

DIFFRACTION DISSOCIATION OF NEUTRONS INTO $(p\pi^-)$ ON PROTONS

IN THE MOMENTUM RANGE 35 TO 65 GeV/c

A. Babaev, E. Brachman, G. Eliseev, A. Ermilov, Yu. Galaktionov,
Yu. Gorodkov, Yu. Kamishkov, E. Leikin, V. Lubimov, L. Ponomarev,
V. Shevchenko, V. Tiunchik and O. Zeldovich

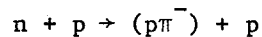
Institute for Theoretical and Experimental Physics, Moscow, USSR
and
Moscow State University, Moscow, USSR

V. Böhmer, J. Engler, W. Flauger, H. Keim, F. Mönning,
K. Pack and H. Schopper

Institut für Experimentelle Kernphysik, Karlsruhe, Germany
and
CERN, Geneva, Switzerland

ABSTRACT

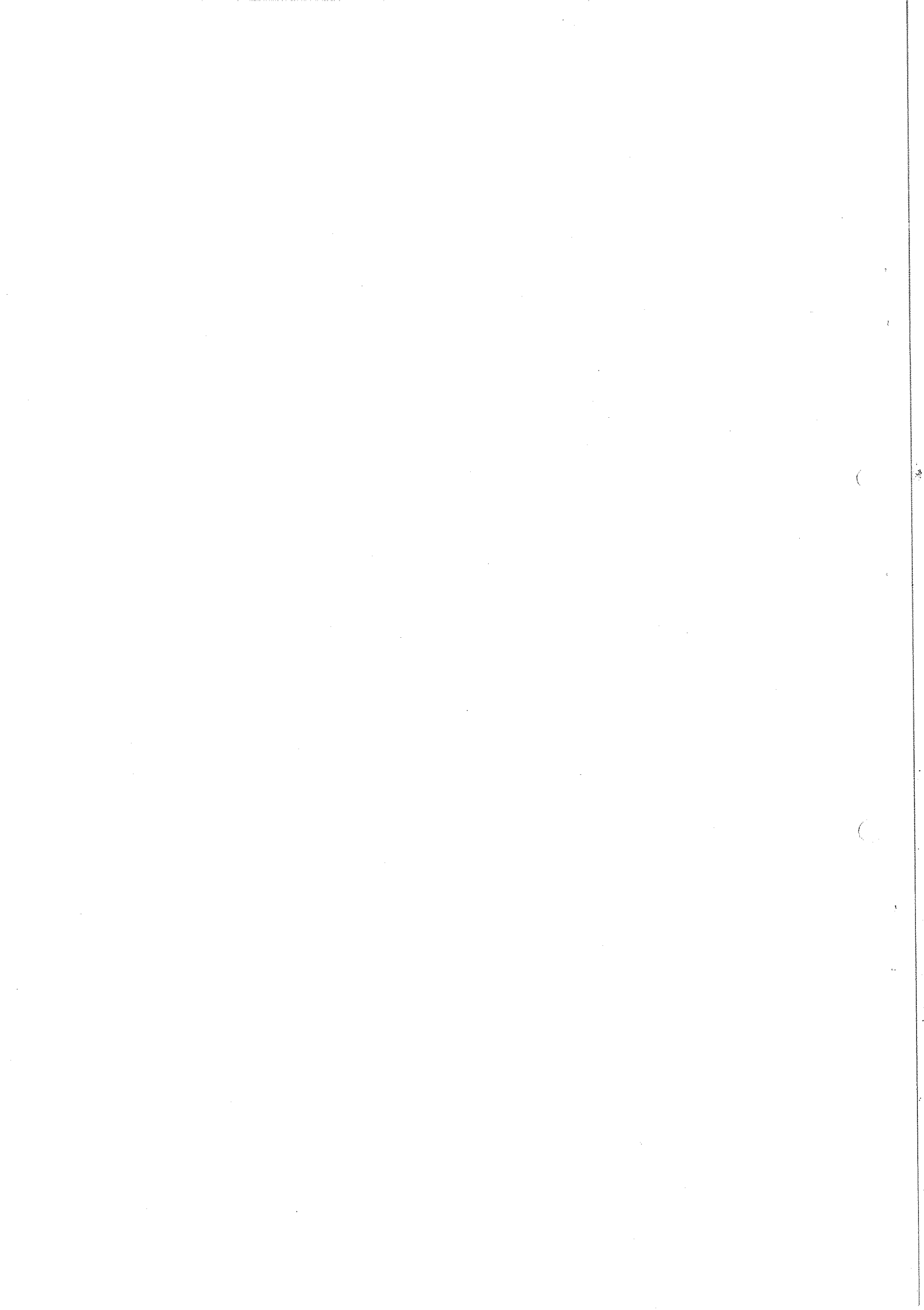
The diffraction dissociation reaction



was studied at the Serpukhov accelerator neutron beam in the momentum range 35-65 GeV/c in an electronics experiment. The differential cross-sections of the reaction are analysed and presented in the five-dimensional phase space $(p_n, m^*, t, \cos \theta^*, \phi^*)$. The backward peak observed in the distribution over $\cos \theta_{GJ}^*$ in the Gottfried-Jackson frame of $(p\pi^-)$ is interpreted as a baryon-exchange effect. The angular distribution of the $(p\pi^-)$ system is compared with Deck-type models.

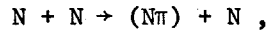
Geneva - 23 June 1976

(Submitted to Nuclear Physics)



1. INTRODUCTION

The nucleon dissociation into $(N\pi)$



as well as other inelastic reactions with many particles in the final state, have up to now mainly been studied in bubble chambers¹⁾. Only recently the nucleon diffraction dissociation was studied in electronics experiments at high energies^{2,3)}.

The main features of the phenomenon observed at intermediate energies (< 30 GeV) are the following⁴⁾.

- i) The $(N\pi)$ system is preferably produced with low invariant mass.
- ii) The energy dependence of the reaction is rather weak.
- iii) The t -distribution shows diffraction-like behaviour ($\sim e^{bt}$) with a slope b , which depends on the mass of the $(N\pi)$ system; the higher the mass the more the slope decreases.
- iv) For the nucleon of the $(N\pi)$ system, the distribution of $\cos \theta_{GJ}$ in the Gottfried-Jackson system is strongly peaked towards $\cos \theta_{GJ} = 1$.

Having to deal with one neutral particle it is convenient, from the experimental point of view, to have it in the initial state where its direction is known. Therefore diffraction dissociation was studied in a neutron beam investigating the following reaction



An electronics experiment, though having the advantage of high statistics, contrary to a bubble chamber, may have essential geometrical restrictions in the detection of multiparticle events and the detection efficiency may be a complex function of the measured variables. In this case, a Monte Carlo procedure, chosen for the calculation of the multi-dimensional detection efficiency, is of great importance.

The experiment reported here was performed in the neutral beam of the Serpukhov machine and was part of a larger programme of an ITEP-Karlsruhe-CERN Collaboration to study np scattering at high energies.

2. THE EXPERIMENTAL METHOD

2.1 The experimental set-up

The basic elements of the apparatus had been used also in an np charge-exchange scattering experiment, and a detailed description is given elsewhere⁵⁾. The set-up used in this experiment is shown schematically in Fig. 1.

The fast forward-going proton was detected and momentum-analysed in the wire chamber magnetic spectrometer; the pion was detected in the hybrid chambers before the magnet, and a set of scintillation counters was used to detect the recoil proton. These counters were $5 \times 10 \text{ cm}^2$ in cross-section and arranged on a circle around the target with a radius of 62.5 cm. The liquid hydrogen target had an effective length of 20 cm and was surrounded by a shield of anticounters with holes for the recoiling proton and the forward-going particles. The anticounters consisted of four layers of scintillator interspersed with 5 mm lead plates.

To trigger the apparatus, the following conditions had to be satisfied:

- i) A charged particle had to pass through the counters P1, P2, P3, and P4, of the forward spectrometer.
- ii) The signal from the counter P4 had to exceed a threshold corresponding to two charged particles.
- iii) At least one of the recoil counters had to be fired.
- iv) There had to be no signal from the anticounters.

For the recoil particle, its time of flight and its pulse height in the scintillator of 5 cm thickness were recorded.

During the running time, about 150,000 triggers were recorded.

2.2 Track reconstruction

The track-finding program⁵⁾ looked for events with at least two tracks before the magnet and at least one of these tracks had to pass through the magnet. No events with two or more tracks passing through the whole spectrometer were found. In order to check the reliability of the track-finding procedure, the data were rescanned by two other programs. They differ from the first one mainly in the grouping of sparks into clusters and in the criterion of sharing sparks for two tracks. They found among the rejected events a sample of an additional 15% of events with at least two tracks. The dependence of the hybrid chambers' efficiency on the track multiplicity and on the distance between them was studied in detail. Up to three tracks, the track-finding probability was 99% in one set of four chambers for tracks more than 2 cm apart from each other. For tracks closer to each other, the decrease of the efficiency was taken into account in the Monte Carlo program used for the efficiency calculation.

About 55,000 events with two or three tracks found in the hybrid chambers were written on the secondary tape.

2.3 Geometrical event reconstruction

At the next step of the analysis the minimum distance ρ between two tracks, which were supposed to correspond to the proton and the pion, was computed. The ρ distribution is shown in Fig. 2. It is peaked at $\rho = 0$ in agreement with the Monte Carlo simulation, which is also shown in Fig. 2. The distribution indicates, on the one hand, that the two tracks are coming from the same origin and, on the other hand, that the background of random crossings is low. For events in which a third track was found, it was checked that this track passed outside the crossing region of the first two trajectories; otherwise the event was considered to be a "star" and rejected. Only the events with $\rho < 0.8$ cm were accepted for the further analysis.

The distributions of the crossing-point coordinates (x, y) in the plane normal to the beam direction are shown in Fig. 3. They reproduce the lateral size of the neutron beam (10×20 mm²), thus showing that the selected events were generated by the beam. The event distribution along the beam is shown in Fig. 4 and compared with the Monte Carlo simulation, which takes into account the reconstruction errors. The comparison demonstrates a good agreement of the distribution with the target length. The cuts on the above-mentioned distributions were applied as shown in Figs. 3 and 4.

The time of flight of the recoil particle and its pulse height in the scintillation counter (kinetic energy) allow one to determine the mass of the traversing particle. The mass spectrum is shown in Fig. 5. It is peaked around the proton mass, and the shape of the peak corresponds to the experimental errors of 0.7 nsec in the time of flight and of typically 8% in the pulse-height measurements. Therefore we see that the selected events originate from neutron beam interactions in the target and have a proton as a recoil particle.

3. THE ANALYSIS OF THE EVENTS

3.1 Kinematical reconstruction of the reaction $n + p \rightarrow (p\pi^-) + p$

In order to recognize events of reaction (1), one has to identify the forward-going particles as a $(p\pi^-)$ state without any additional charged or neutral particles produced.

The coordinate system and the geometrical variables used are shown in Fig. 6. We define the production plane by the direction of the incident neutron and the recoiling proton, and the decay plane by the directions of the two forward-going particles, p and π^- . The intercept of the two planes gives the direction of the motion of the $(p\pi^-)$ system. The trajectory passing through the magnet, corresponding to a positive particle with high momentum, was assumed to belong to

the proton. Then if one assumes that there are no missing particles, one can calculate any kinematical variables of reaction (1) from the measured quantities, assigning the proton and pion masses to the particles. However, if the decay angle of the ($p\pi^-$) or the angle between the decay plane and the production plane are too small, the π momentum is defined only with a big error, due to the finite size of the recoil proton counters. The events of such a geometrical configuration were eliminated.

For the accepted events the momentum transfer from the neutron to the ($p\pi^-$) system ($t_{p\pi}$) was calculated. The same quantity was independently determined from the recoil proton measurements of the time of flight (t_{TOF}) and the pulse height (t_A). The average (t_p) of t_{TOF} and t_A should coincide with $t_{p\pi}$ within the experimental errors. Figure 7 shows the distribution of the difference $t_{p\pi} - t_p$, together with events of the Monte Carlo simulation. The apparent coincidence of the two distributions demonstrates that the events belong to three-body reaction (1); possible background reactions will be discussed in Section 3.2.

From the three measured values of $t_{p\pi}$, t_{TOF} , and t_A , the weighted average t was found and the value of

$$\chi_t^2 = \left(\frac{t - t_{p\pi}}{\sigma_{p\pi}} \right)^2 + \left(\frac{t - t_{TOF}}{\sigma_{TOF}} \right)^2 + \left(\frac{t - t_A}{\sigma_A} \right)^2 \quad (2)$$

was calculated. The corresponding t -dependent variances were determined by the Monte Carlo calculation. In Fig. 8 the χ_t^2 distribution is shown, together with the distribution for Monte Carlo simulated events. The coincidence of the two distributions shows the absence of any visible background processes as indicated by one possible background (random π^- selection, see below).

Figure 9 shows the measured momentum spectrum for the protons of the ($p\pi^-$) system, with the incident neutron momentum spectrum as calculated from the kinematics. The latter is shifted towards higher momenta and has a steep fall towards the kinematical boundary (70 GeV/c). It coincides with the neutron spectrum of the Monte Carlo calculation, in which the neutron spectrum as measured with a total absorption counter⁶⁾ was used. This fact also confirms a small background contribution. The corresponding spectrum, as obtained from the randomly distributed pions, differs significantly.

About 15,000 events in the neutron momentum range 35-65 GeV/c passed the analysis procedure and were written on the summary tape.

3.2 Background

When comparing the χ_t^2 distribution and the neutron momentum spectrum with the Monte Carlo results, we found good agreement. However, for the diffraction

type background processes like $n + p \rightarrow X + p$, where X contains a leading proton, the distribution of the difference to $t_{p\pi} - t_p$ may still be peaked to zero value. The background contamination from these reactions may be essential and needs special consideration.

To eliminate events with more than two forward-going charged particles an upper limit on the linear signal from the counter P4 (see Fig. 1) was set off-line. By this limit, 2.5% of the real events were rejected, whereas the probability to reject two charged particles is 0.5%. The veto system around the target had a detection efficiency of 99% for π^0 's, but it was much less effective ($\sim 20\%$) for neutrons. Moreover, forward-going γ 's could not be vetoed.

Several methods were used to check whether events with some undetected additional particles were misidentified as events of reaction (1) and could be present in the final sample of good events.

Firstly, in the good events the actual pion track was omitted and then the pion direction was taken randomly within the acceptance angle. The events constructed in this way turned out to have also a peak in the $t_{p\pi} - t_p$ distribution. But the peak was much broader than for good events as is seen in the χ_t^2 distribution in Fig. 8. Other kinematical variables, for example, the reconstructed momentum of the neutron, were distributed quite differently as compared to the good events distributions (see Fig. 9). From comparison of these distributions, we evaluate the contamination of the "random pion" events background to be less than 2%.

Secondly, the "stars" were analysed, i.e. the events where three tracks originating from the same point were found in the hybrid chambers. A total of about 100 events of this type were found. These events were converted into two-track events by arbitrarily omitting one of the two tracks which were not coming through the magnet. Then these "events" were analysed in the normal way. One such event out of 100 passed successfully the analysis chain, proving that the analysis procedure suppressed high multiplicity events to a level of 1%.

Thirdly, the contamination of the processes



and



was evaluated by a Monte Carlo technique. The events were generated by a program based on a theoretical Deck-type⁷⁾ model, which satisfactorily describes the experimental data in a broad range of incident momenta and $|t|$. The generated events were then "detected" by a program, imitating the experimental set-up, and analysed by the normal analysis chain. After normalization to the total neutron

flux, it was found that the reaction (3) yields a contamination of 1-2% in the good events sample, whereas the contribution of reaction (4) was 0.3%.

Summarizing, from these considerations, we can conclude that background processes are effectively suppressed. This is due mainly to the veto counter system, the limited geometrical acceptance for background processes, and the kinematical criteria of the process investigated. In the following, we neglect the background and add 3% to the over-all normalization error.

4. THE ACCEPTED PHASE SPACE

4.1 The kinematical variables

The amplitude of reaction (1) with an unpolarized initial state can be described by five independent kinematical variables. The following quantities were chosen

$$p_n, t, m^*, \cos \theta^*, \phi^*, \quad (5)$$

where

- p_n : lab. momentum of the incident neutron (GeV/c).
- t : four-momentum transfer squared to the recoiling proton (GeV/c)².
- m^* : the invariant mass of the system ($p\pi^-$) dissociated from the neutron.
- $\cos \theta^*, \phi^*$: the decay angles of the ($p\pi^-$) system in its c.m.s.

$$\cos \theta^* = - \frac{\vec{P}_2 \cdot \vec{P}_{31}}{|\vec{P}_2| \cdot |\vec{P}_{31}|} \quad (6)$$

$$\cos \phi^* = \frac{[\vec{P}_2 \times \vec{P}_4] \cdot [\vec{P}_{31} \times \vec{P}_2]}{|[\vec{P}_2 \times \vec{P}_4]| \cdot |[\vec{P}_{31} \times \vec{P}_2]|} .$$

These angles are very close to those defined in the so-called "s-channel helicity frame".

We also use the set of variables with standard Gottfried-Jackson angles in the c.m.s. of ($p\pi^-$).

4.2 The experimental accuracies of the kinematical variables

The accuracy of the determination of the five variables (5) was found by a Monte Carlo calculation, using the following experimental findings: (i) the spatial

accuracies of the hybrid and spark chambers were 0.4 and 0.3 mm, respectively; (ii) the time-of-flight measurement accuracy was 0.7 nsec; (iii) the pulse-height measurement accuracy was 8%. One should point out that the accuracies of the quantities (5) were mainly limited by the geometrical sizes of the recoil proton counters. The Monte Carlo program was checked to reproduce all experimentally observed distributions. Some of them were shown in Figs. 2-5 and 7-9.

Table 1 gives an illustration of typical accuracies of the kinematical variables. The accuracies really used were more complex functions of the variables and Table 1 quotes only averaged projections of those functions on the variables' axes.

4.3 Phase space

We determined the total cross-section for neutron momenta p_n between 35 and 65 GeV/c. Outside this interval the absolute normalization error was too large. The remaining four variables could have any values within certain kinematical boundaries.

The parameters (5) were actually measured in a region V_1 for which the boundaries are given in Table 2. Inside V_1 , the event-detection efficiency varied. To study this dependence, the volume V_1 was divided into five-dimensional bins. The bin size was chosen in such a way that the bin length along a variable axis was more than (or sometimes equal to) the corresponding errors. As noted in Table 2, the experimental accessible region V_1 was divided into $3 \times 7 \times 12 \times 6 \times 4 = 6048$ bins.

The detection efficiency in these bins was determined by Monte Carlo calculations. It turned out, for example, in the momentum range of 55-65 GeV/c, that $\sim \frac{1}{2}$ of the whole number of bins had rather high detection efficiency and $\sim \frac{1}{3}$ of them contained the detected experimental events. The volume inside V_1 , where actual experimental events were found, is in the following denoted by V_2 .

4.4 Efficiency calculations

The Monte Carlo program took into account all sources of inaccuracies and inefficiencies, like multiple scattering, ionization loss fluctuations, and hybrid and spark-chamber performance. The five variables were taken randomly inside a bin and then the real events were formed by the program imitating the experimental set-up. This event generation was followed by the geometrical and kinematical reconstruction procedure. Owing to the errors in the measurements, the event originating from a certain bin did not necessarily fall into the same bin after the analysis. Because of the multidimensionality of the phase space,

the transfer into the neighbouring bins could considerably -- up to a factor of 1.5 -- change the local detection efficiency. Therefore, in order to take this transfer into account, in other words to unfold the experimental data, the efficiencies were calculated not using a uniform event density distribution over the volume V_1 , but a real distribution close to the one in nature. Two independent methods were used: an iteration procedure and a theoretical model.

In the iteration procedure, the experimentally detected event density distribution was used as the first approximation for the Monte Carlo calculation input. As the output we had the five-dimensional matrix of the efficiencies, which was used to calculate the differential cross-sections in V_1 . The cross-sections thus obtained were used as input for the next iteration and so on. The change in the cross-section integrated over V_1 from one iteration to the other was used as the convergence criterion. The procedure turned out to be rapidly converging. After four iterations the cross-sections varied less than 10%.

Besides the iteration procedure, the theoretical matrix element⁸⁾ was used to construct the event density distribution for Monte Carlo calculation input. The integrated cross-section, found by this method, was in agreement with the result of the iteration procedure within 10%. The differential cross-section did not differ by more than 20%.

The calculated efficiency varied over the volume V_2 around an average value of 30%. To eliminate the influence of the "edge effects" of the experimental set-up, the boundaries of V_2 were set off-line at limits where the efficiency was less than 10%. By this setting, about 8% of the events were eliminated. It was checked that varying the efficiency threshold in the range 5 to 15% changed the integrated cross-section in accordance with the change in the phase volume.

5. THE CROSS-SECTIONS

Dividing the yields by the detection efficiency, the differential cross-sections $d^5\sigma/dp_n dt dm^* d \cos \theta^* d\phi^*$ were found. These cross-sections with the statistical errors are given in Addendum I (see Ref. 8).

The main sources of the absolute normalization error were the neutron beam monitoring (10%), the Monte Carlo efficiency calculation (15%), the effective target length (6%), and the track-finding efficiency (5%). In Table 3 all the corrections and sources of uncertainties are listed. The total normalization error amounts to $\pm 21\%$.

6. DISCUSSION OF THE RESULTS

6.1 Comparison with theory

All the characteristic features of nucleon diffraction dissociation were understood in terms of the pion-exchange Deck mechanism⁹⁾, which is illustrated by diagram (a) in Fig. 10. We have calculated theoretical cross-sections using a matrix element, as outlined in Addendum II (see Ref. 8), where the Deck mechanism was taken into account through Reggeized one-pion exchange. In the following both experimental and theoretical cross-sections are always compared in the same region of phase space.

Figure 11a shows the angular distribution over $\cos \theta_{GJ}$ and the prediction of the Deck model. One notices that the forward peak ($\cos \theta_{GJ} \sim +1$) is well described, but in the data also a backward peak is quite pronounced, which is not described by this model. This backward peak in the $\cos \theta_{GJ}$ distribution could be created by the decay of the resonances produced via Pomeron exchange (N^*_{520} , N^*_{688})²⁾. To see whether this is an explanation, we weaken the possible influence of the resonance production by plotting the $\cos \theta_{GJ}$ distribution for $m^* < 1.42 \text{ GeV}/c^2$ and $-t < 0.23 \text{ (GeV}/c^2)^2$ (Fig. 11b). As one can see, the backward peak is still pronounced in spite of the above restrictions.

In Fig. 12 the mass distribution of the $(\pi\pi)$ system is compared with the Deck-model prediction for masses smaller than $1.42 \text{ GeV}/c^2$. The Deck model predicts a mass spectrum which peaks at too small mass values.

The backward peak can be explained with a mechanism which is similar to the Deck one, but involving baryon exchange instead of pion exchange, namely by adding the diagrams (b) and (c) in Fig. 10. Such a model, which takes into account all the diagrams of Fig. 10, was developed by one of us (L.P.) and is given in more detail in Addendum II. One should point out that the interference terms were essential when combining all three diagrams. The predictions of this model for the angular distribution and for the mass distribution are given as solid lines in Figs. 11 and 12, respectively. The backward peak as well as the mass spectrum are satisfactorily reproduced. For $m^* \geq 1.4 \text{ GeV}/c^2$ predictions of the model are unreliable.

Figure 13 shows the two-dimensional plots ($\cos \theta^*$, ϕ^*) for the experimental data and Fig. 14 for the pion- and baryon-exchange Deck model, in both cases for the low mass and low $|t|$ region. We present the data in the c.m.s. of the $(\pi\pi)$ system as defined in Eq. (6), because here the regions not observed experimentally are more easily indicated. One notices a good separation of the pion-exchange and the baryon-exchange mechanisms. In Fig. 15 the mass distribution for the two angular regions of (a) baryon- and (b) pion-exchange dominance are shown. As is illustrated in Fig. 15a, the pion Deck exchange alone cannot reproduce the

measured mass distribution. Both exchanges together explain rather well the spectra up to masses of $\sim 1.4 \text{ GeV}/c^2$. Therefore, we can conclude that the present data give clear evidence for the presence of a baryon-exchange contribution according to the graphs of Fig. 10.

The theoretical curves in Figs. 11, 12 and 14, 15 are normalized to the experimentally measured cross-section integrated over the phase space V_2 , under the restrictions $m^* < 1.42 \text{ GeV}/c^2$ and $|t| < 0.23 (\text{GeV}/c)^2$. The absolute cross-sections predicted by theory and those observed experimentally are compared in Table 4. The comparison is done separately for the two angular regions, where the main contribution is the pion-exchange and the baryon-exchange Deck effect, respectively. The integration is done in the momentum range $55 \leq p_n \leq 65 \text{ GeV}/c$. One sees, from Table 4, that the theoretical cross-sections are a factor of 2-3 higher than the experimental cross-section. This discrepancy might indicate that absorption corrections have to be taken into account¹⁰⁾.

6.2 Comparison with other experimental results

The data of other experiments^{2,3)} are not available in differential form. Hence a straightforward comparison is not possible until the phase-space volumes used in different experiments are identical. Nevertheless, we made an attempt to compare our results with those of other measurements in the following way. With the above-mentioned model we empirically constructed a matrix element which described our data and added, for a better description of the mass spectra in the high mass region, the resonance production of $N^*(1520)$ and $N^*(1688)$ via vacuum exchange. Furthermore, the t dependence was made steeper than in the theory to coincide with the experiment. With this parametrization the integration was performed and the difference in the experimental phase spaces taken into account.

We compare mass spectra by integrating the matrix element constructed above in each bin of the mass distribution over the rest of the variables in the phase space of our experiment, as well as in the phase space of other experiments^{2,3)}. The ratio of the two integrations gives the correction to scale our data to those of the other experiments. We investigated the sources of possible errors by taking different variations of the matrix elements and found that the shape of the distributions can be affected up to $\pm 30\%$. Also the normalization error must be increased up to $\pm 30\%$; therefore all these errors should be assigned to the data given below.

In Fig. 16 the $(p\bar{\pi}^-)$ mass distribution for $45 \leq p_n \leq 65 \text{ GeV}/c$ is compared with the corresponding distribution from the FNAL experiment³⁾. Both sets of data are absolutely normalized. For the FNAL data we could only take the absolute

normalization from the mass region $1.25 < m^* < 1.45 \text{ GeV}/c^2$, where absolute cross-sections are quoted. The spectra turned out to be almost identical, apart from the mass region around $1.5 \text{ GeV}/c^2$.

Figure 17 illustrates the energy dependence of the cross-sections in two low-mass intervals and when $0.02 < t < 1.0 \text{ (GeV}/c)^2$. The data are given for three-momentum intervals with the mean values 40, 50, and 60 GeV/c. They compare well with the FNAL data, which are also given in the figure.

Typical t -distributions are shown in Fig. 18 for $m^* < 1.35 \text{ GeV}/c^2$, separately for $\cos \theta_{\text{GJ}} > 0$ and $\cos \theta_{\text{GJ}} < 0$. An exponential e^{-Bt} was fitted to the data. The slope parameters B , as a function of the mass, are given in Fig. 19 and in Table 5, together with the t range used. In Fig. 19a they are determined separately for the forward and the backward region in the Gottfried-Jackson system. For lower masses one observes clearly the difference of the slopes in the two regions, which cannot be said for higher masses. In Fig. 20 the total cross-section of reaction (1) is given for the three incident momenta 40, 50, and 60 GeV/c. The errors shown include also systematic errors. For comparison, the data obtained in experiments at other energies¹⁻³⁾ are also given.

7. CONCLUSION

The data on diffraction dissociation above 30 GeV/c presented here show new phenomena not observed at lower energies. These are the presence of the backward peak in $\cos \theta_{\text{GJ}}$ and the shift of the mass peak to higher masses. The effect can be explained by the Deck mechanism when taking baryon exchange into account as well as the usual pion exchange.

REFERENCES

- 1) E. Dahl-Jensen et al., Scandinavian Bubble Chamber Collaboration, Nuclear Phys. B87, 426 (1975) and references quoted therein.
- 2) E. Nagy et al., Experimental result on inelastic diffractive scattering in pp collisions at the ISR, Paper submitted to the 17th Internat. Conf. on High-Energy Physics, London, 1974.
C. Broll, Etude de $pp \rightarrow p(n\pi^+)$ aux anneaux de stockage du CERN, Thesis, Orsay, 1976.
- 3) J. Biel et al., Investigation of the reaction $n + p \rightarrow (p\pi^-) + p$ at Fermilab energies, Paper submitted to the EPS Internat. Conf. on High-Energy Physics, Palermo, 1975 and Phys. Rev. Letters 36, 504 (1976).
- 4) For a review consult, for example:
M.I. Miettinen, Invited talk at EPS Internat. Conf. on High-Energy Physics, Palermo, 1975, preprint TH.2072-CERN, and
G. Goggi, in Proc. Internat. Colloquium on Multiparticle Reactions, Oxford, 1975 (Science Research Council, Rutherford Lab., Chilton, Didcot, 1975), RL75-143.
- 5) A. Babaev et al., Neutron-proton charge exchange in the momentum region 25-65 GeV/c, Submitted to Nuclear Phys. B.
- 6) V. Böhmer et al., Nuclear Instrum. Methods 122, 313 (1974).
- 7) L.A. Ponomarev, Yadernaya Fiz. 22, 807 (1975).
- 8) Addenda I and II to this article, not published, but available on request from the authors: (J.E.) at CERN, Geneva, Switzerland, (V.L.) at ITEP, Moscow, USSR, and (F.M.) at IEKP, Karlsruhe, Germany.
- 9) R.T. Deck, Phys. Rev. Letters 13, 169 (1964).
E.L. Berger, A critic of the Reggeized Deck model, Argonne report ANL/HEP 7506, Daresbury Study Weekend series No. 8.
K.G. Boreskov et al., Yadernaya Fiz. 15, 361 (1972) [English translation: Soviet J. Nuclear Phys. 15, 203 (1972)].
K.G. Boreskov et al., Yadernaya Fiz. 15, 557 (1972) [English translation: Soviet J. Nuclear Phys. 15, 309 (1972)].
- 10) E.L. Berger and P. Pirilä, Phys. Letters 59B, 361 (1975).
V.A. Tsarev, Phys. Rev. D 11, 1864 (1975).

Table 1

The experimental accuracies of the kinematical variables

Variable	Standard deviation	Units
p_n	$\sigma_{p_n} = 0.022 p_n + 0.65$	GeV/c
t	$\sigma_t = 0.11 t$	(GeV/c) ²
m^*	$\sigma_{m^*} = 0.135 \times (m^* - 1)$	GeV/c ²
$\cos \theta^*$	$\sigma_{\cos \theta^*} = 0.04 \cos \theta^* + 0.054$	
ϕ^*	$\sigma_{\phi^*} = 0.08$	rad

Table 2

The boundary of the phase space accepted by the apparatus (volume V_1)

Variable	Interval	Units	Number of intervals
p_n	35-65	GeV/c	3
$-t$	0.05-0.62	(GeV/c) ²	7
m^*	1.08-1.86	GeV/c ²	12
$\cos \theta^*$	$-0.96 \leq \cos \theta^* \leq 0.96$		6
ϕ^*	$0.04\pi \leq \phi^* \leq 0.96\pi$	rad	4

Table 3

Correction factors and uncertainties

Source	Correction factor	Uncertainty %
Beam monitoring	1.0	±10
Dead-time of antisystem	1.14	±5
Beam loss between target and monitor	0.91	±2
Track-finding efficiency	1.05	±5
Background contamination	1.00	±3
Effective target length	1.00	±6
Threshold in P4	1.01	±1
Efficiency calculation	1.00	±15
Total	1.10	±21

Table 4

Integrated cross-sections in μb for $0.05 \leq -t < 0.23 \text{ (GeV/c)}^2$,
 $m^* < 1.42 \text{ GeV/c}^2$, and $55 \leq p_n \leq 65 \text{ GeV/c}$

	$0.7\pi < \phi^* < 0.96\pi$ $-0.4 < \cos \theta^* < 0.6$	$0.04\pi < \phi^* < 0.4\pi$ $-0.96 < \cos \theta^* < 0$
Experiment	12 ± 2.5	7.6 ± 1.5
Pion exchange Deck	28.4	6.8
Pion + baryon exchange Deck	26.3	18.4

Table 5

The slope B of the exponential fall-off in the t distribution
 $55 \leq p_n \leq 65 \text{ GeV}/c$

M($\pi\pi$) intervals	all $\cos \theta_{GJ}$		$\cos \theta_{GJ} > 0$		$\cos \theta_{GJ} < 0$	
	B [(GeV/c) ⁻²]	-t range	B [(GeV/c) ⁻²]	-t range	B [(GeV/c) ⁻²]	-t range
1.08-1.18	17.8 ± 1.8	0.05-0.17	15.8 ± 1.8	0.05-0.17	21.4 ± 4.3	0.05-0.17
1.18-1.3	15.3 ± 0.82	0.05-0.17	12.0 ± 0.9	0.05-0.17	22.0 ± 1.6	0.05-0.17
1.3 -1.42	16.6 ± 0.83	0.05-0.17	14.7 ± 1.0	0.05-0.17	20.1 ± 1.4	0.05-0.17
1.42-1.54	10.3 ± 1.0	0.05-0.17	8.7 ± 1.3	0.05-0.17	13.5 ± 1.8	0.05-0.17
1.54-1.86	4.9 ± 0.64	0.05-0.45	9.0 ± 1.3	0.11-0.41	5.9 ± 1.0	0.05-0.35

Figure captions

- Fig. 1 : The experimental arrangement
- Fig. 2 : The minimal distance ρ between two tracks crossing in the target region.
- Fig. 3 : The distributions of the crossing points of two tracks in the plane normal to the beam direction. The shadowed region shows the beam cross-section as defined by the collimators at the target position.
- Fig. 4 : The distribution of the crossing points along the beam direction.
- Fig. 5 : The mass distribution of the recoiling particle as determined from time of flight and pulse height.
- Fig. 6 : Schematic view of the reaction and the variables used in the analysis.
- Fig. 7 : The difference of $|t|$ as calculated from the recoil proton and the $(\pi^- p)$ system.
- Fig. 8 : The χ^2 -distribution according to Eq. (2).
- Fig. 9 : The momentum spectra of the detected protons and the neutrons in the beam.
- Fig. 10 : The pion- and baryon-exchange Deck graphs.
- Fig. 11 : The polar angular distribution in the Gottfried-Jackson system:
a) integrated for all masses m^* and momentum transfers $|t|$;
b) for $m^* < 1.42$ GeV and $|t| < 0.23$ (GeV/c)². The full line represents a pion- and baryon-exchange Deck model calculation and the dotted line only a pion-exchange Deck model.
- Fig. 12 : The mass distribution of the $(p\pi)$ system for $|t| < 0.23$ (GeV/c)². The full line represents a pion- and baryon-exchange Deck-model calculation and the dotted line only a pion-exchange Deck-model calculation. The models apply in the low-mass region.
- Fig. 13 : The experimental cross-sections in $\mu\text{b}/\text{sr}$ for $55 < p_n < 65$ GeV/c, $m^* < 1.42$ GeV/c² and $0.05 < |t| < 0.23$ (GeV/c)². The lines are hand-drawn isobarns to guide the eye; they are taken from a more refined grid. The hatched region is not covered by the experimental acceptance.

- Fig. 14 : The theoretical cross-sections in $\mu\text{b}/\text{sr}$ for the Deck-model calculation for (a) pion and baryon exchange and (b) pion exchange alone. The kinematical restrictions are the same as in Fig. 13.
- Fig. 15 : The (πp) mass distribution in the angular region of (a) baryon-exchange dominance and (b) pion-exchange dominance. The lines are Deck-model calculations for baryon and pion exchange (full) and pion exchange alone (dotted).
- Fig. 16 : The integrated (πp) mass distribution for $0.02 < |t| < 1.0$. In the error bars the integration error is included. For comparison the distribution of Ref. 3 is shown.
- Fig. 17 : Energy dependence of the cross-section for the mass intervals 1.25-1.35 and 1.35-1.45 GeV/c^2 , integrated over $0.02 < |t| < 1.0$ $(\text{GeV}/c)^2$. The error bars include experimental and integration error.
- Fig. 18 : t dependence of the cross-sections for low masses and for the forward and backward angular regions in the Gottfried-Jackson system. The lines are fitted exponentials in the region $0.05 < |t| < 0.17$ $(\text{GeV}/c)^2$.
- Fig. 19 : The mass-slope correlation: a) for the forward and backward regions in the Gottfried-Jackson system; b) for the whole angular region compared with data from other experiments.
- Fig. 20 : The total diffraction dissociation cross-section compared with data from other experiments; the error bars include all errors. The pp cross-sections are divided by two. The cross-section level for 50-300 GeV/c is estimated by us from the FNAL data³⁾.

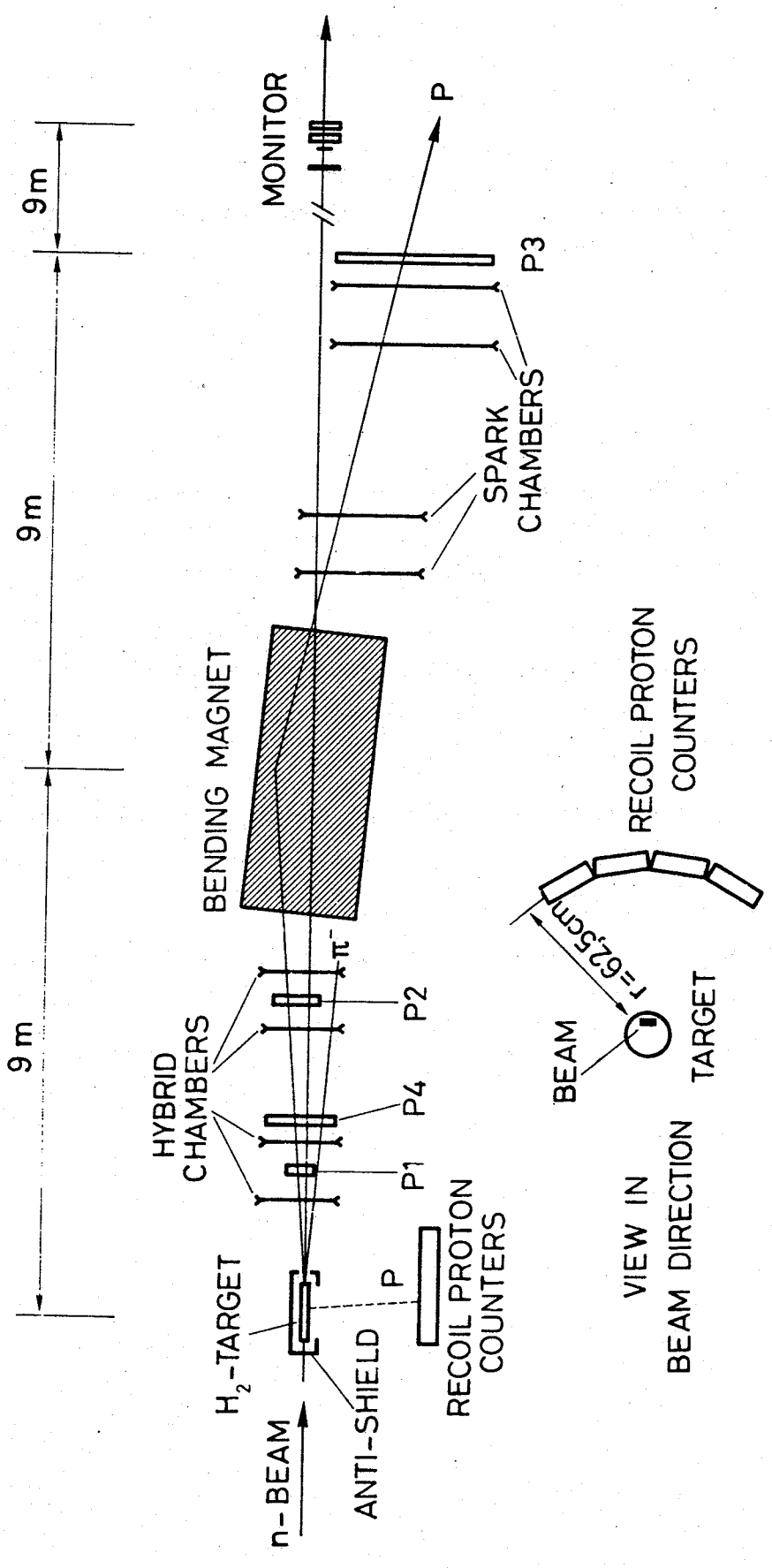


Fig. 1

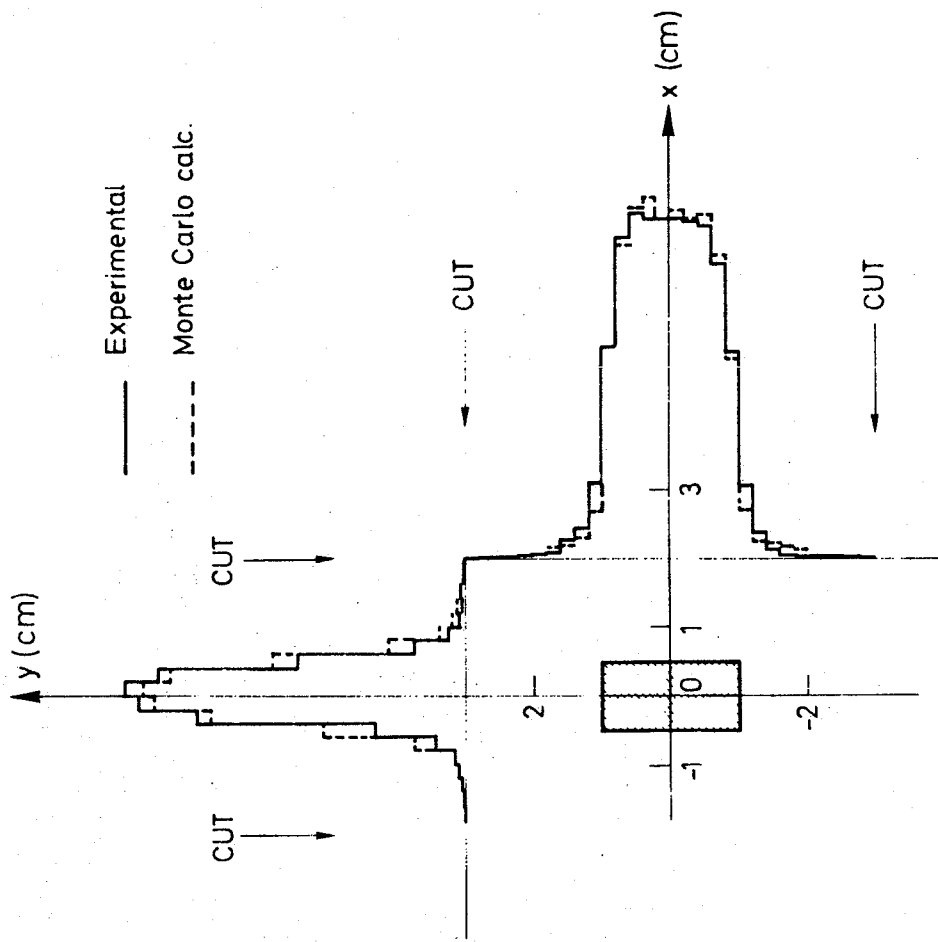


Fig. 3

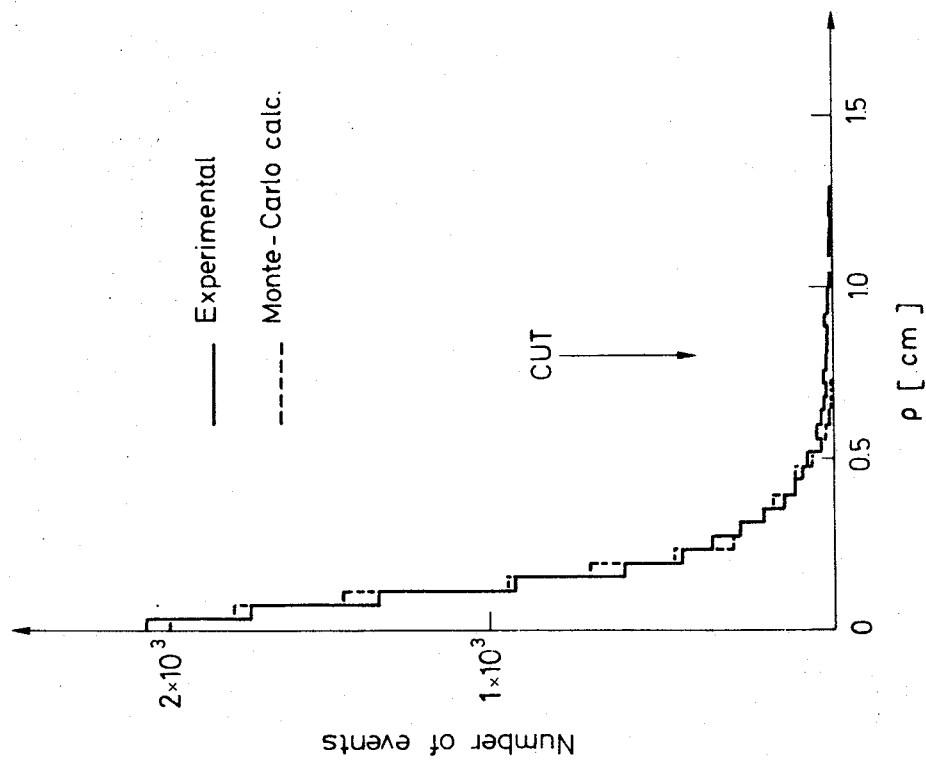


Fig. 2

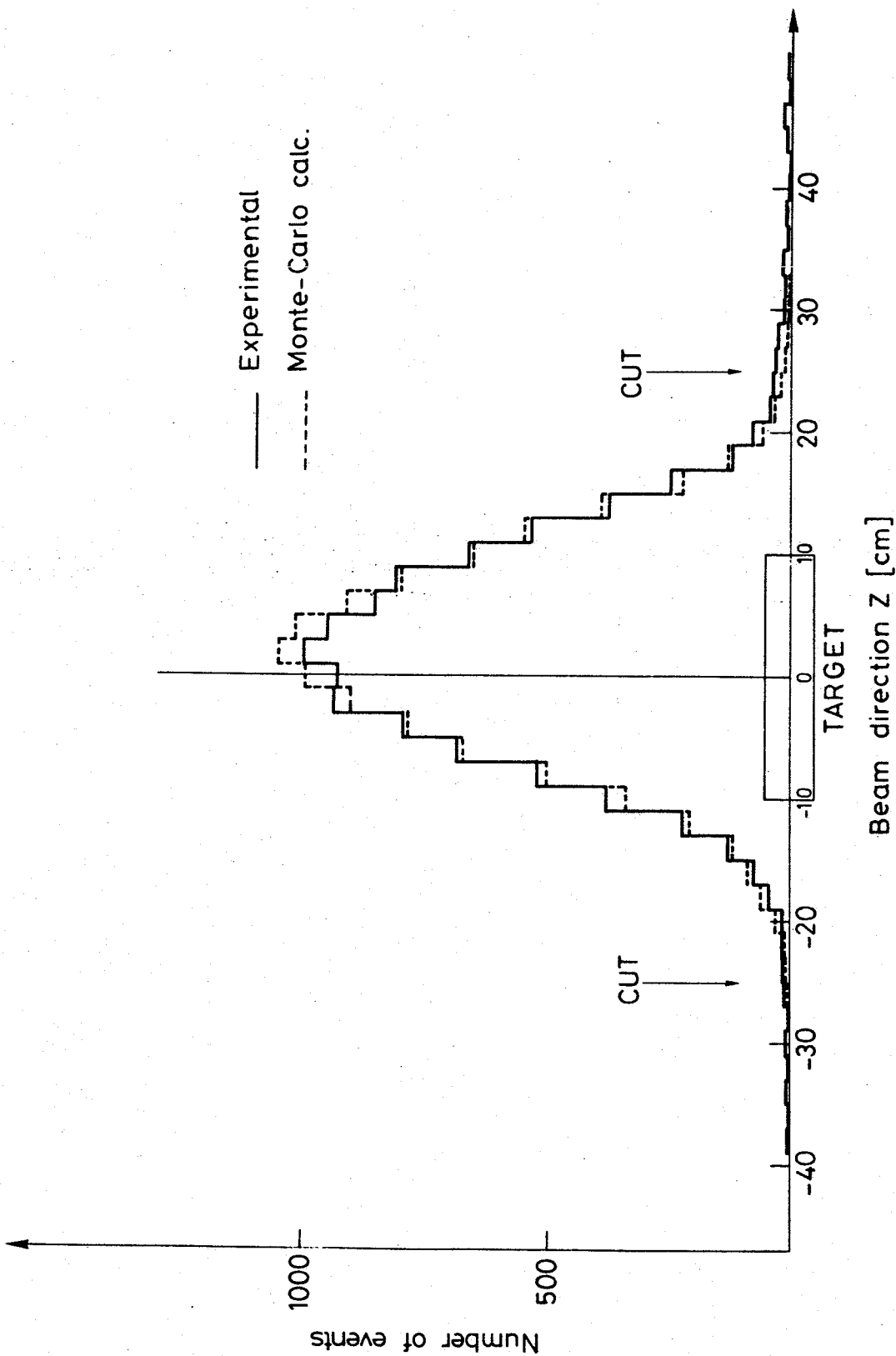


Fig. 4

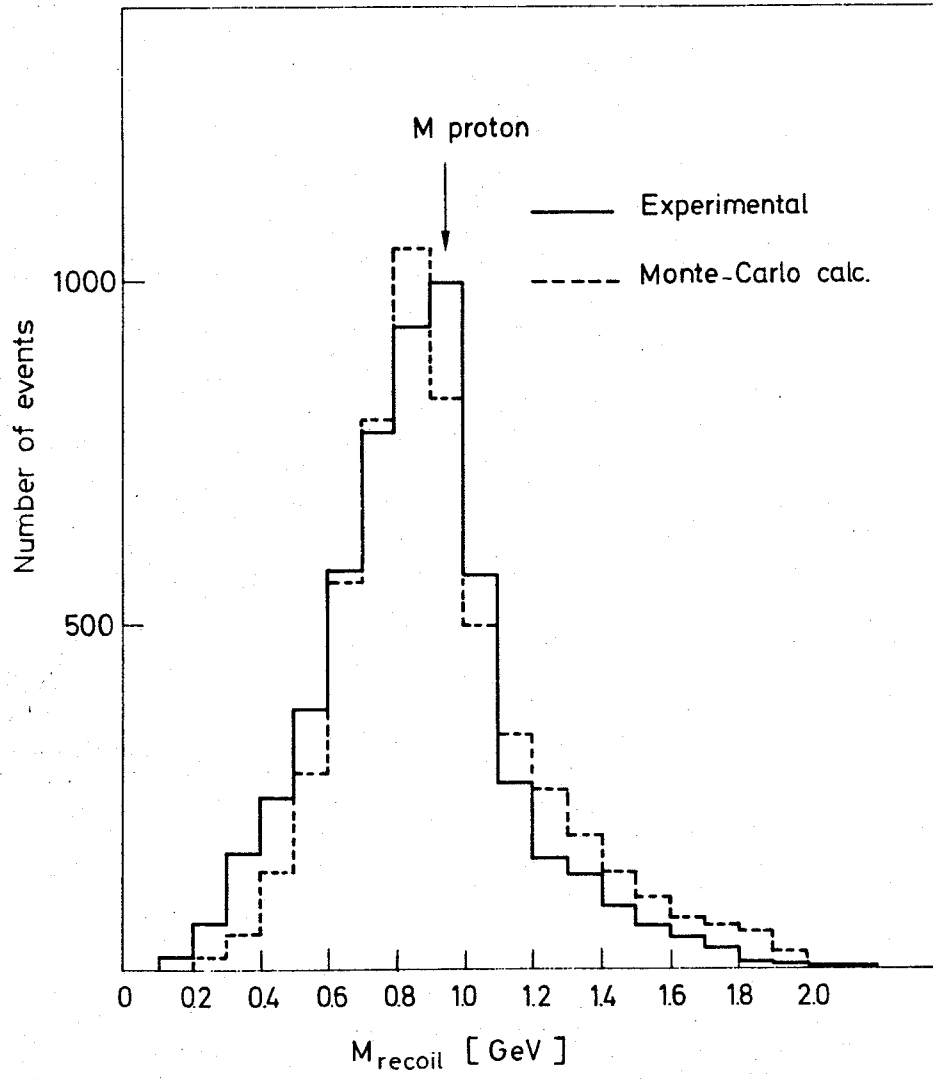


Fig. 5

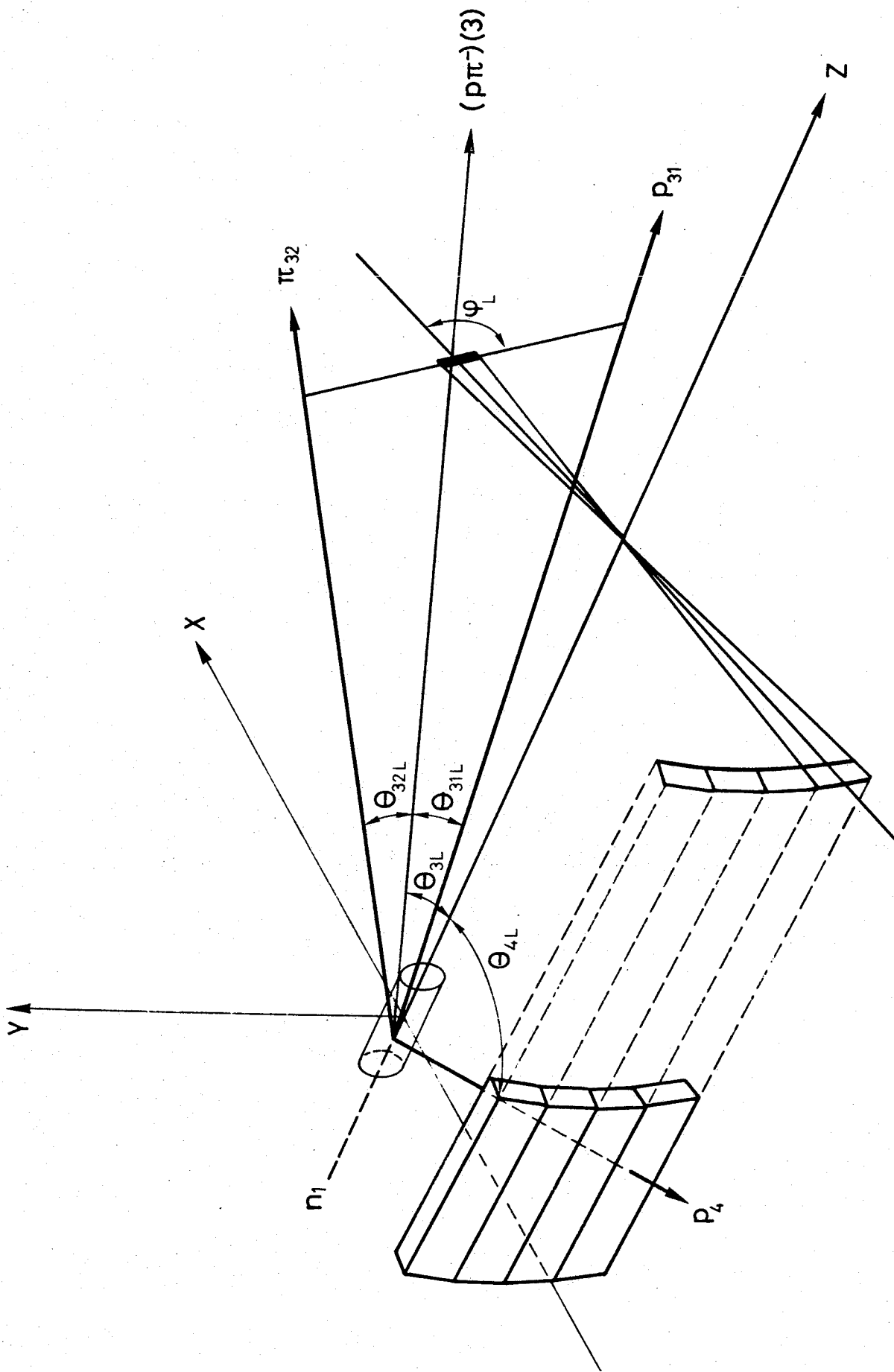


Fig. 6

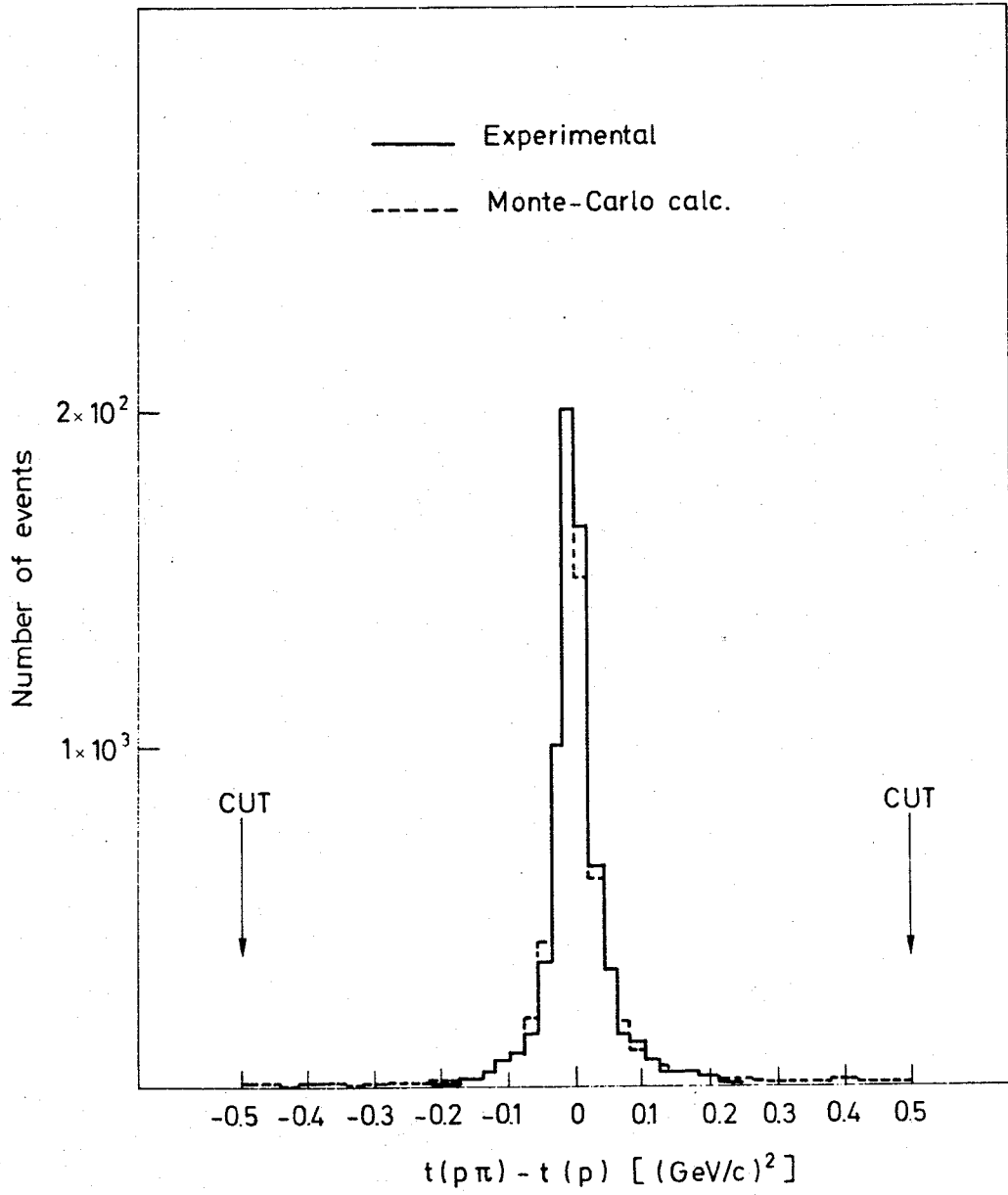


Fig. 7

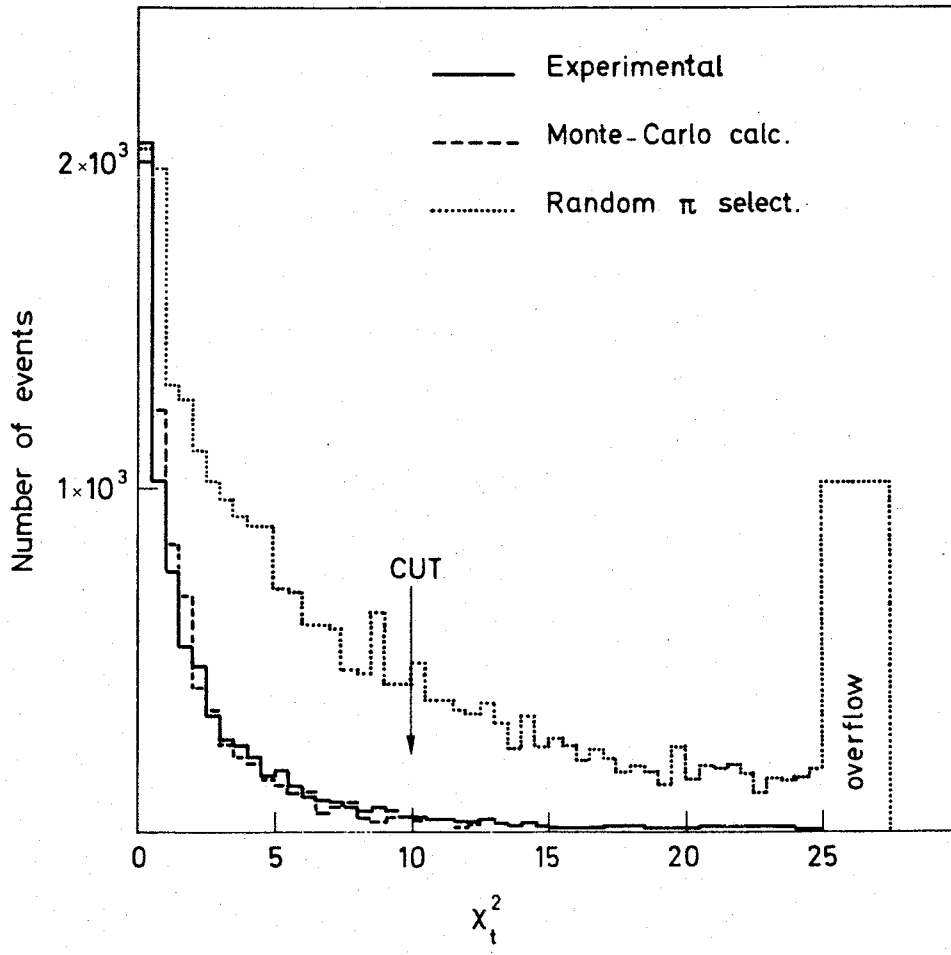


Fig. 8

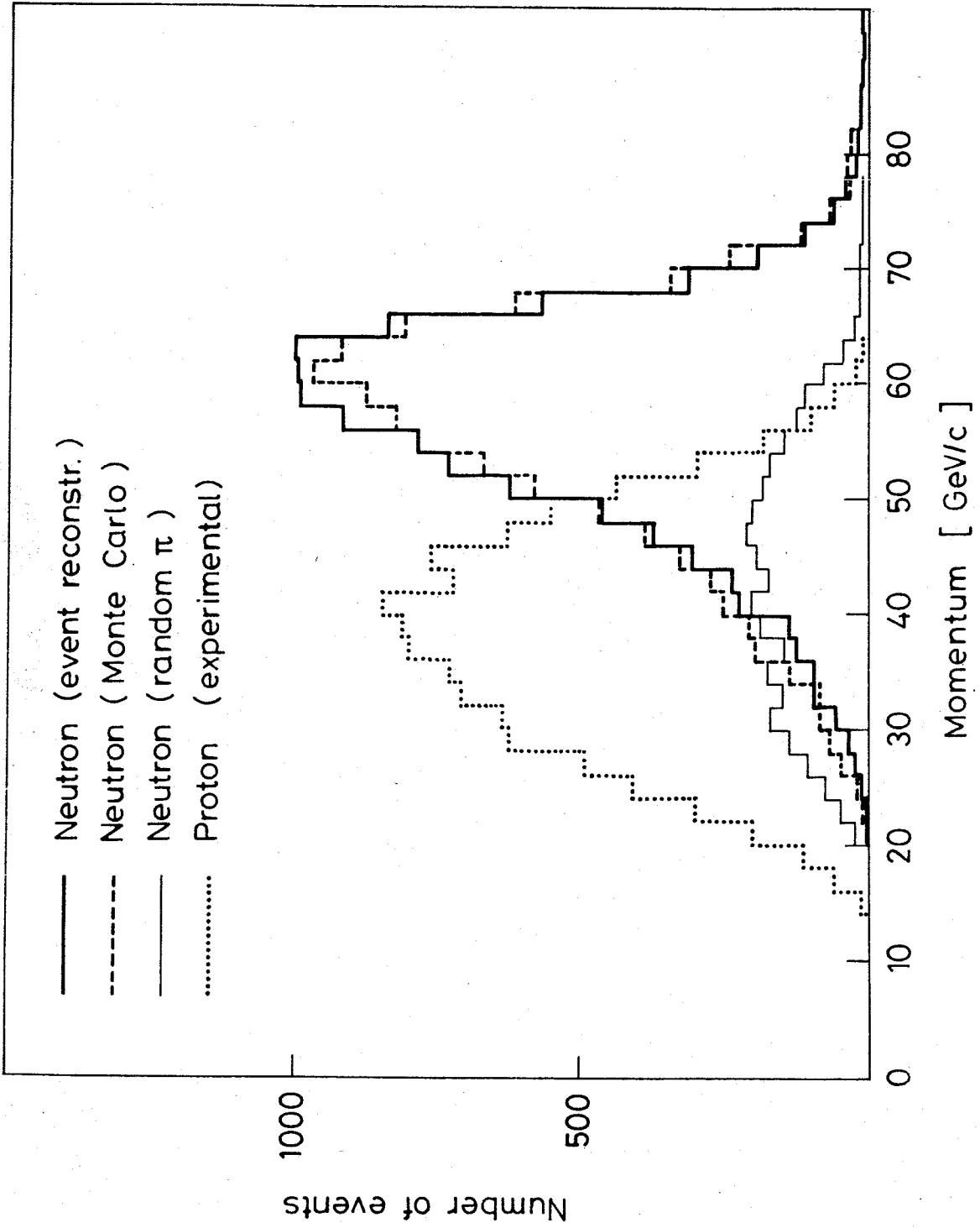


Fig. 9

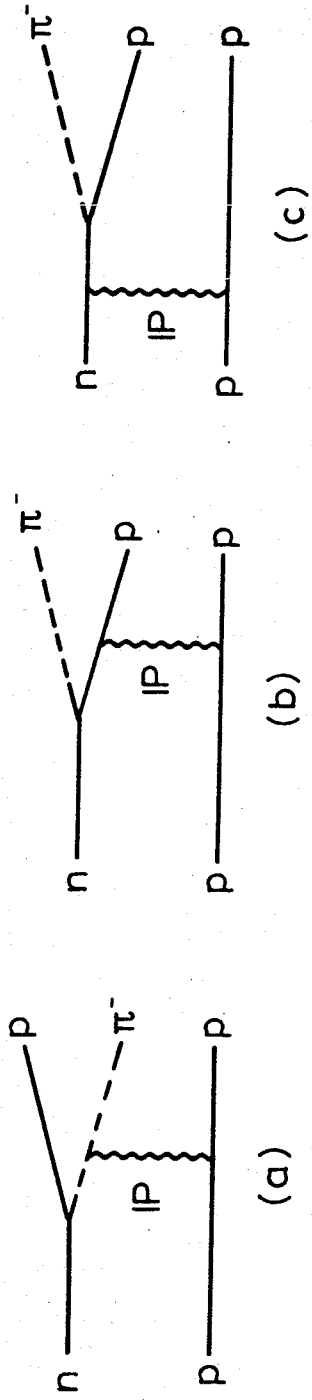


Fig. 10

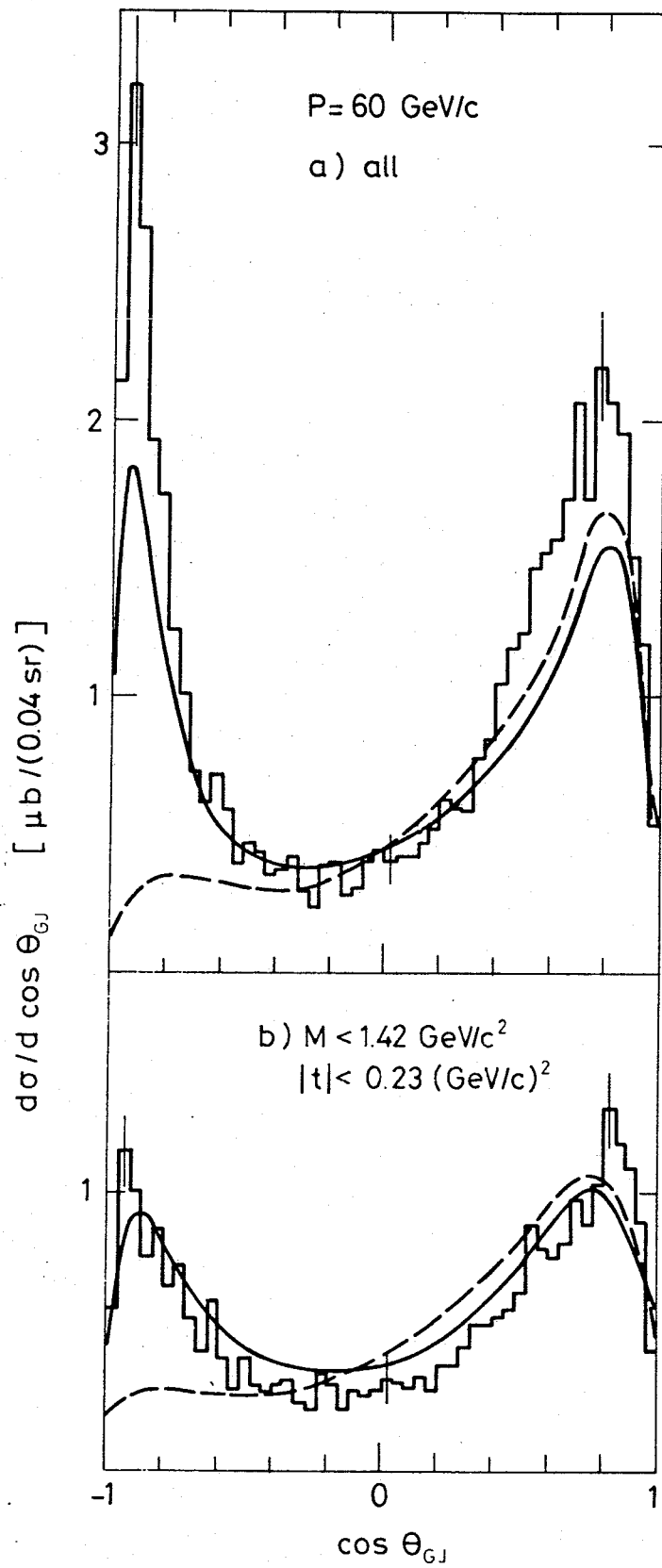


Fig. 11

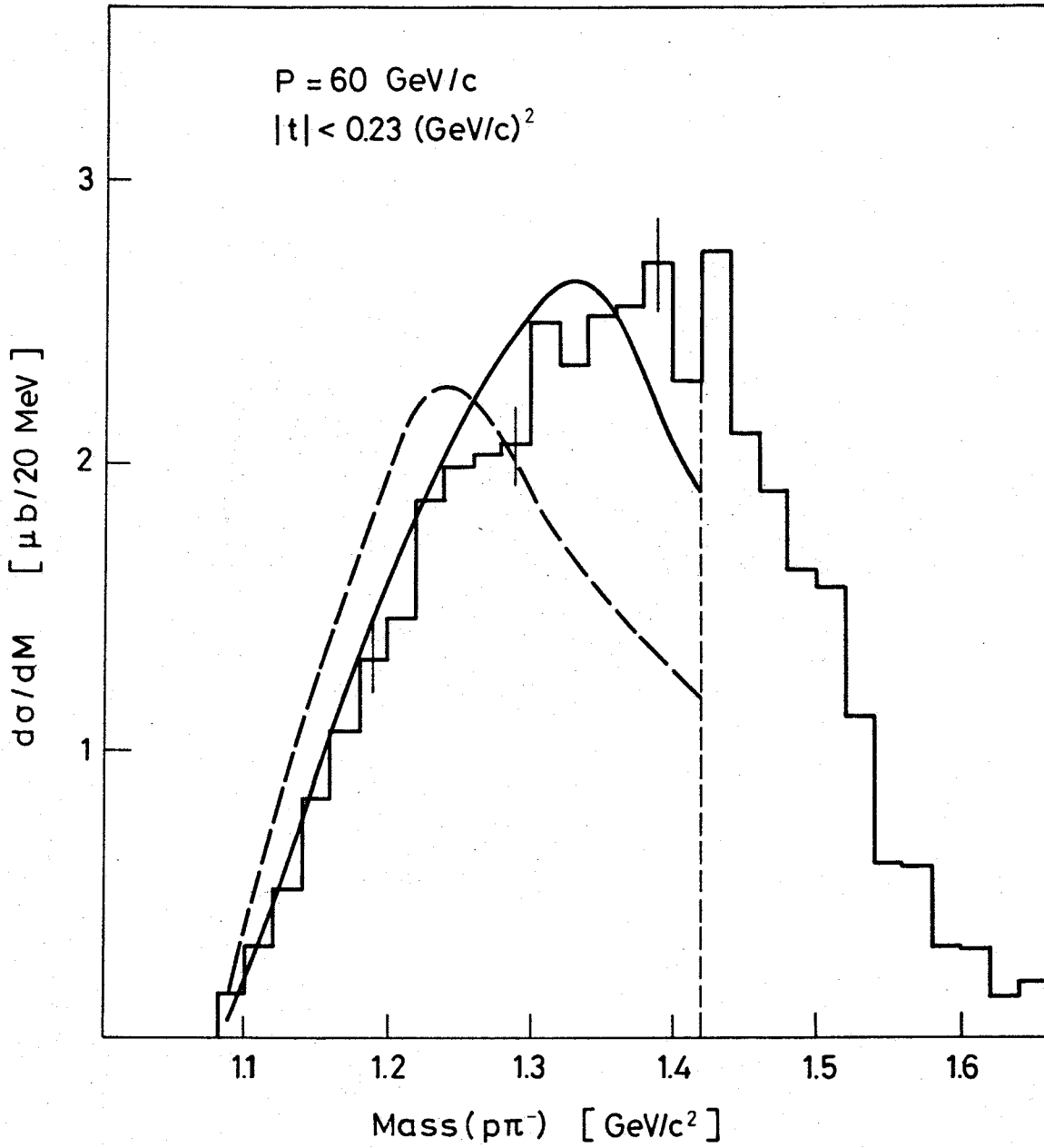


Fig. 12

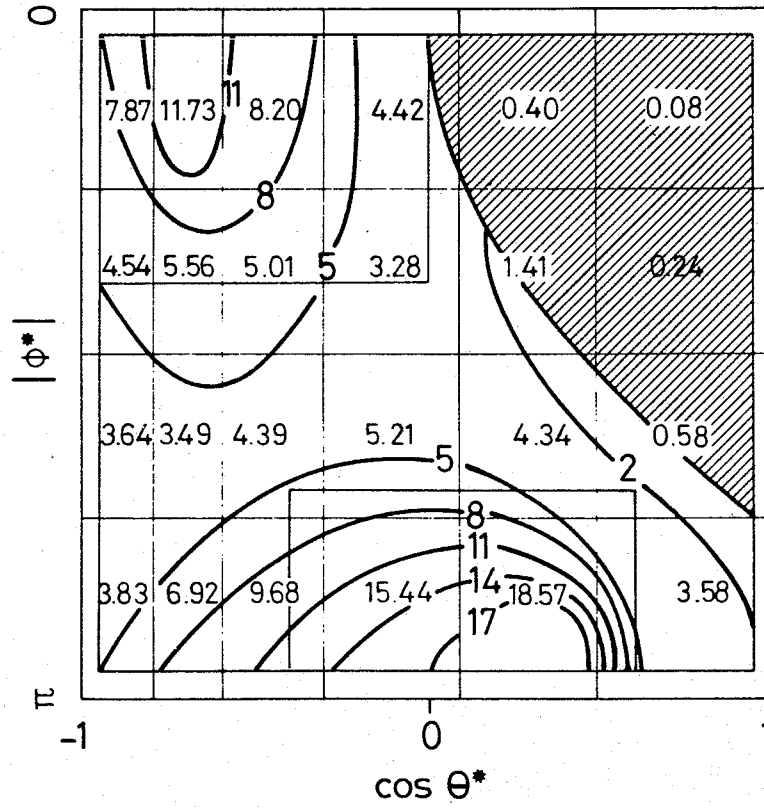


Fig. 13

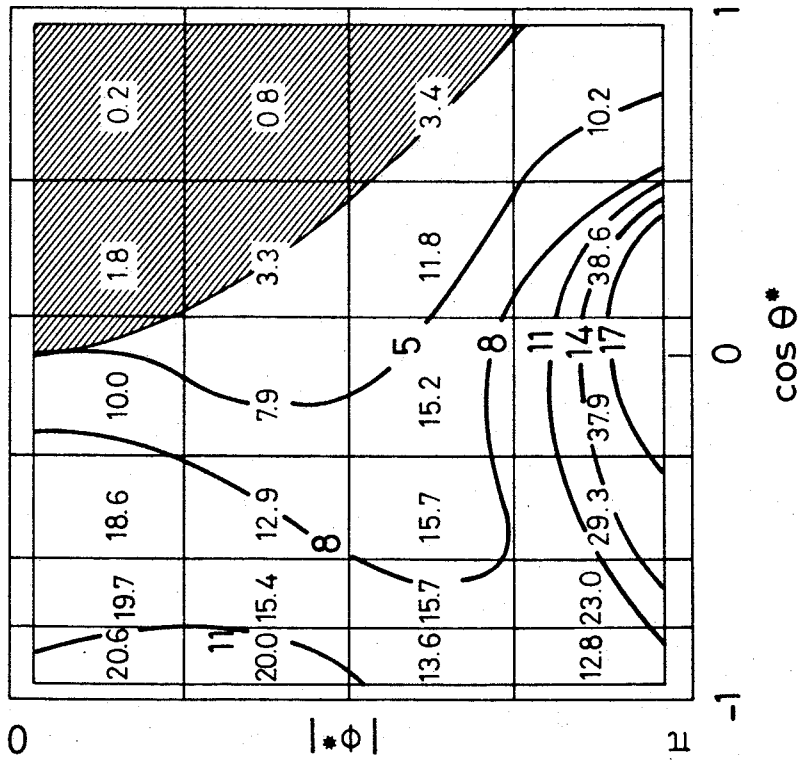
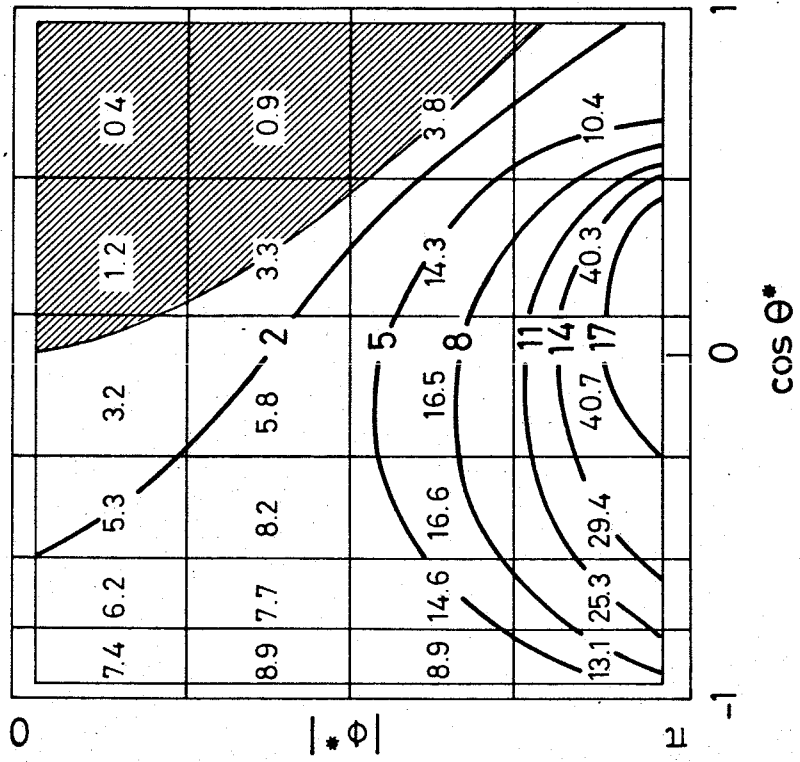


Fig. 14

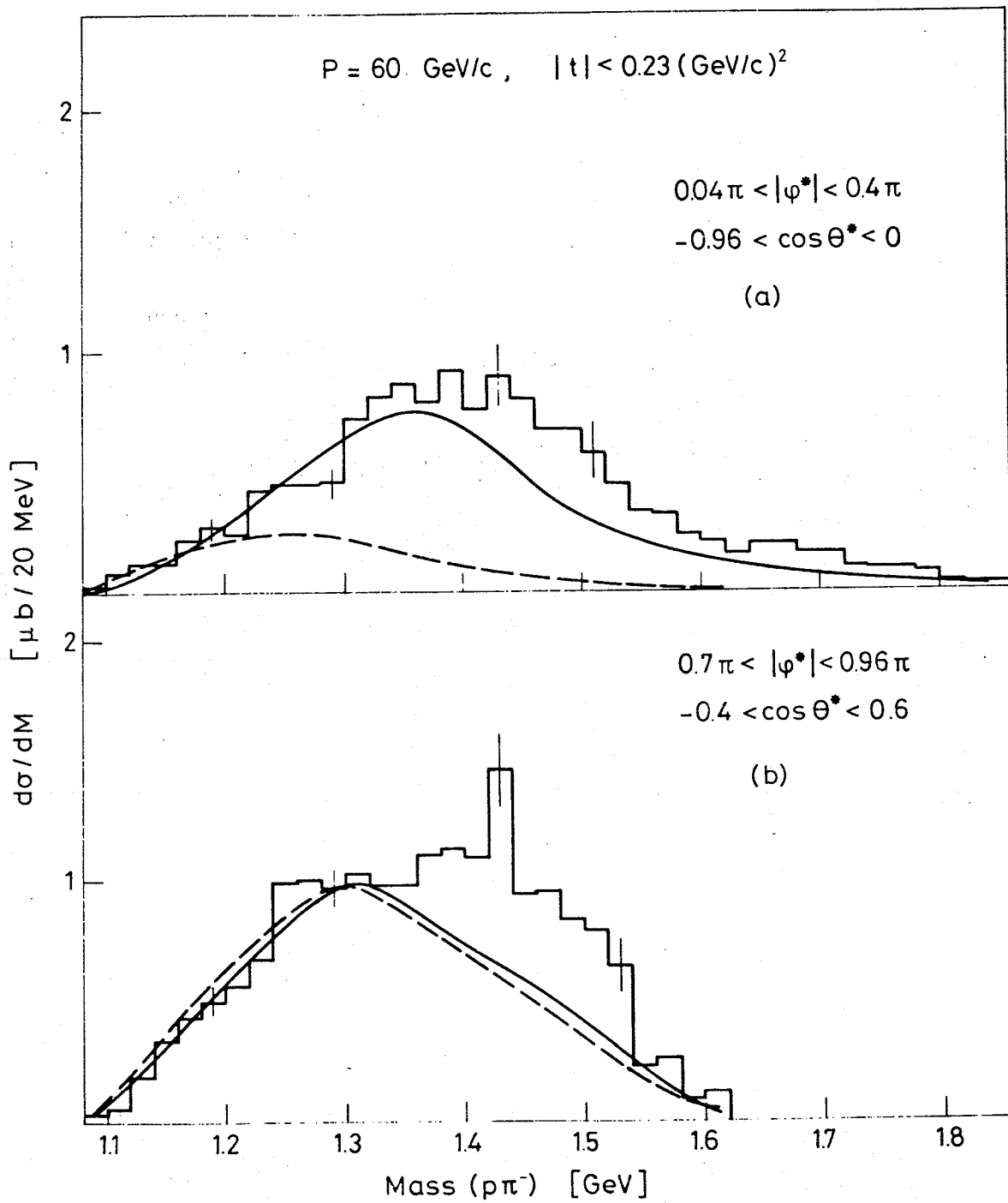


Fig. 15

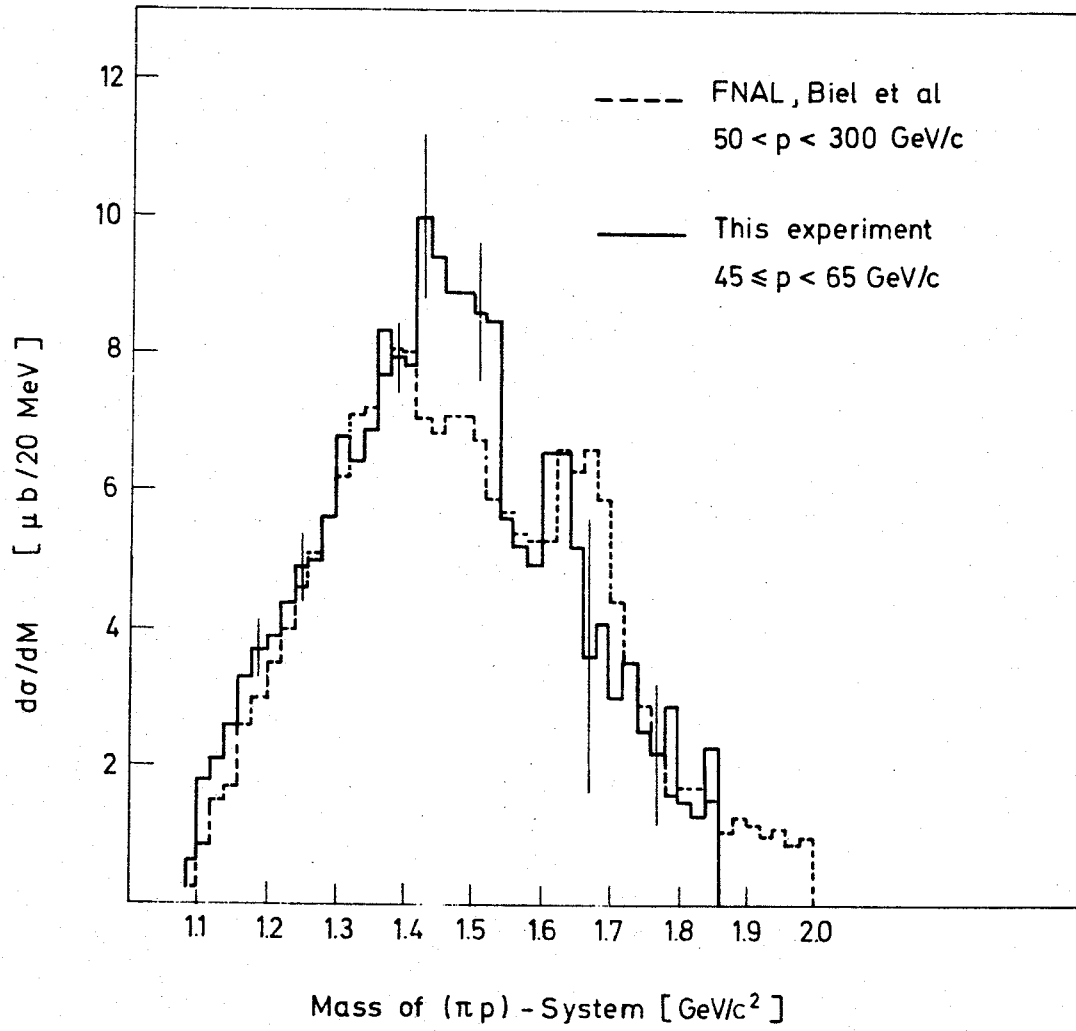


Fig. 16

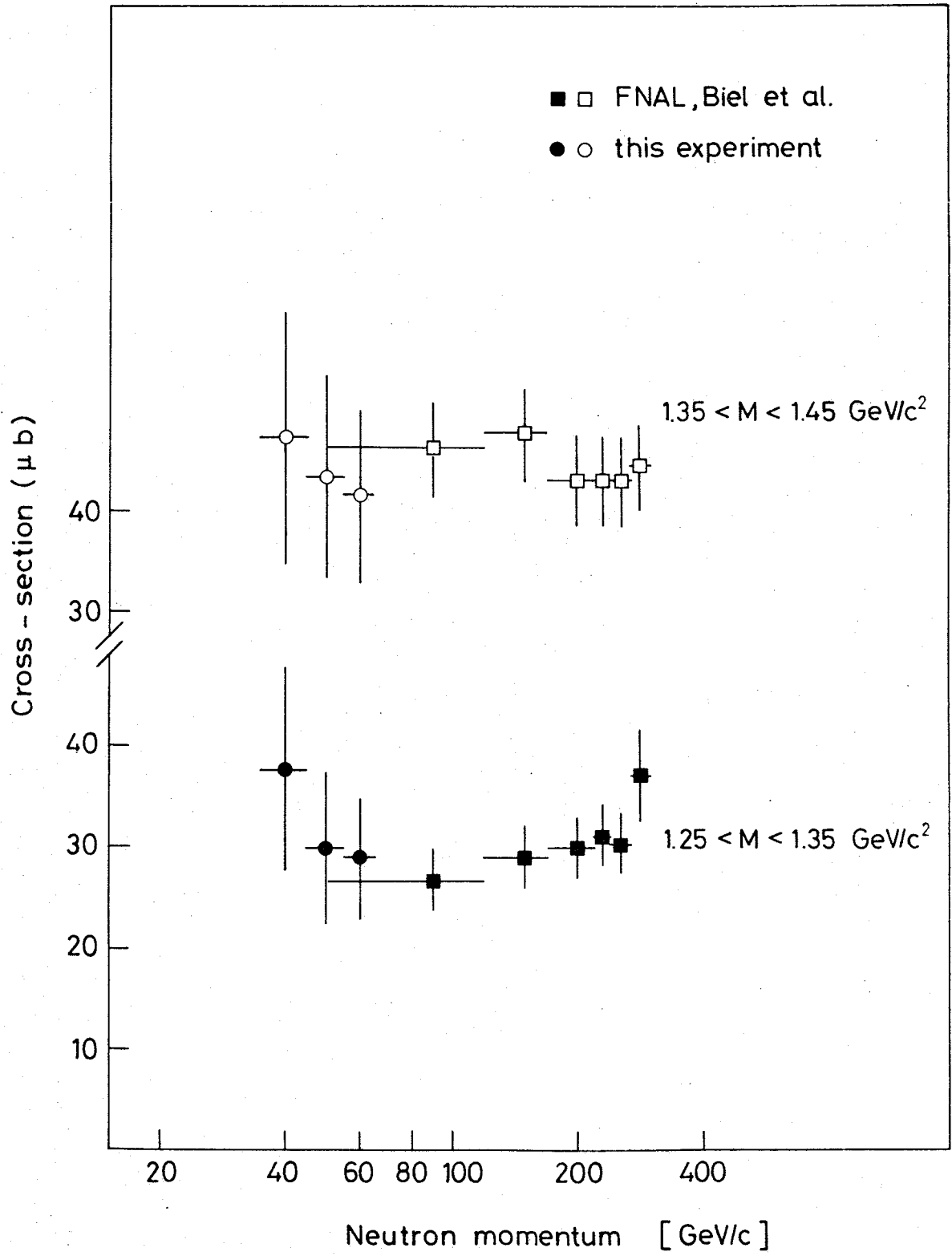


Fig. 17

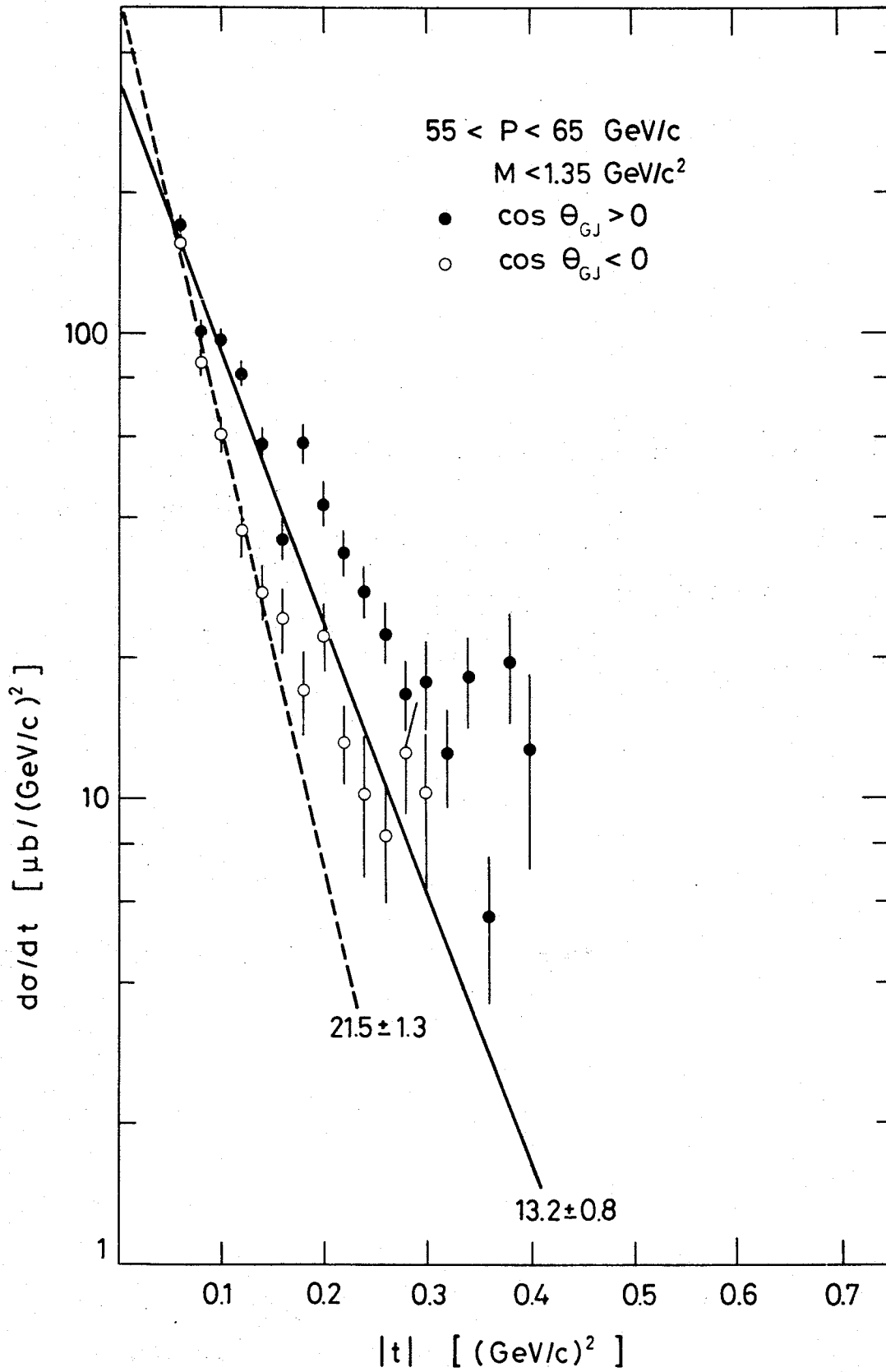


Fig. 18

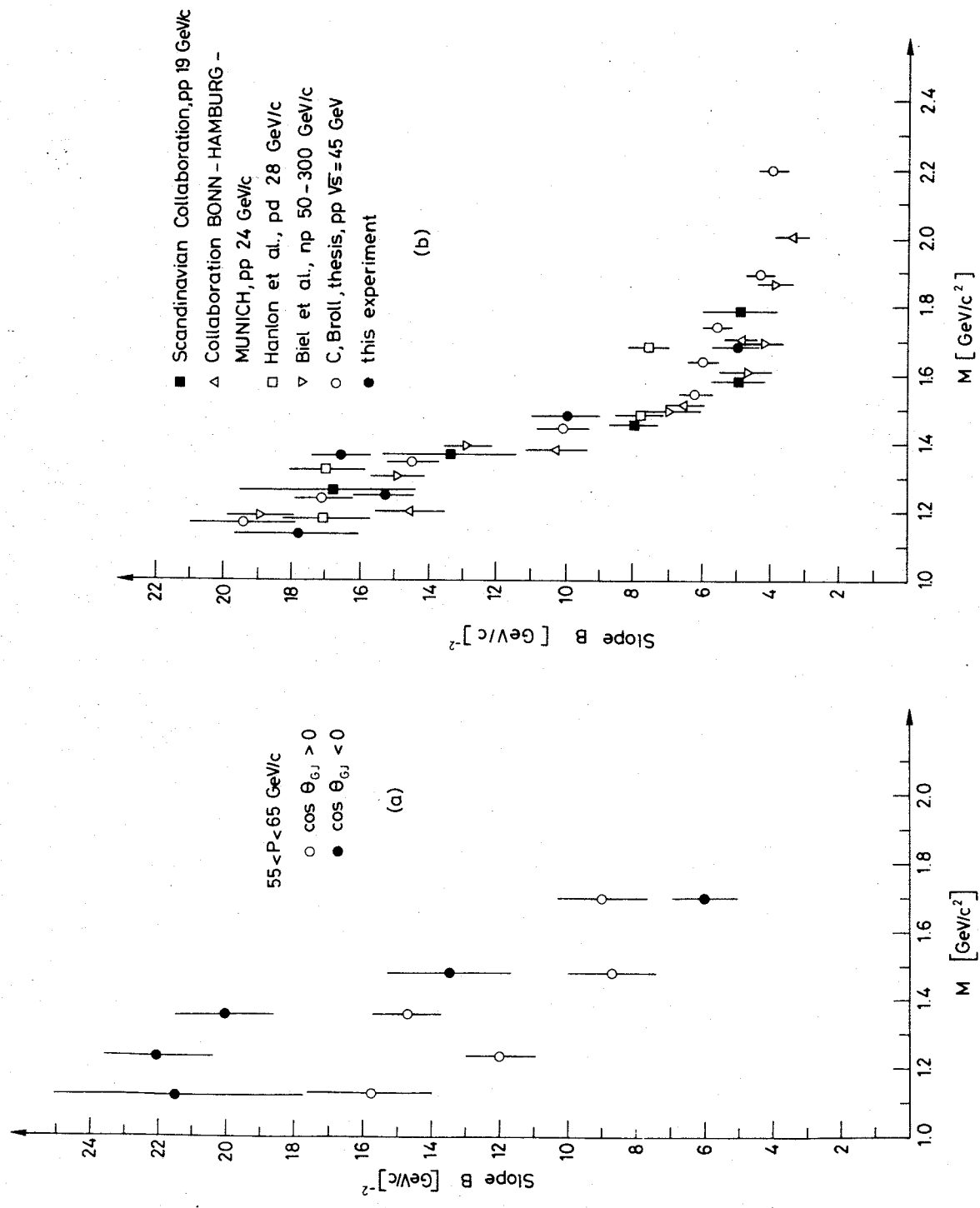


Fig. 19

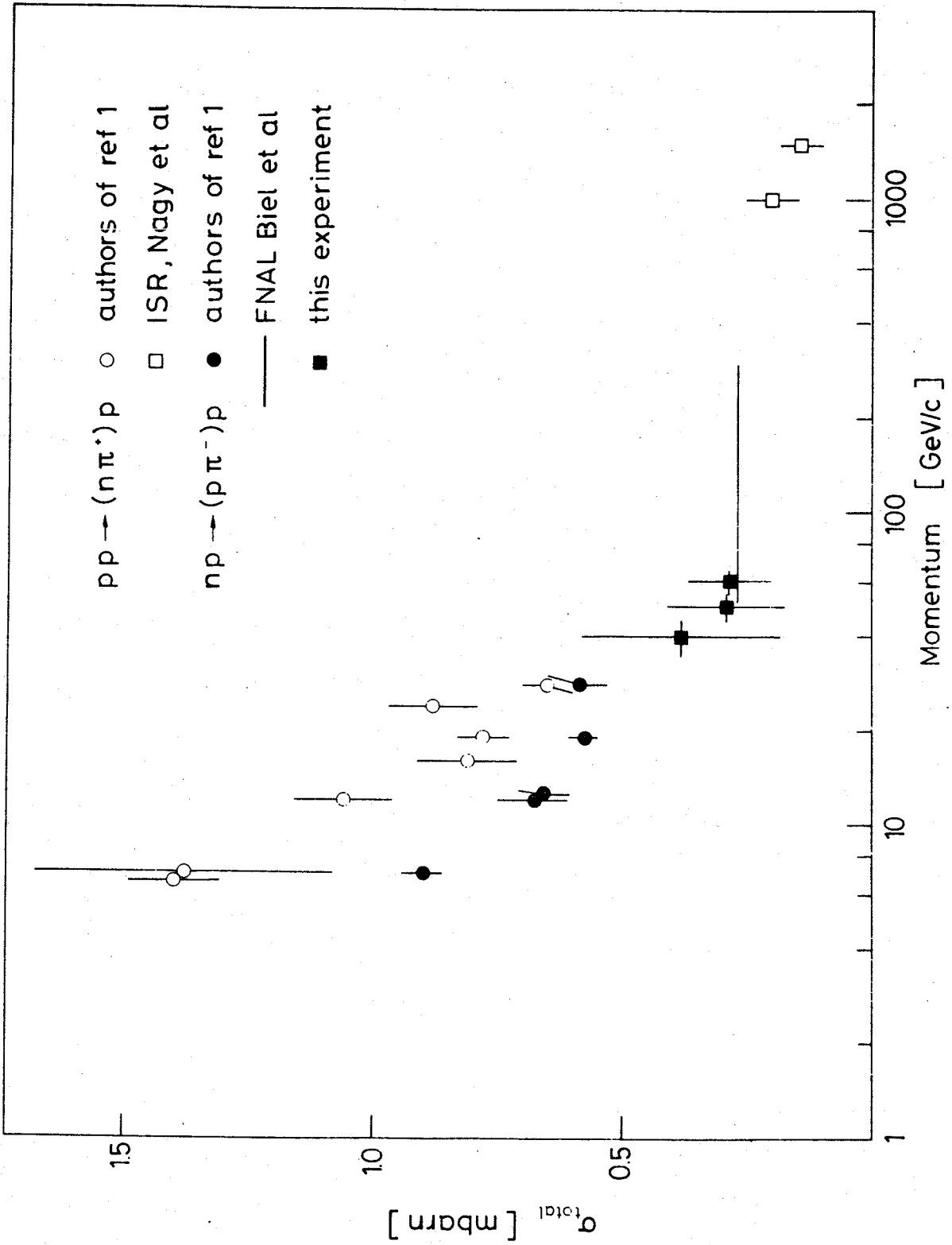


Fig. 20

ADDENDUM I

to

DIFFRACTION DISSOCIATION OF NEUTRONS INTO $(p\pi^-)$ ON PROTONS
IN THE MOMENTUM RANGE 35 TO 65 GeV/c

by

A. Babaev et al.,

ITEP, Moscow, IEKP, Karlsruhe and CERN, Geneva

In the tables are given the differential cross-sections $d\sigma/(dp, dM, dt, d\Omega)$ in $\mu\text{b}/(\text{GeV}^4/c^5\text{sr})$ for the reaction $n + p \rightarrow (p + \pi^-) + p$.

Geneva - June 1976

DIFFERENTIAL CROSS SECTION OF $\mu^+\mu^-\rightarrow(\mu^+\pi^-\mu^+\pi^+)$ REACTION FOR THE MOMENTUM RANGE 35 \pm 45 GEV/C,
COS THETA* INTERVAL -0.94 \pm -0.89 (IN MICROBARN/(GEV**4/C**5*STERAD))

P* GEV: 1.08+1.12 1.12+1.18 1.16+1.24 1.24+1.30 1.30+1.36 1.36+1.42 1.42+1.48 1.48+1.54 1.54+1.62 1.62+1.70 1.70+1.78 1.78+1.86
C**2

0*/3.14
.04+26 0.0+ 0.0 14.4* 7.4 38.2*28.4 22.9* 8.9 42.9*17.3 47.1*19.1 17.3*17.6 -0.0* 0.0 24.8*20.2 -0.0* 0.0 -0.0* 0.0 -0.0* 0.0
.26+50 0.0* 0.0 26.2*14.3 23.6*11.3 29.0*11.7 65.9*34.6 -0.0* 0.0 -0.0* 0.0 -0.0* 0.0 -0.0* 0.0 -0.0* 0.0 -0.0* 0.0 -0.0* 0.0
.50+74 0.0* 0.0 3.8* 3.9 4.4* 2.7 21.4*10.2 3.0* 0.0 -0.0* 0.0 -0.0* 0.0 -0.0* 0.0 -0.0* 0.0 -0.0* 0.0 -0.0* 0.0 -0.0* 0.0
.74+96 -0.0* 0.0 2.2* 1.6 14.3* 4.0 30.4*14.9 -0.0* 0.0 -0.0* 0.0 -0.0* 0.0 -0.0* 0.0 -0.0* 0.0 -0.0* 0.0 -0.0* 0.0 -0.0* 0.0 -0.0* 0.0

-T INTERVAL: 0.05 \pm 0.10 (GEV/C)**2

0*/3.14
.04+26 4.5* 5.0 16.1*11.7 6.1* 4.1 3.0* 1.6 15.0* 7.4 29.5*12.8 13.9* 7.7 28.7*23.4 -0.0* 0.0 -0.0* 0.0 -0.0* 0.0 -0.0* 0.0
.26+50 0.0* 0.0 0.0* 0.0 3.7* 3.1 2.7* 2.8 4.2* 4.5 -0.0* 0.0 -0.0* 0.0 -0.0* 0.0 -0.0* 0.0 -0.0* 0.0 -0.0* 0.0 -0.0* 0.0
.50+74 0.0* 0.0 0.0* 0.0 3.7* 3.8 2.7* 3.0 0.0* 0.0 -0.0* 0.0 -0.0* 0.0 -0.0* 0.0 -0.0* 0.0 -0.0* 0.0 -0.0* 0.0 -0.0* 0.0
.74+96 -0.0* 0.0 1.3* 0.9 1.9* 1.4 0.0* 0.0 0.0* 0.0 -0.0* 0.0 -0.0* 0.0 -0.0* 0.0 -0.0* 0.0 -0.0* 0.0 -0.0* 0.0 -0.0* 0.0

-T INTERVAL: 0.10 \pm 0.16 (GEV/C)**2

0*/3.14
.04+26 -0.0* 0.0 3.6* 2.6 9.8* 0.8 3.5* 2.2 7.9* 5.0 25.6*14.2 5.0* 5.3 -0.0* 0.0 0.0* 0.0 -0.0* 0.0 -0.0* 0.0
.26+50 -0.0* 0.0 0.0* 0.0 1.9* 1.9 0.0* 0.0 5.0* 5.3 0.0* 0.0 -0.0* 0.0 -0.0* 0.0 -0.0* 0.0 -0.0* 0.0 -0.0* 0.0 -0.0* 0.0
.50+74 -0.0* 0.0 0.0* 0.0 2.1* 2.2 4.1* 4.3 0.0* 0.0 -0.0* 0.0 -0.0* 0.0 -0.0* 0.0 -0.0* 0.0 -0.0* 0.0 -0.0* 0.0 -0.0* 0.0
.74+96 0.0* 0.0 0.0* 0.0 5.9* 6.8 10.6*12.2 3.0* 0.0 -0.0* 0.0 -0.0* 0.0 -0.0* 0.0 -0.0* 0.0 -0.0* 0.0 -0.0* 0.0 -0.0* 0.0

-T INTERVAL: 0.15 \pm 0.23 (GEV/C)**2

0*/3.14
.04+26 -0.0* 0.0 0.0* 0.0 1.5* 1.6 2.5* 2.6 3.0* 0.0 14.3*12.0 17.3*14.5 0.9* 0.0 -0.0* 0.0 -0.0* 0.0 -0.0* 0.0
.26+50 -0.0* 0.0 0.0* 0.0 0.0* 0.0 0.0* 0.0 0.0* 0.0 0.0* 0.0 0.0* 0.0 -0.0* 0.0 -0.0* 0.0 -0.0* 0.0 -0.0* 0.0
.50+74 -0.0* 0.0 1.2* 1.4 0.0* 0.0 0.0* 0.0 2.0* 2.2 0.0* 0.0 -0.0* 0.0 -0.0* 0.0 -0.0* 0.0 -0.0* 0.0 -0.0* 0.0
.74+96 -0.0* 0.0 0.0* 0.0 0.0* 0.0 4.5* 5.5 -0.0* 0.0 -0.0* 0.0 -0.0* 0.0 -0.0* 0.0 -0.0* 0.0 -0.0* 0.0 -0.0* 0.0

-T INTERVAL: 0.23 \pm 0.31 (GEV/C)**2

0*/3.14
.04+26 -0.0* 0.0 1.6* 1.8 0.6* 0.9 0.0* 0.0 0.0* 0.0 1.7* 1.9 3.0* 0.0 9.4*10.3 -0.0* 0.0 -0.0* 0.0 -0.0* 0.0
.26+50 -0.0* 0.0 2.4* 2.7 0.0* 0.0 0.0* 0.0 0.0* 0.0 7.2*10.1 3.0* 0.0 -0.0* 0.0 -0.0* 0.0 -0.0* 0.0 -0.0* 0.0
.50+74 -0.0* 0.0 1.1* 1.1 0.0* 0.0 0.0* 0.0 -0.0* 0.0 -0.0* 0.0 -0.0* 0.0 -0.0* 0.0 -0.0* 0.0 -0.0* 0.0 -0.0* 0.0
.74+96 -0.0* 0.0 3.0* 3.0 0.0* 0.0 3.3* 3.6 0.0* 0.0 -0.0* 0.0 -0.0* 0.0 -0.0* 0.0 -0.0* 0.0 -0.0* 0.0 -0.0* 0.0

-T INTERVAL: 0.31 \pm 0.40 (GEV/C)**2

0*/3.14
.04+26 -0.0* 0.0 4.4* 6.1 0.0* 0.0 0.0* 0.0 0.0* 0.0 3.0* 0.0 0.0* 0.0 -0.0* 0.0 -0.0* 0.0 -0.0* 0.0
.26+50 -0.0* 0.0 0.0* 0.0 3.4* 4.1 -0.0* 0.0 0.0* 0.0 0.0* 0.0 -0.0* 0.0 -0.0* 0.0 -0.0* 0.0 -0.0* 0.0
.50+74 -0.0* 0.0 0.0* 0.0 0.0* 0.0 0.0* 0.0 0.0* 0.0 -0.0* 0.0 -0.0* 0.0 -0.0* 0.0 -0.0* 0.0 -0.0* 0.0
.74+96 -0.0* 0.0 0.0* 0.0 0.0* 0.0 -0.0* 0.0 -0.0* 0.0 -0.0* 0.0 -0.0* 0.0 -0.0* 0.0 -0.0* 0.0 -0.0* 0.0

-T INTERVAL: 0.40 \pm 0.50 (GEV/C)**2

0*/3.14
.04+26 -0.0* 0.0 -0.0* 0.0 0.0* 0.0 0.0* 0.0 0.0* 0.0 -0.0* 0.0 -0.0* 0.0 -0.0* 0.0 -0.0* 0.0 -0.0* 0.0
.26+50 -0.0* 0.0 -0.0* 0.0 -0.0* 0.0 -0.0* 0.0 -0.0* 0.0 -0.0* 0.0 -0.0* 0.0 -0.0* 0.0 -0.0* 0.0 -0.0* 0.0
.50+74 -0.0* 0.0 -0.0* 0.0 -0.0* 0.0 -0.0* 0.0 -0.0* 0.0 -0.0* 0.0 -0.0* 0.0 -0.0* 0.0 -0.0* 0.0 -0.0* 0.0
.74+96 -0.0* 0.0 -0.0* 0.0 -0.0* 0.0 -0.0* 0.0 -0.0* 0.0 -0.0* 0.0 -0.0* 0.0 -0.0* 0.0 -0.0* 0.0 -0.0* 0.0

-T INTERVAL: 0.50 \pm 0.62 (GEV/C)**2

DIFFERENTIAL CROSS SECTION OF $N+p \rightarrow (p, \pi^-) + p$ REACTION FOR THE MOMENTUM RANGE 35 \pm 45 GEV/C ,

COS THETA* INTERVAL -0.80 \pm -0.60 (IN MICROBARN/(GEV**4/C**5*STERAD))

* GEV: 1.08+1.12 1.12+1.18 1.18+1.24 1.24+1.30 1.30+1.36 1.36+1.42 1.42+1.48 1.48+1.54 1.54+1.62 1.62+1.70 1.70+1.78 1.78+1.86 C**2

0*/3.14
.04+.26 0.0+ 0.0 17.4+ 7.4 26.5+10.2 17.5+ 7.6 69.7+19.5 71.5+23.3 94.2+39.1 56.4+23.8 8.8+ 6.6 -0.0+ 0.0 -0.0+ 0.0 -0.0+ 0.0 -0.0+ 0.0
.26+.50 2.6+ 2.9 5.7+ 3.3 37.6+11.4 61.7+26.6 41.2+24.0 32.3+29.5 21.5+14.6 -0.0+ 0.0 -0.0+ 0.0 -0.0+ 0.0 -0.0+ 0.0 -0.0+ 0.0
.50+.74 3.1+ 3.3 16.0+ 6.8 4.3+ 4.4 -0.0+ 0.0 -0.0+ 0.0 -0.0+ 0.0 -0.0+ 0.0 -0.0+ 0.0 -0.0+ 0.0 -0.0+ 0.0
.74+.96 5.0+ 3.9 10.8+ 5.1 15.4+ 6.2 37.3+15.3 9.0+ 0.0 -0.0+ 0.0 -0.0+ 0.0 -0.0+ 0.0 -0.0+ 0.0 -0.0+ 0.0 -0.0+ 0.0

-T INTERVAL: 0.05 \pm 0.10 (GEV/C)**2

0*/3.14
.04+.26 0.0+ 0.0 1.5+ 1.5 16.7+ 7.0 14.7+ 6.1 45.2+22.3 4.3+ 2.6 19.0+17.2 34.0+12.2 8.2+ 8.6 -0.0+ 0.0 -0.0+ 0.0 -0.0+ 0.0
.26+.50 0.0+ 0.0 0.0+ 0.0 1.3+ 1.4 10.1+ 7.5 3.9+ 4.1 -0.0+ 0.0 -0.0+ 0.0 -0.0+ 0.0 -0.0+ 0.0 -0.0+ 0.0 -0.0+ 0.0
.50+.74 0.0+ 0.0 4.6+ 3.4 1.3+ 1.7 12.4+ 7.6 0.0+ 0.0 -0.0+ 0.0 -0.0+ 0.0 -0.0+ 0.0 -0.0+ 0.0 -0.0+ 0.0 -0.0+ 0.0
.74+.96 0.0+ 0.0 11.4+ 5.3 10.2+ 5.5 12.0+ 6.3 14.4+ 9.0 -0.0+ 0.0 -0.0+ 0.0 -0.0+ 0.0 -0.0+ 0.0 -0.0+ 0.0 -0.0+ 0.0

-T INTERVAL: 0.10 \pm 0.16 (GEV/C)**2

0*/3.14
.04+.26 0.0+ 0.0 0.0+ 0.0 9.9+ 4.4 11.2+ 5.0 4.3+ 4.5 7.4+ 7.7 28.1+18.0 10.0+ 7.5 -0.0+ 0.0 -0.0+ 0.0 -0.0+ 0.0 -0.0+ 0.0
.26+.50 0.0+ 0.0 0.0+ 0.0 2.7+ 2.9 2.4+ 2.6 4.4+ 4.7 0.0+ 0.0 -0.0+ 0.0 -0.0+ 0.0 -0.0+ 0.0 -0.0+ 0.0 -0.0+ 0.0
.50+.74 0.0+ 0.0 0.0+ 0.0 0.0+ 0.0 0.0+ 0.0 0.0+ 0.0 -0.0+ 0.0 -0.0+ 0.0 -0.0+ 0.0 -0.0+ 0.0 -0.0+ 0.0 -0.0+ 0.0
.74+.96 0.0+ 0.0 0.0+ 0.0 7.7+ 10.9+ 5.4 5.9+ 6.2 -0.0+ 0.0 -0.0+ 0.0 -0.0+ 0.0 -0.0+ 0.0 -0.0+ 0.0 -0.0+ 0.0 -0.0+ 0.0

-T INTERVAL: 0.16 \pm 0.23 (GEV/C)**2

0*/3.14
.04+.26 -0.0+ 0.0 3.6+ 3.3 7.0+ 0.0 3.1+ 2.9 8.1+ 4.4 4.6+ 4.9 3.1+ 3.4 -0.0+ 0.0 -0.0+ 0.0 -0.0+ 0.0 -0.0+ 0.0
.26+.50 0.0+ 0.0 0.5+ 0.6 6.7+ 7.2 0.0+ 0.0 0.0+ 0.0 0.0+ 0.0 -0.0+ 0.0 -0.0+ 0.0 -0.0+ 0.0 -0.0+ 0.0 -0.0+ 0.0
.50+.74 -0.0+ 0.0 0.7+ 0.8 0.6+ 0.6 0.0+ 0.0 0.0+ 0.0 -0.0+ 0.0 -0.0+ 0.0 -0.0+ 0.0 -0.0+ 0.0 -0.0+ 0.0 -0.0+ 0.0
.74+.96 9.8+10.0 4.8+ 4.2 0.0+ 0.0 12.8+ 8.4 5.2+ 4.1 -0.0+ 0.0 -0.0+ 0.0 -0.0+ 0.0 -0.0+ 0.0 -0.0+ 0.0 -0.0+ 0.0

-T INTERVAL: 0.23 \pm 0.31 (GEV/C)**2

0*/3.14
.04+.26 -0.0+ 0.0 0.0+ 0.0 17.3+10.8 19.4+12.5 15.3+10.4 -0.0+ 0.0 -0.0+ 0.0 -0.0+ 0.0 -0.0+ 0.0 -0.0+ 0.0 -0.0+ 0.0
.26+.50 0.0+ 0.0 0.0+ 0.0 0.0+ 0.0 8.9+ 6.9 0.0+ 0.0 0.0+ 0.0 0.0+ 0.0 0.0+ 0.0 -0.0+ 0.0 -0.0+ 0.0 -0.0+ 0.0
.50+.74 0.0+ 0.0 0.0+ 0.0 1.5+ 1.7 -0.0+ 0.0 -0.0+ 0.0 -0.0+ 0.0 -0.0+ 0.0 -0.0+ 0.0 -0.0+ 0.0 -0.0+ 0.0
.74+.96 6.0+ 0.0 1.0+ 0.0 1.1+ 1.3+ 9.1 0.0+ 0.0 2.3+ 2.5 5.0+ 4.0 -0.0+ 0.0 -0.0+ 0.0 -0.0+ 0.0 -0.0+ 0.0

-T INTERVAL: 0.31 \pm 0.40 (GEV/C)**2

0*/3.14
.04+.26 -0.0+ 0.0 -0.0+ 0.0 0.0+ 0.0 3.0+ 5.3 0.0+ 0.0 -0.0+ 0.0 -0.0+ 0.0 -0.0+ 0.0 -0.0+ 0.0 -0.0+ 0.0
.26+.50 -0.0+ 0.0 -0.0+ 0.0 3.2+ 4.5 0.0+ 0.0 6.3+ 6.9 0.0+ 0.0 -0.0+ 0.0 -0.0+ 0.0 -0.0+ 0.0 -0.0+ 0.0
.50+.74 -0.0+ 0.0 0.0+ 0.0 0.0+ 0.0 -0.0+ 0.0 -0.0+ 0.0 -0.0+ 0.0 -0.0+ 0.0 -0.0+ 0.0 -0.0+ 0.0 -0.0+ 0.0
.74+.96 0.0+ 0.0 -0.0+ 0.0 0.0+ 0.0 2.0+ 2.2 0.0+ 0.0 -0.0+ 0.0 -0.0+ 0.0 -0.0+ 0.0 -0.0+ 0.0 -0.0+ 0.0

-T INTERVAL: 0.40 \pm 0.50 (GEV/C)**2

0*/3.14
.04+.26 -0.0+ 0.0 -0.0+ 0.0 0.0+ 0.0 0.0+ 0.0 -0.0+ 0.0 -0.0+ 0.0 -0.0+ 0.0 -0.0+ 0.0 -0.0+ 0.0 -0.0+ 0.0
.26+.50 -0.0+ 0.0 -0.0+ 0.0 0.0+ 0.0 0.0+ 0.0 0.0+ 0.0 -0.0+ 0.0 -0.0+ 0.0 -0.0+ 0.0 -0.0+ 0.0 -0.0+ 0.0
.50+.74 -0.0+ 0.0 -0.0+ 0.0 -0.0+ 0.0 -0.0+ 0.0 -0.0+ 0.0 -0.0+ 0.0 -0.0+ 0.0 -0.0+ 0.0 -0.0+ 0.0 -0.0+ 0.0
.74+.96 -0.0+ 0.0 0.0+ 0.0 0.0+ 0.0 0.0+ 0.0 -0.0+ 0.0 -0.0+ 0.0 -0.0+ 0.0 -0.0+ 0.0 -0.0+ 0.0 -0.0+ 0.0

-T INTERVAL: 0.50 \pm 0.62 (GEV/C)**2

DIFFERENTIAL CROSS SECTION OF N+P->(P+PI-)+P REACTION FOR THE MOMENTUM RANGE 35 ± 45 GEV/C ,

COS THETA INTERVAL -0.67 ± -0.39 (IN MICROBARN/(GEV**4/C**5*STERAD))

M* GEV: 1.08±1.12 1.12±1.19 1.18±1.24 1.24±1.30 1.30±1.36 1.36±1.42 1.42±1.48 1.48±1.54 1.54±1.62 1.62±1.70 1.70±1.78 1.78±1.86

C**2

φ*/3.14
 .04±.26
 .26±.50
 .50±.74
 .74±.96
 9.2± 5.9 6.6± 3.5 19.7± 6.2 10.9± 6.6 9.5± 5.3 -0.0± 0.0 -0.0± 0.0 -0.0± 0.0 -0.0± 0.0 -0.0± 0.0 -0.0± 0.0
 3.7± 4.0 9.4± 4.5 16.1± 6.1 29.9±12.9 6.7± 6.9 -0.0± 0.0 -0.0± 0.0 -0.0± 0.0 -0.0± 0.0 -0.0± 0.0 -0.0± 0.0
 5.1± 2.3 17.2± 5.9 16.0± 5.2 34.2±15.1 0.0± 0.0 -0.0± 0.0 -0.0± 0.0 -0.0± 0.0 -0.0± 0.0 -0.0± 0.0 -0.0± 0.0
 .74±.96 8.1± 5.2 22.3± 7.4 24.7± 5.6 65.2±15.4 63.1±22.6 -0.0± 0.0 -0.0± 0.0 -0.0± 0.0 -0.0± 0.0 -0.0± 0.0 -0.0± 0.0

-T INTERVAL: 0.05 ± 0.10 (GEV/C)**2

φ*/3.14
 .04±.26
 .26±.50
 .50±.74
 .74±.96
 0.0± 0.0 4.0± 2.1 6.4± 2.4 15.7± 6.9 37.3±13.6 30.4±14.4 0.0± 0.0 -0.0± 0.0 -0.0± 0.0 -0.0± 0.0 -0.0± 0.0
 0.0± 0.0 3.3± 2.8 7.3± 5.7 10.2± 5.0 0.0± 0.0 -0.0± 0.0 -0.0± 0.0 -0.0± 0.0 -0.0± 0.0 -0.0± 0.0 -0.0± 0.0
 0.0± 0.0 3.0± 2.2 4.9± 3.0 16.1± 9.8 -0.0± 0.0 -0.0± 0.0 -0.0± 0.0 -0.0± 0.0 -0.0± 0.0 -0.0± 0.0 -0.0± 0.0
 4.8± 4.4 9.2± 3.4 14.6± 4.2 17.5± 5.3 7.6± 3.6 -0.0± 0.0 -0.0± 0.0 -0.0± 0.0 -0.0± 0.0 -0.0± 0.0 -0.0± 0.0

-T INTERVAL: 0.16 ± 0.23 (GEV/C)**2

φ*/3.14
 .04±.26
 .26±.50
 .50±.74
 .74±.96
 0.0± 0.0 1.8± 1.5 13.8± 5.7 1.9± 1.9 30.5±11.8 37.4±14.3 31.9±14.0 -0.0± 0.0 -0.0± 0.0 -0.0± 0.0 -0.0± 0.0
 0.0± 0.0 1.1± 1.2 4.3± 5.3 16.5±13.5 2.1± 2.1 -0.0± 0.0 -0.0± 0.0 -0.0± 0.0 -0.0± 0.0 -0.0± 0.0 -0.0± 0.0
 0.0± 0.0 0.0± 0.0 7.1± 5.2 3.3± 3.8 -0.0± 0.0 -0.0± 0.0 -0.0± 0.0 -0.0± 0.0 -0.0± 0.0 -0.0± 0.0 -0.0± 0.0
 3.2± 3.6 3.7± 2.8 3.6± 2.2 20.9± 6.8 14.2± 7.2 -0.0± 0.0 -0.0± 0.0 -0.0± 0.0 -0.0± 0.0 -0.0± 0.0 -0.0± 0.0

-T INTERVAL: 0.23 ± 0.31 (GEV/C)**2

φ*/3.14
 .04±.26
 .26±.50
 .50±.74
 .74±.96
 0.0± 0.0 0.0± 0.0 1.6± 1.2 1.7± 1.7 6.0± 5.1 0.0± 0.0 3.7± 4.3 -0.0± 0.0 -0.0± 0.0 -0.0± 0.0 -0.0± 0.0
 -0.0± 0.0 1.4± 1.2 3.9± 4.5 0.0± 0.0 0.0± 0.0 -0.0± 0.0 -0.0± 0.0 -0.0± 0.0 -0.0± 0.0 -0.0± 0.0 -0.0± 0.0
 0.0± 0.0 0.0± 0.0 9.0± 0.0 0.0± 0.0 -0.0± 0.0 -0.0± 0.0 -0.0± 0.0 -0.0± 0.0 -0.0± 0.0 -0.0± 0.0 -0.0± 0.0
 7.4±.96 0.0± 0.0 2.6± 2.5 7.4± 3.5 4.8± 2.9 0.0± 0.0 0.0± 0.0 -0.0± 0.0 -0.0± 0.0 -0.0± 0.0 -0.0± 0.0

-T INTERVAL: 0.31 ± 0.40 (GEV/C)**2

φ*/3.14
 .04±.26
 .26±.50
 .50±.74
 .74±.96
 0.0± 0.0 0.0± 0.0 1.3± 1.0 4.4± 2.4 1.1± 1.2 0.0± 0.0 -0.0± 0.0 -0.0± 0.0 -0.0± 0.0 -0.0± 0.0
 -0.0± 0.0 0.0± 0.0 0.0± 0.0 1.7± 2.0 0.0± 0.0 0.0± 0.0 -0.0± 0.0 -0.0± 0.0 -0.0± 0.0 -0.0± 0.0 -0.0± 0.0
 0.0± 0.0 0.0± 0.0 0.0± 0.0 0.0± 0.0 4.6± 5.6 -0.0± 0.0 -0.0± 0.0 -0.0± 0.0 -0.0± 0.0 -0.0± 0.0 -0.0± 0.0
 13.8±15.8 3.2± 2.9 0.0± 0.0 3.5± 2.6 0.0± 0.0 -0.0± 0.0 -0.0± 0.0 -0.0± 0.0 -0.0± 0.0 -0.0± 0.0 -0.0± 0.0

-T INTERVAL: 0.40 ± 0.50 (GEV/C)**2

φ*/3.14
 .04±.26
 .26±.50
 .50±.74
 .74±.96
 0.0± 0.0 -0.0± 0.0 9.7± 0.7 0.0± 0.0 -0.0± 0.0 -0.0± 0.0 -0.0± 0.0 -0.0± 0.0 -0.0± 0.0 -0.0± 0.0
 -0.0± 0.0 0.0± 0.0 0.0± 0.0 0.0± 0.0 0.0± 0.0 0.0± 0.0 -0.0± 0.0 -0.0± 0.0 -0.0± 0.0 -0.0± 0.0 -0.0± 0.0
 -0.0± 0.0 0.0± 0.0 2.7± 2.8 0.0± 0.0 -0.0± 0.0 -0.0± 0.0 -0.0± 0.0 -0.0± 0.0 -0.0± 0.0 -0.0± 0.0 -0.0± 0.0
 13.8±15.8 9.0± 0.0 0.0± 0.0 0.0± 0.0 0.0± 0.0 -0.0± 0.0 -0.0± 0.0 -0.0± 0.0 -0.0± 0.0 -0.0± 0.0 -0.0± 0.0

-T INTERVAL: 0.50 ± 0.62 (GEV/C)**2

φ*/3.14
 .04±.26
 .26±.50
 .50±.74
 .74±.96
 0.0± 0.0 0.0± 0.0 9.0± 0.0 -0.0± 0.0 0.0± 0.0 0.0± 0.0 -0.0± 0.0 -0.0± 0.0 -0.0± 0.0 -0.0± 0.0
 -0.0± 0.0 0.0± 0.0 0.0± 0.0 -0.0± 0.0 -0.0± 0.0 -0.0± 0.0 -0.0± 0.0 -0.0± 0.0 -0.0± 0.0 -0.0± 0.0 -0.0± 0.0
 -0.0± 0.0 0.0± 0.0 0.0± 0.0 -0.0± 0.0 -0.0± 0.0 -0.0± 0.0 -0.0± 0.0 -0.0± 0.0 -0.0± 0.0 -0.0± 0.0 -0.0± 0.0
 -0.0± 0.0 -0.0± 0.0 -0.0± 0.0 0.0± 0.0 0.0± 0.0 -0.0± 0.0 -0.0± 0.0 -0.0± 0.0 -0.0± 0.0 -0.0± 0.0 -0.0± 0.0

DIFFERENTIAL CROSS SECTION OF N+P->(P+PI-)P REACTION FOR THE MOMENTUM RANGE 35 ± 45 GEV/C ,

COS THETA* INTERVAL -0.30 + 0.10 (IN MICROBARN/(SEV**4/C**5*STERAD))

* GEV: 1.08±1.12 1.12±1.18 1.18±1.24 1.24±1.30 1.30±1.36 1.36±1.42 1.42±1.48 1.48±1.54 1.54±1.62 1.62±1.70 1.70±1.78 1.78±1.86 C**2

0*/3.14
 .04±.26 1.0± 1.0 5.6± 3.4 -0.0± 0.0 -0.0± 0.0 -0.0± 0.0 -0.0± 0.0 -0.0± 0.0 -0.0± 0.0 -0.0± 0.0 -0.0± 0.0 -0.0± 0.0
 .26±.50 5.8± 3.3 5.3± 2.9 17.3±10.1 0.0± 0.0 -0.0± 0.0 -0.0± 0.0 -0.0± 0.0 -0.0± 0.0 -0.0± 0.0 -0.0± 0.0 -0.0± 0.0 -0.0± 0.0
 .50±.74 3.9± 3.0 14.1± 4.7 19.8± 6.5 -0.0± 0.0 -0.0± 0.0 -0.0± 0.0 -0.0± 0.0 -0.0± 0.0 -0.0± 0.0 -0.0± 0.0 -0.0± 0.0 -0.0± 0.0
 .74±.96 14.2± 5.1 29.8± 6.2 67.8±10.5 53.3± 8.8 59.3±14.0 -0.0± 0.0 -0.0± 0.0 -0.0± 0.0 -0.0± 0.0 -0.0± 0.0 -0.0± 0.0 -0.0± 0.0

0*/3.14
 .04±.26 4.8± 3.7 4.1± 2.2 11.1± 7.6 -0.0± 0.0 -0.0± 0.0 -0.0± 0.0 -0.0± 0.0 -0.0± 0.0 -0.0± 0.0 -0.0± 0.0 -0.0± 0.0 -0.0± 0.0
 .26±.50 2.6± 2.1 1.8± 1.3 2.5± 2.7 0.0± 0.0 -0.0± 0.0 -0.0± 0.0 -0.0± 0.0 -0.0± 0.0 -0.0± 0.0 -0.0± 0.0 -0.0± 0.0
 .50±.74 9.7± 0.7 2.3± 1.7 2.6± 1.9 19.7±10.0 -0.0± 0.0 -0.0± 0.0 -0.0± 0.0 -0.0± 0.0 -0.0± 0.0 -0.0± 0.0 -0.0± 0.0
 .74±.96 3.8± 1.7 15.5± 3.6 21.1± 4.2 39.3± 7.7 27.0± 6.8 23.1± 9.9 -0.0± 0.0 -0.0± 0.0 -0.0± 0.0 -0.0± 0.0 -0.0± 0.0

0*/3.14
 .04±.26 9.0± 0.0 1.9± 1.4 1.1± 1.1 0.0± 0.0 3.2± 3.5 -0.0± 0.0 -0.0± 0.0 -0.0± 0.0 -0.0± 0.0 -0.0± 0.0 -0.0± 0.0
 .26±.50 0.0± 0.0 0.8± 0.9 3.1± 3.5 4.5± 3.5 -0.0± 0.0 -0.0± 0.0 -0.0± 0.0 -0.0± 0.0 -0.0± 0.0 -0.0± 0.0
 .50±.74 0.0± 0.0 0.0± 0.0 5.5± 3.7 3.6± 3.8 -0.0± 0.0 -0.0± 0.0 -0.0± 0.0 -0.0± 0.0 -0.0± 0.0 -0.0± 0.0
 .74±.96 7.3± 7.3 7.1± 2.9 15.5± 5.0 17.1± 6.1 14.7± 8.0 -0.0± 0.0 -0.0± 0.0 -0.0± 0.0 -0.0± 0.0 -0.0± 0.0

0*/3.14
 .04±.26 6.0± 0.0 1.4± 1.1 4.4± 3.4 0.0± 0.0 -0.0± 0.0 -0.0± 0.0 -0.0± 0.0 -0.0± 0.0 -0.0± 0.0 -0.0± 0.0
 .26±.50 0.0± 0.0 2.7± 2.5 2.4± 2.6 0.0± 0.0 -0.0± 0.0 -0.0± 0.0 -0.0± 0.0 -0.0± 0.0 -0.0± 0.0
 .50±.74 0.7± 0.8 0.7± 0.7 9.0± 0.0 -0.0± 0.0 -0.0± 0.0 -0.0± 0.0 -0.0± 0.0 -0.0± 0.0 -0.0± 0.0
 .74±.96 4.8± 5.6 4.6± 2.4 8.7± 3.7 6.1± 3.3 0.0± 0.0 7.1± 5.8 -0.0± 0.0 -0.0± 0.0 -0.0± 0.0 -0.0± 0.0

0*/3.14
 .04±.26 1.0± 1.1 0.7± 0.7 2.0± 1.6 0.0± 0.0 0.0± 0.0 -0.0± 0.0 -0.0± 0.0 -0.0± 0.0 -0.0± 0.0 -0.0± 0.0
 .26±.50 0.0± 0.0 0.0± 0.0 2.1± 2.5 2.0± 2.3 -0.0± 0.0 -0.0± 0.0 -0.0± 0.0 -0.0± 0.0 -0.0± 0.0
 .50±.74 -0.0± 0.0 0.0± 0.0 0.0± 0.0 0.0± 0.0 -0.0± 0.0 -0.0± 0.0 -0.0± 0.0 -0.0± 0.0 -0.0± 0.0
 .74±.96 0.0± 0.0 1.9± 1.2 0.0± 0.0 7.4± 4.8 0.0± 0.0 0.0± 0.0 -0.0± 0.0 -0.0± 0.0 -0.0± 0.0 -0.0± 0.0

0*/3.14
 .04±.26 0.0± 0.0 0.3± 0.3 0.0± 0.0 -0.0± 0.0 0.0± 0.0 -0.0± 0.0 -0.0± 0.0 -0.0± 0.0 -0.0± 0.0 -0.0± 0.0
 .26±.50 0.0± 0.0 0.0± 0.0 0.0± 0.0 0.0± 0.0 -0.0± 0.0 -0.0± 0.0 -0.0± 0.0 -0.0± 0.0 -0.0± 0.0
 .50±.74 0.0± 0.0 0.0± 0.0 -0.0± 0.0 -0.0± 0.0 -0.0± 0.0 -0.0± 0.0 -0.0± 0.0 -0.0± 0.0 -0.0± 0.0
 .74±.96 -0.0± 0.0 0.0± 0.0 0.0± 0.0 -0.0± 0.0 -0.0± 0.0 -0.0± 0.0 -0.0± 0.0 -0.0± 0.0 -0.0± 0.0

0*/3.14
 .04±.26 -0.0± 0.0 0.0± 0.0 0.0± 0.0 0.0± 0.0 -0.0± 0.0 -0.0± 0.0 -0.0± 0.0 -0.0± 0.0 -0.0± 0.0
 .26±.50 -0.0± 0.0 -0.0± 0.0 -0.0± 0.0 -0.0± 0.0 -0.0± 0.0 -0.0± 0.0 -0.0± 0.0 -0.0± 0.0 -0.0± 0.0
 .50±.74 -0.0± 0.0 -0.0± 0.0 -0.0± 0.0 -0.0± 0.0 -0.0± 0.0 -0.0± 0.0 -0.0± 0.0 -0.0± 0.0 -0.0± 0.0
 .74±.96 -0.0± 0.0 1.0± 0.0 -0.0± 0.0 -0.0± 0.0 -0.0± 0.0 -0.0± 0.0 -0.0± 0.0 -0.0± 0.0 -0.0± 0.0

-T INTERVAL: 0.05 ± 0.10 (GEV/C)**2

-T INTERVAL: 0.10 ± 0.16 (GEV/C)**2

-T INTERVAL: 0.16 ± 0.23 (GEV/C)**2

-T INTERVAL: 0.23 ± 0.31 (GEV/C)**2

-T INTERVAL: 0.31 ± 0.40 (GEV/C)**2

-T INTERVAL: 0.40 ± 0.50 (GEV/C)**2

-T INTERVAL: 0.50 ± 0.62 (GEV/C)**2

DIFFERENTIAL CROSS SECTION OF N_pP->(P+PI-)P REACTION FOR THE MOMENTUM RANGE 45 ± 55 GEV/C,
COS THETA* INTERVAL -0.96 ± -0.80 (IN MICROBARN/(GEV**4/C**5*STERAD))

M*GEV: 1.00±1.12 1.12±1.16 1.16±1.24 1.24±1.30 1.30±1.36 1.36±1.42 1.42±1.48 1.48±1.54 1.54±1.62 1.62±1.70 1.70±1.78 1.78±1.86
C**2

φ*/3.14
.04±.26 -0.0±0.0 5.1±3.8 39.2±13.2 31.1±9.5 37.5±11.5 40.5±8.8 43.4±12.2 41.0±21.2 30.3±10.1 18.1±10.0 4.5±4.6 -0.0±0.0
.26±.50 0.0±0.0 8.7±5.3 29.4±7.3 13.3±4.6 20.1±5.8 36.3±10.6 69.4±22.1 15.1±11.3 -0.0±0.0 -0.0±0.0 -0.0±0.0 -0.0±0.0
.50±.74 0.0±0.0 7.0±3.8 9.5±3.4 16.2±5.4 14.4±5.1 26.6±9.9 0.0±0.0 -0.0±0.0 -0.0±0.0 -0.0±0.0 -0.0±0.0 -0.0±0.0
.74±.96 0.0±0.0 3.5±3.5 15.6±5.9 29.3±9.1 28.8±6.2 33.0±18.0 -0.0±0.0 -0.0±0.0 -0.0±0.0 -0.0±0.0 -0.0±0.0 -0.0±0.0

-T INTERVAL: 0.05 ± 0.10 (GEV/C)**2

φ*/3.14
.04±.26 6.1±8.6 2.7±2.1 11.5±5.5 12.2±4.3 35.3±11.9 43.5±14.8 71.2±20.0 39.5±12.6 31.6±11.3 16.8±8.2 7.1±5.4 0.0±0.0
.26±.50 0.0±0.0 3.3±2.1 9.4±5.9 4.1±2.2 6.9±2.5 16.7±8.8 19.2±7.9 21.0±12.9 14.6±9.9 -0.0±0.0 -0.0±0.0 -0.0±0.0
.50±.74 0.0±0.0 0.0±0.0 1.3±0.9 2.0±1.5 6.3±3.3 12.0±4.8 1.1±1.1 -0.0±0.0 -0.0±0.0 -0.0±0.0 -0.0±0.0 -0.0±0.0
.74±.96 0.0±0.0 5.5±4.1 1.9±2.0 9.1±4.3 5.5±2.4 8.3±5.0 4.5±4.8 -0.0±0.0 -0.0±0.0 -0.0±0.0 -0.0±0.0 -0.0±0.0

-T INTERVAL: 0.10 ± 0.16 (GEV/C)**2

φ*/3.14
.04±.26 -0.0±0.0 0.0±0.0 2.2±1.7 0.0±0.0 1.7±1.3 18.6±10.0 11.4±6.1 5.7±3.3 9.2±4.8 9.3±7.0 -0.0±0.0 -0.0±0.0
.26±.50 -0.0±0.0 -0.0±0.0 0.0±0.0 0.0±0.0 0.0±0.0 2.4±2.5 2.1±2.2 17.1±9.9 2.5±2.7 -0.0±0.0 -0.0±0.0 -0.0±0.0
.50±.74 -0.0±0.0 0.0±0.0 0.3±0.3 0.0±0.0 0.0±0.0 4.1±4.2 5.1±6.6 -0.0±0.0 -0.0±0.0 -0.0±0.0 -0.0±0.0 -0.0±0.0
.74±.96 -0.0±0.0 0.0±0.0 0.0±0.0 0.0±0.0 0.0±0.0 5.2±5.5 5.5±5.8 0.0±0.0 -0.0±0.0 -0.0±0.0 -0.0±0.0 -0.0±0.0

-T INTERVAL: 0.16 ± 0.23 (GEV/C)**2

φ*/3.14
.04±.26 -0.0±0.0 0.0±0.0 1.2±1.2 3.9±2.0 6.9±4.0 3.6±3.7 1.3±1.4 27.9±15.1 0.0±0.0 0.0±0.0 0.0±0.0 0.0±0.0
.26±.50 -0.0±0.0 0.0±0.0 3.6±2.9 0.9±0.9 0.0±0.0 9.0±0.0 3.0±3.1 -0.0±0.0 0.8±0.9 -0.0±0.0 0.0±0.0 -0.0±0.0
.50±.74 -0.0±0.0 1.4±1.6 9.0±0.0 1.5±1.7 2.1±2.2 0.0±0.0 0.0±0.0 -0.0±0.0 -0.0±0.0 -0.0±0.0 -0.0±0.0 -0.0±0.0
.74±.96 -0.0±0.0 4.6±5.3 7.1±4.9 1.2±1.2 0.0±0.0 2.8±2.9 -0.0±0.0 -0.0±0.0 -0.0±0.0 -0.0±0.0 -0.0±0.0 -0.0±0.0

-T INTERVAL: 0.23 ± 0.31 (GEV/C)**2

φ*/3.14
.04±.26 -0.0±0.0 0.0±0.0 1.9±1.2 9.1±7.4 2.7±2.1 2.0±1.6 5.9±4.6 3.8±4.2 2.4±2.6 0.8±0.8 -0.0±0.0 -0.0±0.0
.26±.50 -0.0±0.0 0.0±0.0 3.6±3.8 0.0±0.0 1.6±1.7 3.4±3.5 0.0±0.0 0.0±0.0 0.0±0.0 -0.0±0.0 -0.0±0.0 -0.0±0.0
.50±.74 -0.0±0.0 0.0±0.0 1.4±1.2 0.0±0.0 0.0±0.0 0.0±0.0 0.0±0.0 -0.0±0.0 -0.0±0.0 -0.0±0.0 -0.0±0.0 -0.0±0.0
.74±.96 -0.0±0.0 5.4±6.6 9.5±0.5 6.8±8.2 0.0±0.0 -0.0±0.0 0.0±0.0 -0.0±0.0 -0.0±0.0 -0.0±0.0 -0.0±0.0 -0.0±0.0

-T INTERVAL: 0.31 ± 0.40 (GEV/C)**2

φ*/3.14
.04±.26 -0.0±0.0 0.0±0.0 1.2±1.5 -0.0±0.0 0.0±0.0 1.0±1.1 0.0±0.0 0.0±0.0 0.0±0.0 -0.0±0.0 -0.0±0.0 -0.0±0.0
.26±.50 -0.0±0.0 0.0±0.0 0.0±0.0 0.0±0.0 0.0±0.0 4.9±4.0 3.8±4.1 -0.0±0.0 -0.0±0.0 -0.0±0.0 -0.0±0.0 -0.0±0.0
.50±.74 -0.0±0.0 0.0±0.0 0.0±0.0 0.0±0.0 -0.0±0.0 -0.0±0.0 0.0±0.0 -0.0±0.0 -0.0±0.0 -0.0±0.0 -0.0±0.0 -0.0±0.0
.74±.96 -0.0±0.0 0.0±0.0 -0.0±0.0 0.0±0.0 -0.0±0.0 0.0±0.0 0.0±0.0 -0.0±0.0 -0.0±0.0 -0.0±0.0 -0.0±0.0 -0.0±0.0

-T INTERVAL: 0.40 ± 0.50 (GEV/C)**2

φ*/3.14
.04±.26 -0.0±0.0 -0.0±0.0 0.0±0.0 0.0±0.0 0.0±0.0 -0.0±0.0 0.0±0.0 0.0±0.0 0.0±0.0 -0.0±0.0 -0.0±0.0 -0.0±0.0
.26±.50 -0.0±0.0 0.0±0.0 -0.0±0.0 -0.0±0.0 -0.0±0.0 -0.0±0.0 -0.0±0.0 -0.0±0.0 -0.0±0.0 -0.0±0.0 -0.0±0.0 -0.0±0.0
.50±.74 -0.0±0.0 -0.0±0.0 0.0±0.0 2.8±4.0 -0.0±0.0 0.0±0.0 0.0±0.0 -0.0±0.0 -0.0±0.0 -0.0±0.0 -0.0±0.0 -0.0±0.0
.74±.96 -0.0±0.0 -0.0±0.0 -0.0±0.0 0.0±0.0 -0.0±0.0 -0.0±0.0 -0.0±0.0 -0.0±0.0 -0.0±0.0 -0.0±0.0 -0.0±0.0 -0.0±0.0

-T INTERVAL: 0.50 ± 0.62 (GEV/C)**2

DIFFERENTIAL CROSS SECTION OF N+P->(P+PI-)+P REACTION FOR THE MOMENTUM RANGE 45 + 55 GEV/C ,
COS THETA* INTERVAL -0.30 + 0.10 (IN MICROBARN/(GEV**4/C**5*STERAD))

M* GEV: 1.08+1.12 1.12+1.18 1.18+1.24 1.24+1.30 1.30+1.36 1.36+1.42 1.42+1.48 1.48+1.54 1.54+1.62 1.62+1.70 1.70+1.78 1.78+1.86
C**2

o*/3.14
.04+.26 3.5* 1.7 9.3* 2.7 8.2* 3.1 15.0* 7.3 -0.0* 0.0 0.0* 0.0 -0.0* 0.0 -0.0* 0.0 -0.0* 0.0 -0.0* 0.0
.26+.50 5.7* 3.2 7.3* 2.1 12.5* 3.2 12.1* 3.9 12.9* 6.1 -0.0* 0.0 -0.0* 0.0 -0.0* 0.0 -0.0* 0.0 -0.0* 0.0
.50+.74 1.4* 1.0 11.6* 2.7 10.1* 2.2 22.4* 5.0 17.1* 5.5 -0.0* 0.0 -0.0* 0.0 -0.0* 0.0 -0.0* 0.0 -0.0* 0.0
.74+.96 11.0* 4.5 27.5* 4.5 35.0* 5.2 62.0* 7.4 79.1* 9.0 37.9* 7.3 -0.0* 0.0 -0.0* 0.0 -0.0* 0.0 -0.0* 0.0 -0.0* 0.0

-T INTERVAL: 0.05 + 0.10 (GEV/C)**2

o*/3.14
.04+.26 1.3* 1.4 4.1* 1.8 2.7* 1.4 2.7* 1.6 12.6* 6.3 -0.0* 0.0 -0.0* 0.0 -0.0* 0.0 -0.0* 0.0 -0.0* 0.0 -0.0* 0.0
.26+.50 1.5* 1.2 3.4* 1.5 1.2* 0.7 3.8* 2.3 1.2* 1.2 0.0* 0.0 -0.0* 0.0 -0.0* 0.0 -0.0* 0.0 -0.0* 0.0 -0.0* 0.0
.50+.74 1.0* 0.6 3.7* 1.5 4.8* 1.7 6.8* 2.7 5.9* 3.4 -0.0* 0.0 -0.0* 0.0 -0.0* 0.0 -0.0* 0.0 -0.0* 0.0 -0.0* 0.0
.74+.96 3.0* 1.5 12.7* 2.5 16.9* 2.8 21.4* 3.6 25.4* 3.6 46.7* 6.6 43.4* 8.2 -0.0* 0.0 -0.0* 0.0 -0.0* 0.0 -0.0* 0.0

-T INTERVAL: 0.10 + 0.16 (GEV/C)**2

o*/3.14
.04+.26 1.0* 1.0 1.7* 0.8 3.5* 1.8 6.1* 2.9 0.0* 0.0 -0.0* 0.0 -0.0* 0.0 -0.0* 0.0 -0.0* 0.0 -0.0* 0.0 -0.0* 0.0
.26+.50 0.0* 0.0 0.9* 0.9 2.4* 0.8 0.0* 0.0 2.2* 2.3 -0.0* 0.0 -0.0* 0.0 -0.0* 0.0 -0.0* 0.0 -0.0* 0.0 -0.0* 0.0
.50+.74 1.0* 0.6 1.0* 0.6 5.0* 2.2 1.9* 2.3 1.9* 1.4 -0.0* 0.0 -0.0* 0.0 -0.0* 0.0 -0.0* 0.0 -0.0* 0.0 -0.0* 0.0
.74+.96 0.3* 0.3 10.9* 3.0 22.5* 5.0 16.9* 4.3 18.1* 4.3 23.6* 4.6 32.4* 7.8 24.3* 7.7 -0.0* 0.0 -0.0* 0.0 -0.0* 0.0

-T INTERVAL: 0.23 + 0.31 (GEV/C)**2

o*/3.14
.04+.26 2.3* 2.6 0.7* 0.5 0.7* 0.5 0.5* 0.5 4.0* 2.3 0.0* 0.0 -0.0* 0.0 -0.0* 0.0 -0.0* 0.0 -0.0* 0.0 -0.0* 0.0
.26+.50 0.0* 0.0 0.3* 0.1 1.4* 1.1 0.7* 0.8 2.0* 2.2 -0.0* 0.0 -0.0* 0.0 -0.0* 0.0 -0.0* 0.0 -0.0* 0.0 -0.0* 0.0
.50+.74 1.3* 1.6 2.0* 1.1 9.0* 0.0 2.2* 1.7 -0.0* 0.0 -0.0* 0.0 -0.0* 0.0 -0.0* 0.0 -0.0* 0.0 -0.0* 0.0 -0.0* 0.0
.74+.96 0.0* 0.0 1.7* 0.9 3.2* 1.3 12.6* 3.4 5.0* 1.4 15.6* 4.4 16.2* 4.8 7.6* 3.6 0.0* 0.0 -0.0* 0.0 -0.0* 0.0

-T INTERVAL: 0.31 + 0.40 (GEV/C)**2

o*/3.14
.04+.26 2.5* 2.2 0.7* 0.4 0.7* 0.4 0.0* 0.0 0.0* 0.0 2.3* 1.8 0.0* 0.0 -0.0* 0.0 -0.0* 0.0 -0.0* 0.0 -0.0* 0.0
.26+.50 -0.0* 0.0 0.2* 0.2 1.7* 1.3 0.6* 0.6 2.5* 2.1 1.6* 1.7 0.0* 0.0 -0.0* 0.0 -0.0* 0.0 -0.0* 0.0 -0.0* 0.0
.50+.74 -0.0* 0.0 0.3* 0.4 0.8* 0.6 2.0* 1.9 0.0* 0.0 -0.0* 0.0 -0.0* 0.0 -0.0* 0.0 -0.0* 0.0 -0.0* 0.0 -0.0* 0.0
.74+.96 1.6* 2.5 1.1* 0.6 8.6* 2.9 2.2* 1.0 1.8* 1.3 3.0* 1.8 1.2* 0.9 5.7* 2.9 -0.0* 0.0 -0.0* 0.0 -0.0* 0.0

-T INTERVAL: 0.40 + 0.50 (GEV/C)**2

o*/3.14
.04+.26 0.0* 0.0 0.0* 0.0 0.4* 0.3 0.0* 0.0 0.0* 0.0 0.0* 0.0 -0.0* 0.0 -0.0* 0.0 -0.0* 0.0 -0.0* 0.0 -0.0* 0.0
.26+.50 0.0* 0.0 0.0* 0.0 0.0* 0.0 2.2* 1.8 0.0* 0.0 -0.0* 0.0 -0.0* 0.0 -0.0* 0.0 -0.0* 0.0 -0.0* 0.0 -0.0* 0.0
.50+.74 -0.0* 0.0 0.0* 0.0 0.0* 0.0 0.0* 0.0 0.0* 0.0 -0.0* 0.0 -0.0* 0.0 -0.0* 0.0 -0.0* 0.0 -0.0* 0.0 -0.0* 0.0
.74+.96 0.0* 0.0 0.0* 0.0 0.7* 0.5 2.0* 1.4 0.0* 0.0 1.2* 0.9 0.0* 0.0 -0.0* 0.0 -0.0* 0.0 -0.0* 0.0 -0.0* 0.0

-T INTERVAL: 0.50 + 0.62 (GEV/C)**2

o*/3.14
.04+.26 -0.0* 0.0 0.0* 0.0 0.0* 0.0 0.0* 0.0 0.0* 0.0 -0.0* 0.0 -0.0* 0.0 -0.0* 0.0 -0.0* 0.0 -0.0* 0.0 -0.0* 0.0
.26+.50 -0.0* 0.0 0.0* 0.0 0.0* 0.0 -0.0* 0.0 -0.0* 0.0 -0.0* 0.0 -0.0* 0.0 -0.0* 0.0 -0.0* 0.0 -0.0* 0.0 -0.0* 0.0
.50+.74 -0.0* 0.0 0.0* 0.0 0.0* 0.0 1.0* 1.4 -0.0* 0.0 -0.0* 0.0 -0.0* 0.0 -0.0* 0.0 -0.0* 0.0 -0.0* 0.0 -0.0* 0.0
.74+.96 -0.0* 0.0 0.0* 0.0 -0.0* 0.0 -0.0* 0.0 0.0* 0.0 0.0* 0.0 1.4* 2.0 -0.0* 0.0 -0.0* 0.0 -0.0* 0.0 -0.0* 0.0

DIFFERENTIAL CROSS SECTION OF $n+p \rightarrow (p+\pi^-)+p$ REACTION FOR THE MOMENTUM RANGE 45 + 55 GEV/C ,

COS THETA* INTERVAL 0.10 + 0.50 (IN MICROBARN/(GEV**4/C**5*STERAD))

M* GEV: 1.63+1.12 1.12+1.10 1.16+1.24 1.24+1.30 1.30+1.36 1.36+1.42 1.42+1.48 1.48+1.54 1.54+1.62 1.62+1.70 1.70+1.76 1.76+1.86
C**2

0*/3.14
0.04+26 3.0+ 1.7 6.6+ 4.2 -0.0+ 0.0 -0.0+ 0.0 -0.0+ 0.0 -0.0+ 0.0 -0.0+ 0.0 -0.0+ 0.0 -0.0+ 0.0 -0.0+ 0.0 -0.0+ 0.0
.26+50 0.9+ 1.0 6.9+ 2.4 3.0+ 2.2 0.0+ 0.0 -0.0+ 0.0 -0.0+ 0.0 -0.0+ 0.0 -0.0+ 0.0 -0.0+ 0.0 -0.0+ 0.0 -0.0+ 0.0 -0.0+ 0.0
.50+74 2.0+ 1.2 11.3+ 3.1 16.2+ 6.2 14.2+ 4.7 -0.0+ 0.0 -0.0+ 0.0 -0.0+ 0.0 -0.0+ 0.0 -0.0+ 0.0 -0.0+ 0.0 -0.0+ 0.0 -0.0+ 0.0 -0.0+ 0.0
.74+96 6.2+ 2.3 21.0+ 3.6 50.3+ 6.3 50.5+ 6.0 68.4+ 9.8 83.8+14.7 45.1+15.0 -0.0+ 0.0 -0.0+ 0.0 -0.0+ 0.0 -0.0+ 0.0 -0.0+ 0.0 -0.0+ 0.0 -0.0+ 0.0
-T INTERVAL: 0.05 + 0.10 (GEV/C)**2

0*/3.14
0.04+26 0.0+ 0.0 3.0+ 1.8 -0.0+ 0.0 -0.0+ 0.0 -0.0+ 0.0 -0.0+ 0.0 -0.0+ 0.0 -0.0+ 0.0 -0.0+ 0.0 -0.0+ 0.0 -0.0+ 0.0 -0.0+ 0.0
.26+50 0.0+ 0.0 0.3+ 0.3 1.4+ 1.5 -0.0+ 0.0 -0.0+ 0.0 -0.0+ 0.0 -0.0+ 0.0 -0.0+ 0.0 -0.0+ 0.0 -0.0+ 0.0 -0.0+ 0.0 -0.0+ 0.0
.50+74 2.0+ 1.7 3.1+ 1.4 9.5+ 3.3 15.2+ 5.6 -0.0+ 0.0 -0.0+ 0.0 -0.0+ 0.0 -0.0+ 0.0 -0.0+ 0.0 -0.0+ 0.0 -0.0+ 0.0 -0.0+ 0.0
.74+96 1.7+ 0.9 11.4+ 2.1 20.6+ 3.3 35.1+ 4.9 36.7+ 6.4 39.6+ 8.5 -0.0+ 0.0 -0.0+ 0.0 -0.0+ 0.0 -0.0+ 0.0 -0.0+ 0.0 -0.0+ 0.0
-T INTERVAL: 0.10 + 0.16 (GEV/C)**2

0*/3.14
0.04+26 0.0+ 0.0 0.2+ 0.2 0.0+ 0.0 0.0+ 0.0 -0.0+ 0.0 -0.0+ 0.0 -0.0+ 0.0 -0.0+ 0.0 -0.0+ 0.0 -0.0+ 0.0 -0.0+ 0.0
.26+50 1.9+ 2.3 0.6+ 0.6 1.4+ 1.5 0.0+ 0.0 -0.0+ 0.0 -0.0+ 0.0 -0.0+ 0.0 -0.0+ 0.0 -0.0+ 0.0 -0.0+ 0.0 -0.0+ 0.0
.50+74 0.0+ 0.0 0.4+ 0.4 3.0+ 1.9 1.6+ 1.7 -0.0+ 0.0 -0.0+ 0.0 -0.0+ 0.0 -0.0+ 0.0 -0.0+ 0.0 -0.0+ 0.0 -0.0+ 0.0
.74+96 0.0+ 0.0 5.8+ 2.2 7.3+ 2.2 18.0+ 6.0 32.8+ 9.4 -0.0+ 0.0 -0.0+ 0.0 -0.0+ 0.0 -0.0+ 0.0 -0.0+ 0.0 -0.0+ 0.0
-T INTERVAL: 0.16 + 0.23 (GEV/C)**2

0*/3.14
0.04+26 0.9+ 1.1 0.3+ 0.3 0.0+ 0.0 -0.0+ 0.0 -0.0+ 0.0 -0.0+ 0.0 -0.0+ 0.0 -0.0+ 0.0 -0.0+ 0.0 -0.0+ 0.0
.26+50 0.0+ 0.0 0.0+ 0.0 0.0+ 0.0 -0.0+ 0.0 -0.0+ 0.0 -0.0+ 0.0 -0.0+ 0.0 -0.0+ 0.0 -0.0+ 0.0 -0.0+ 0.0
.50+74 0.0+ 0.0 0.4+ 0.3 0.0+ 0.0 2.2+ 2.4 -0.0+ 0.0 -0.0+ 0.0 -0.0+ 0.0 -0.0+ 0.0 -0.0+ 0.0 -0.0+ 0.0 -0.0+ 0.0
.74+96 0.4+ 0.4 0.9+ 0.5 0.3+ 0.3 2.7+ 1.6 4.8+ 2.3 -0.0+ 0.0 -0.0+ 0.0 -0.0+ 0.0 -0.0+ 0.0 -0.0+ 0.0 -0.0+ 0.0
-T INTERVAL: 0.23 + 0.31 (GEV/C)**2

0*/3.14
0.04+26 3.3+ 4.0 0.2+ 0.2 1.6+ 1.4 0.0+ 0.0 -0.0+ 0.0 -0.0+ 0.0 -0.0+ 0.0 -0.0+ 0.0 -0.0+ 0.0 -0.0+ 0.0
.26+50 -0.0+ 0.0 0.4+ 0.5 0.0+ 0.0 -0.0+ 0.0 -0.0+ 0.0 -0.0+ 0.0 -0.0+ 0.0 -0.0+ 0.0 -0.0+ 0.0 -0.0+ 0.0
.50+74 0.0+ 0.0 0.6+ 0.5 0.0+ 0.0 -0.0+ 0.0 -0.0+ 0.0 -0.0+ 0.0 -0.0+ 0.0 -0.0+ 0.0 -0.0+ 0.0 -0.0+ 0.0
.74+96 0.0+ 0.0 1.1+ 0.7 0.6+ 0.6 4.2+ 3.2 -0.0+ 0.0 -0.0+ 0.0 -0.0+ 0.0 -0.0+ 0.0 -0.0+ 0.0 -0.0+ 0.0
-T INTERVAL: 0.31 + 0.40 (GEV/C)**2

0*/3.14
0.04+26 -0.0+ 0.0 0.0+ 0.0 0.0+ 0.0 -0.0+ 0.0 -0.0+ 0.0 -0.0+ 0.0 -0.0+ 0.0 -0.0+ 0.0 -0.0+ 0.0
.26+50 0.0+ 0.0 0.0+ 0.0 0.0+ 0.0 -0.0+ 0.0 -0.0+ 0.0 -0.0+ 0.0 -0.0+ 0.0 -0.0+ 0.0 -0.0+ 0.0
.50+74 -0.0+ 0.0 0.0+ 0.0 0.0+ 0.0 -0.0+ 0.0 -0.0+ 0.0 -0.0+ 0.0 -0.0+ 0.0 -0.0+ 0.0 -0.0+ 0.0
.74+96 -0.0+ 0.0 1.4+ 1.2 0.0+ 0.0 0.0+ 0.0 -0.0+ 0.0 -0.0+ 0.0 -0.0+ 0.0 -0.0+ 0.0 -0.0+ 0.0
-T INTERVAL: 0.40 + 0.50 (GEV/C)**2

0*/3.14
0.04+26 -0.0+ 0.0 0.0+ 0.0 0.0+ 0.0 -0.0+ 0.0 -0.0+ 0.0 -0.0+ 0.0 -0.0+ 0.0 -0.0+ 0.0 -0.0+ 0.0
.26+50 1.3+ 1.4 0.0+ 0.0 -0.0+ 0.0 -0.0+ 0.0 -0.0+ 0.0 -0.0+ 0.0 -0.0+ 0.0 -0.0+ 0.0 -0.0+ 0.0
.50+74 0.0+ 0.0 0.0+ 0.0 -0.0+ 0.0 -0.0+ 0.0 -0.0+ 0.0 -0.0+ 0.0 -0.0+ 0.0 -0.0+ 0.0 -0.0+ 0.0
.74+96 0.0+ 0.0 0.0+ 0.0 -0.0+ 0.0 -0.0+ 0.0 -0.0+ 0.0 -0.0+ 0.0 -0.0+ 0.0 -0.0+ 0.0 -0.0+ 0.0
-T INTERVAL: 0.50 + 0.62 (GEV/C)**2

DIFFERENTIAL CROSS SECTION OF N+P->(P+PI-)+P REACTION FOR THE MOMENTUM RANGE 55 ± 65 GEV/C ,

COS THETA INTERVAL -0.95 + -0.80 (IN MICROBARN/(GEV**4/C**5*STERAD))

M* GEV: 1.08±1.12 1.12±1.18 1.12±1.24 1.24±1.30 1.30±1.36 1.36±1.42 1.42±1.48 1.48±1.54 1.54±1.62 1.62±1.70 1.70±1.76 1.78±1.86

C**2
0*/3.14
.04±.26 0.0± 0.0 3.4± 3.5 16.5± 7.4 33.2±10.2 56.6±15.1 74.6±17.0 66.0±16.5 54.0±13.8 27.0± 6.6 33.0±10.3 21.2± 9.5 16.9± 9.4
.26±.50 0.0± 0.0 2.8± 2.8 11.9± 4.5 18.9± 5.4 38.5± 9.3 22.0± 6.9 67.9±15.3 23.8± 8.3 20.6± 9.4 -0.0± 0.0 -0.0± 0.0 -0.0± 0.0
.50±.74 0.0± 0.0 5.0± 3.0 13.1± 4.8 18.6± 5.0 23.5± 5.8 38.1± 8.8 12.8± 4.1 16.2± 7.7 -0.0± 0.0 -0.0± 0.0 -0.0± 0.0 -0.0± 0.0
.74±.96 -0.0± 0.0 4.5± 4.6 14.3± 5.6 23.6± 7.3 25.0± 8.0 27.8± 7.1 50.3±13.9 3.9± 4.1 -0.0± 0.0 -0.0± 0.0 -0.0± 0.0 -0.0± 0.0

-T INTERVAL: 0.05 + 0.10 (GEV/C)**2
0*/3.14
-0.0± 0.0 -0.0± 0.0 5.3± 4.1 10.9± 6.6 22.2± 9.1 10.6± 5.5 26.3± 7.2 40.8±10.9 7.4± 2.3 20.3± 7.0 1.8± 1.0 3.4± 2.6
.04±.26 0.0± 0.0 2.0± 2.0 5.2± 2.6 15.2± 5.0 18.8± 6.9 13.4± 5.4 16.5± 9.2 9.5± 3.7 -0.0± 0.0 -0.0± 0.0 -0.0± 0.0
.26±.50 0.0± 0.0 1.8± 1.3 3.9± 1.8 4.3± 1.8 15.5± 5.3 2.7± 2.1 -0.0± 0.0 -0.0± 0.0 -0.0± 0.0 -0.0± 0.0
.50±.74 -0.0± 0.0 4.8± 5.1 1.0± 0.7 1.3± 1.3 11.6± 6.2 3.8± 2.3 4.9± 5.5 -0.0± 0.0 -0.0± 0.0 -0.0± 0.0 -0.0± 0.0

-T INTERVAL: 0.10 + 0.16 (GEV/C)**2
0*/3.14
0.0± 0.0 0.0± 0.0 1.6± 1.9 0.0± 0.0 9.8± 4.6 2.0± 2.0 2.6± 2.6 30.5±10.9 23.1± 8.0 1.0± 1.1 4.5± 2.8 2.9± 3.1
.04±.26 0.0± 0.0 3.0± 3.5 0.0± 0.0 0.6± 0.6 2.2± 2.3 9.5± 4.4 9.6± 6.0 1.3± 1.4 -0.0± 0.0 -0.0± 0.0 -0.0± 0.0
.26±.50 0.0± 0.0 1.6± 1.7 2.3± 2.4 0.0± 0.0 3.8± 4.0 0.0± 0.0 0.0± 0.0 -0.0± 0.0 -0.0± 0.0 -0.0± 0.0
.50±.74 0.0± 0.0 3.0± 3.0 0.0± 0.0 0.0± 0.0 7.0± 4.2 3.6± 0.6 2.0± 2.1 -0.0± 0.0 -0.0± 0.0 -0.0± 0.0 -0.0± 0.0

-T INTERVAL: 0.15 + 0.23 (GEV/C)**2
0*/3.14
-0.0± 0.0 0.0± 0.0 0.0± 0.0 0.0± 0.0 5.3± 4.0 2.7± 2.6 14.1± 8.1 2.6± 2.6 30.5±10.9 23.1± 8.0 1.0± 1.1 4.5± 2.8 2.9± 3.1
.04±.26 0.0± 0.0 2.0± 2.0 2.0± 2.0 2.0± 2.0 1.7± 1.8 0.0± 0.0 1.9± 2.0 5.2± 3.4 0.0± 0.0 -0.0± 0.0 -0.0± 0.0
.26±.50 0.0± 0.0 1.1± 1.2 0.0± 0.0 0.7± 0.8 0.0± 0.0 0.0± 0.0 0.0± 0.0 0.0± 0.0 0.0± 0.0 -0.0± 0.0 -0.0± 0.0
.50±.74 -0.0± 0.0 2.6± 2.0 0.0± 0.0 3.0± 3.0 2.6± 2.7 1.3± 1.3 2.9± 2.0 0.0± 0.0 -0.0± 0.0 -0.0± 0.0 -0.0± 0.0

-T INTERVAL: 0.31 + 0.40 (GEV/C)**2
0*/3.14
-0.0± 0.0 -0.0± 0.0 1.3± 1.4 0.0± 0.0 3.5± 3.9 -0.0± 0.0 2.6± 3.0 0.0± 0.0 0.0± 0.0 0.0± 0.0 0.0± 0.0 2.1± 2.3
.04±.26 0.0± 0.0 0.0± 0.0 1.0± 1.0 0.0± 0.0 0.0± 0.0 0.0± 0.0 0.0± 0.0 0.0± 0.0 0.0± 0.0 0.0± 0.0 0.0± 0.0
.26±.50 0.0± 0.0 1.6± 1.7 2.1± 1.7 3.6± 3.3 0.0± 0.0 0.0± 0.0 0.0± 0.0 0.0± 0.0 0.0± 0.0 0.0± 0.0 0.0± 0.0
.50±.74 -0.0± 0.0 -0.0± 0.0 -0.0± 0.0 3.6± 4.2 0.0± 0.0 0.0± 0.0 1.0± 1.1 0.0± 0.0 -0.0± 0.0 -0.0± 0.0 -0.0± 0.0

-T INTERVAL: 0.40 + 0.50 (GEV/C)**2
0*/3.14
-0.0± 0.0 -0.0± 0.0 0.0± 0.0 0.0± 0.0 0.0± 0.0 0.0± 0.0 0.0± 0.0 0.0± 0.0 0.0± 0.0 0.0± 0.0 0.0± 0.0 0.0± 0.0
.04±.26 0.0± 0.0 1.3± 1.5 -0.0± 0.0 0.0± 0.0 0.0± 0.0 0.0± 0.0 1.6± 1.7 0.0± 0.0 -0.0± 0.0 -0.0± 0.0 -0.0± 0.0
.26±.50 0.0± 0.0 0.9± 1.2 -0.0± 0.0 -0.0± 0.0 0.0± 0.0 0.0± 0.0 0.0± 0.0 -0.0± 0.0 -0.0± 0.0 -0.0± 0.0 -0.0± 0.0
.50±.74 -0.0± 0.0 -0.0± 0.0 -0.0± 0.0 3.2± 3.2 -0.0± 0.0 1.8± 2.1 -0.0± 0.0 3.7± 3.2 -0.0± 0.0 -0.0± 0.0 -0.0± 0.0

-T INTERVAL: 0.50 + 0.62 (GEV/C)**2
0*/3.14
-0.0± 0.0 0.0± 0.0 0.0± 0.0 0.0± 0.0 0.0± 0.0 0.0± 0.0 0.0± 0.0 0.0± 0.0 0.0± 0.0 0.0± 0.0 0.0± 0.0
.04±.26 0.0± 0.0 -0.0± 0.0 -0.0± 0.0 -0.0± 0.0 -0.0± 0.0 -0.0± 0.0 -0.0± 0.0 -0.0± 0.0 -0.0± 0.0 -0.0± 0.0
.26±.50 0.0± 0.0 2.5± 3.5 -0.0± 0.0 -0.0± 0.0 -0.0± 0.0 -0.0± 0.0 -0.0± 0.0 -0.0± 0.0 -0.0± 0.0 -0.0± 0.0
.50±.74 -0.0± 0.0 -0.0± 0.0 -0.0± 0.0 0.0± 0.0 0.0± 0.0 0.0± 0.0 0.0± 0.0 0.0± 0.0 0.0± 0.0 0.0± 0.0 -0.0± 0.0

DIFFERENTIAL CROSS SECTION OF N+P->(P+P+)-+P REACTION FOR THE MOMENTUM RANGE 55 + 65 GEV/C ,
COS THETA* INTERVAL -0.80 + -0.60 (IN MICROBARN/(GEV**4/C**5*STERAD))

** GEV: 1.08+1.12 1.12+1.16 1.16+1.24 1.24+1.30 1.30+1.36 1.36+1.42 1.42+1.48 1.48+1.54 1.54+1.62 1.62+1.70 1.70+1.78 1.78+1.86
C**2

-T INTERVAL: 0.05 + 0.10 (GEV/C)**2
0*/3.14 0.0* 0.0 19.4* 5.3 30.3* 7.5 34.7* 7.5 61.1* 9.7 99.9*17.1 50.8* 9.1 30.7* 9.2 20.1* 5.2 29.0* 8.0 26.4* 9.6 4.1* 31.1
.04+.26 0.0* 0.0 9.7* 4.1 20.8* 5.2 31.7* 6.7 51.5*11.2 70.9*18.0 0.0* 0.0 -0.0* 0.0 -0.0* 0.0 -0.0* 0.0 -0.0* 0.0 -0.0* 0.0
.26+.50 6.6* 7.2 9.7* 4.1 20.8* 5.2 31.7* 6.7 51.5*11.2 70.9*18.0 0.0* 0.0 -0.0* 0.0 -0.0* 0.0 -0.0* 0.0 -0.0* 0.0 -0.0* 0.0
.50+.74 9.0* 0.0 4.1* 2.1 9.5* 3.3 11.3* 2.6 18.3* 4.5 34.3* 8.0 -9.0* 0.0 -9.0* 0.0 -0.0* 0.0 -0.0* 0.0 -0.0* 0.0 -0.0* 0.0
.74+.96 3.2* 3.3 10.5* 3.7 19.2* 5.0 38.5* 7.6 32.0* 7.4 34.7* 7.5 33.1* 9.2 -0.0* 0.0 -0.0* 0.0 -0.0* 0.0 -0.0* 0.0 -0.0* 0.0

-T INTERVAL: 0.10 + 0.16 (GEV/C)**2
0*/3.14 0.0* 0.0 1.7* 1.7 8.6* 4.2 17.8* 5.4 20.2* 5.4 16.0* 5.0 48.0*13.5 41.3* 9.7 29.7* 9.2 13.8* 5.0 6.6* 3.0 5.9* 3.8
.04+.26 -0.0* 0.0 1.7* 1.7 8.6* 4.2 17.8* 5.4 20.2* 5.4 16.0* 5.0 48.0*13.5 41.3* 9.7 29.7* 9.2 13.8* 5.0 6.6* 3.0 5.9* 3.8
.26+.50 0.0* 0.0 1.2* 0.9 2.3* 1.4 10.1* 4.7 11.9* 3.9 5.1* 2.7 4.9* 3.7 -9.0* 0.0 -0.0* 0.0 -0.0* 0.0 -0.0* 0.0 -0.0* 0.0
.50+.74 4.4* 4.9 0.6* 0.4 2.5* 1.5 5.3* 1.9 9.3* 3.4 7.2* 3.1 0.0* 0.0 -0.0* 0.0 -0.0* 0.0 -0.0* 0.0 -0.0* 0.0 -0.0* 0.0
.74+.96 0.0* 0.0 9.2* 4.4 5.1* 1.8 14.7* 5.3 5.3* 2.0 8.7* 2.8 14.0* 4.2 3.5* 3.7 -0.0* 0.0 -0.0* 0.0 -0.0* 0.0 -0.0* 0.0

-T INTERVAL: 0.15 + 0.23 (GEV/C)**2
0*/3.14 0.0* 0.0 3.5* 3.4 3.7* 2.1 18.0* 5.7 23.2* 7.1 24.0* 8.2 36.3*10.2 8.5* 3.6 9.2* 4.0 10.3* 6.0 0.0* 0.0
.04+.26 -0.0* 0.0 3.5* 3.4 3.7* 2.1 18.0* 5.7 23.2* 7.1 24.0* 8.2 36.3*10.2 8.5* 3.6 9.2* 4.0 10.3* 6.0 0.0* 0.0
.26+.50 0.0* 0.0 0.0* 0.0 0.0* 0.0 6.1* 3.3 5.0* 3.3 2.1* 1.6 -0.0* 0.0 -0.0* 0.0 -0.0* 0.0 -0.0* 0.0 -0.0* 0.0
.50+.74 0.0* 0.0 1.5* 1.1 0.9* 0.0 2.2* 1.4 8.0* 0.0 3.4* 3.5 -0.0* 0.0 -0.0* 0.0 -0.0* 0.0 -0.0* 0.0 -0.0* 0.0
.74+.96 -0.0* 0.0 4.5* 2.6 6.3* 3.7 6.1* 2.6 7.5* 3.2 5.6* 2.2 3.0* 2.2 1.3* 1.0 0.0* 0.0 -0.0* 0.0 -0.0* 0.0

-T INTERVAL: 0.23 + 0.31 (GEV/C)**2
0*/3.14 0.0* 0.0 0.3* 0.3 1.8* 1.4 0.6* 0.6 3.9* 2.9 6.4* 3.4 7.3* 3.9 2.0* 1.3 6.5* 3.2 3.2* 2.7 8.0* 5.3 0.0* 0.0
.04+.26 -0.0* 0.0 0.3* 0.3 1.8* 1.4 0.6* 0.6 3.9* 2.9 6.4* 3.4 7.3* 3.9 2.0* 1.3 6.5* 3.2 3.2* 2.7 8.0* 5.3 0.0* 0.0
.26+.50 0.0* 0.0 2.2* 2.6 0.3* 0.3 1.0* 1.1 0.3* 0.0 1.5* 1.5 2.8* 2.1 1.7* 1.9 -0.0* 0.0 -0.0* 0.0 -0.0* 0.0 -0.0* 0.0
.50+.74 0.9* 0.0 0.3* 0.3 0.4* 0.4 0.6* 0.4 0.3* 0.0 4.3* 3.3 -0.0* 0.0 -0.0* 0.0 -0.0* 0.0 -0.0* 0.0 -0.0* 0.0
.74+.96 -0.0* 0.0 5.9* 2.0 5.2* 3.0 6.2* 4.1 6.3* 2.5 3.9* 0.9 1.9* 1.5 2.4* 2.5 0.3* 0.3 -0.0* 0.0 -0.0* 0.0

-T INTERVAL: 0.31 + 0.40 (GEV/C)**2
0*/3.14 0.0* 0.0 4.3* 5.2 4.0* 3.1 2.8* 2.2 -0.0* 0.0 4.8* 3.7 5.7* 4.0 1.7* 1.9 3.0* 0.0 2.1* 1.8 0.0* 0.0
.04+.26 -0.0* 0.0 4.3* 5.2 4.0* 3.1 2.8* 2.2 -0.0* 0.0 4.8* 3.7 5.7* 4.0 1.7* 1.9 3.0* 0.0 2.1* 1.8 0.0* 0.0
.26+.50 -0.0* 0.0 1.8* 1.6 1.8* 1.9 0.5* 0.5 0.9* 0.0 1.6* 1.7 -0.0* 0.0 -0.0* 0.0 -0.0* 0.0 -0.0* 0.0 -0.0* 0.0
.50+.74 0.0* 0.0 0.7* 0.8 1.9* 1.4 1.0* 1.1 0.0* 0.0 -0.0* 0.0 -0.0* 0.0 -0.0* 0.0 -0.0* 0.0 -0.0* 0.0
.74+.96 -0.0* 0.0 1.0* 1.1 7.4* 5.7 -0.0* 0.0 2.3* 1.1 4.2* 2.6 0.0* 0.0 -0.0* 0.0 -0.0* 0.0 -0.0* 0.0

-T INTERVAL: 0.40 + 0.50 (GEV/C)**2
0*/3.14 0.0* 0.0 -0.0* 0.0 1.1* 1.2 -0.0* 0.0 2.1* 2.2 2.6* 2.7 2.5* 2.7 -0.0* 0.0 0.0* 0.0 -0.0* 0.0
.04+.26 -0.0* 0.0 -0.0* 0.0 1.1* 1.2 -0.0* 0.0 2.1* 2.2 2.6* 2.7 2.5* 2.7 -0.0* 0.0 0.0* 0.0 -0.0* 0.0
.26+.50 -0.0* 0.0 1.6* 2.2 0.0* 0.0 0.7* 0.8 0.0* 0.0 -0.0* 0.0 -0.0* 0.0 -0.0* 0.0 -0.0* 0.0 -0.0* 0.0
.50+.74 -0.0* 0.0 0.4* 0.4 0.0* 0.0 0.0* 0.0 0.0* 0.0 0.0* 0.0 -0.0* 0.0 -0.0* 0.0 -0.0* 0.0 -0.0* 0.0
.74+.96 -0.0* 0.0 1.3* 1.0 0.0* 0.0 4.0* 3.0 0.8* 0.0 0.0* 0.0 4.2* 3.4 1.1* 1.3 0.0* 0.0 -0.0* 0.0

-T INTERVAL: 0.50 + 0.62 (GEV/C)**2
0*/3.14 0.0* 0.0 0.0* 0.0 0.0* 0.0 0.0* 0.0 0.0* 0.0 -0.0* 0.0 0.8* 1.0 -0.0* 0.0 -0.0* 0.0
.04+.26 -0.0* 0.0 0.0* 0.0 0.0* 0.0 0.0* 0.0 0.0* 0.0 -0.0* 0.0 0.8* 1.0 -0.0* 0.0 -0.0* 0.0
.26+.50 -0.0* 0.0 0.0* 0.0 -0.0* 0.0 0.0* 0.0 0.0* 0.0 -0.0* 0.0 -0.0* 0.0 -0.0* 0.0 -0.0* 0.0 -0.0* 0.0
.50+.74 -0.0* 0.0 0.6* 0.0 1.3* 1.3 0.0* 0.0 0.0* 0.0 -0.0* 0.0 -0.0* 0.0 -0.0* 0.0 -0.0* 0.0
.74+.96 -0.0* 0.0 0.0* 0.0 0.0* 0.0 0.0* 0.0 0.0* 0.0 0.0* 0.0 -0.0* 0.0 -0.0* 0.0 -0.0* 0.0

DIFFERENTIAL CROSS SECTION OF N*P->(P+PI-)+P REACTION FOR THE MOMENTUM RANGE 55 + 65 GEV/C ,

COS THETA* INTERVAL -0.30 + 0.10 (IN MICROBARN/(GEV**4/C**5*STERAD))

M* GEV: 1.38+1.12 1.12+1.18 1.16+1.24 1.24+1.30 1.30+1.36 1.36+1.42 1.42+1.48 1.48+1.54 1.54+1.62 1.62+1.70 1.70+1.78 1.78+1.86

C**2

-T INTERVAL: 0.05 + 0.10 (GEV/C)**2

0.73+14	2.0*	2.1	8.5*	2.4	12.4*	3.2	14.7*	3.8	30.4*	9.3	4.7*	3.5	-0.0*	0.0	-0.0*	0.0	-0.0*	0.0	-0.0*	0.0	-0.0*	0.0	-0.0*	0.0	-0.0*	0.0
.04+.26	0.0*	0.7	5.4*	1.8	15.3*	3.1	13.0*	2.8	21.0*	4.9	5.3*	2.8	-0.0*	0.0	-0.0*	0.0	-0.0*	0.0	-0.0*	0.0	-0.0*	0.0	-0.0*	0.0	-0.0*	0.0
.26+.50	0.0*	1.5	7.6*	1.7	25.9*	4.2	15.8*	4.2	29.9*	4.6	20.2*	5.7	-0.0*	0.0	-0.0*	0.0	-0.0*	0.0	-0.0*	0.0	-0.0*	0.0	-0.0*	0.0	-0.0*	0.0
.50+.74	0.0*	1.1	19.4*	3.6	33.3*	4.4	51.4*	5.6	58.7*	6.1	63.9*	6.6	76.5*	10.3	34.8*	10.3	-0.0*	0.0	-0.0*	0.0	-0.0*	0.0	-0.0*	0.0	-0.0*	0.0

-T INTERVAL: 0.10 + 0.16 (GEV/C)**2

0.73+14	0.0*	0.0	2.0*	1.2	10.9*	2.9	3.6*	4.1	1.6*	1.6	0.0*	0.0	-0.0*	0.0	-0.0*	0.0	-0.0*	0.0	-0.0*	0.0	-0.0*	0.0	-0.0*	0.0	-0.0*	0.0
.04+.26	0.0*	0.0	3.0*	1.2	2.4*	1.2	4.2*	1.8	7.1*	3.0	0.0*	0.0	-0.0*	0.0	-0.0*	0.0	-0.0*	0.0	-0.0*	0.0	-0.0*	0.0	-0.0*	0.0	-0.0*	0.0
.26+.50	0.0*	0.0	5.5*	1.7	6.0*	1.5	10.1*	2.1	7.7*	2.4	10.5*	3.7	-0.0*	0.0	-0.0*	0.0	-0.0*	0.0	-0.0*	0.0	-0.0*	0.0	-0.0*	0.0	-0.0*	0.0
.50+.74	1.0*	1.0	10.8*	2.2	16.0*	2.3	43.5*	4.7	28.4*	3.3	29.7*	3.6	49.8*	6.0	38.8*	6.5	-0.0*	0.0	-0.0*	0.0	-0.0*	0.0	-0.0*	0.0	-0.0*	0.0

-T INTERVAL: 0.16 + 0.23 (GEV/C)**2

0.73+14	2.1*	1.6	4.5*	1.6	4.6*	1.9	4.5*	2.2	10.3*	4.2	-0.0*	0.0	-0.0*	0.0	-0.0*	0.0	-0.0*	0.0	-0.0*	0.0	-0.0*	0.0	-0.0*	0.0	-0.0*	0.0
.04+.26	0.0*	0.0	2.0*	1.0	0.6*	0.5	3.4*	1.5	5.0*	2.8	5.8*	3.2	-0.0*	0.0	-0.0*	0.0	-0.0*	0.0	-0.0*	0.0	-0.0*	0.0	-0.0*	0.0	-0.0*	0.0
.26+.50	0.0*	0.0	2.6*	1.1	9.7*	0.4	2.7*	1.2	4.1*	1.5	3.0*	0.0	-0.0*	0.0	-0.0*	0.0	-0.0*	0.0	-0.0*	0.0	-0.0*	0.0	-0.0*	0.0	-0.0*	0.0
.50+.74	0.0*	0.0	11.6*	3.4	8.7*	1.9	27.6*	4.4	26.4*	4.3	19.7*	3.0	25.7*	3.7	29.8*	5.1	15.8*	4.0	-0.0*	0.0	-0.0*	0.0	-0.0*	0.0	-0.0*	0.0

-T INTERVAL: 0.23 + 0.31 (GEV/C)**2

0.73+14	0.0*	0.0	1.5*	0.3	0.0*	0.0	0.7*	0.7	2.2*	1.4	1.6*	1.2	0.0*	0.0	0.0*	0.0	-0.0*	0.0	-0.0*	0.0	-0.0*	0.0	-0.0*	0.0	-0.0*	0.0
.04+.26	0.0*	0.0	0.6*	0.5	0.2*	0.2	0.9*	0.2	0.9*	0.2	0.0*	0.0	2.2*	1.3	1.3*	1.3	-0.0*	0.0	-0.0*	0.0	-0.0*	0.0	-0.0*	0.0	-0.0*	0.0
.26+.50	0.7*	0.9	1.3*	0.0	0.9*	0.0	2.0*	0.9	2.2*	1.1	4.0*	0.0	-0.0*	0.0	-0.0*	0.0	-0.0*	0.0	-0.0*	0.0	-0.0*	0.0	-0.0*	0.0	-0.0*	0.0
.74+.96	0.0*	0.0	1.0*	0.6	5.2*	1.6	11.3*	2.4	10.3*	2.1	11.4*	2.5	9.6*	2.0	9.0*	2.4	13.3*	3.2	5.4*	2.9	-0.0*	0.0	-0.0*	0.0	-0.0*	0.0

-T INTERVAL: 0.31 + 0.40 (GEV/C)**2

0.73+14	0.0*	0.0	0.9*	0.6	0.2*	0.2	1.3*	0.6	0.5*	0.5	2.8*	1.8	0.6*	0.6	0.0*	0.0	-0.0*	0.0	-0.0*	0.0	-0.0*	0.0	-0.0*	0.0	-0.0*	0.0
.04+.26	0.0*	0.0	0.8*	0.7	0.0*	0.0	0.2*	0.2	0.0*	0.0	0.0*	0.0	2.2*	1.7	0.0*	0.0	-0.0*	0.0	-0.0*	0.0	-0.0*	0.0	-0.0*	0.0	-0.0*	0.0
.26+.50	0.0*	0.0	0.0*	0.0	0.0*	0.0	1.1*	0.8	1.4*	1.1	1.3*	1.4	-0.0*	0.0	-0.0*	0.0	-0.0*	0.0	-0.0*	0.0	-0.0*	0.0	-0.0*	0.0	-0.0*	0.0
.74+.96	0.0*	0.0	1.0*	0.7	2.8*	1.0	3.3*	1.1	4.3*	1.9	4.8*	1.7	2.9*	1.0	9.0*	3.0	5.4*	2.7	1.0*	0.9	-0.0*	0.0	-0.0*	0.0	-0.0*	0.0

-T INTERVAL: 0.40 + 0.50 (GEV/C)**2

0.73+14	-0.0*	0.0	0.9*	0.6	0.9*	0.6	1.6*	1.3	0.8*	0.8	1.1*	1.2	0.0*	0.0	0.0*	0.0	0.0*	0.0	-0.0*	0.0	-0.0*	0.0	-0.0*	0.0	-0.0*	0.0
.04+.26	0.0*	0.0	0.2*	0.2	0.0*	0.0	0.0*	0.0	-0.0*	0.0	0.0*	0.0	0.8*	0.9	-0.0*	0.0	-0.0*	0.0	-0.0*	0.0	-0.0*	0.0	-0.0*	0.0	-0.0*	0.0
.26+.50	0.0*	0.0	0.6*	0.5	1.6*	1.0	0.0*	0.0	0.0*	0.0	0.0*	0.0	-0.0*	0.0	-0.0*	0.0	-0.0*	0.0	-0.0*	0.0	-0.0*	0.0	-0.0*	0.0	-0.0*	0.0
.74+.96	0.0*	0.0	0.2*	0.3	1.0*	0.6	0.2*	0.2	1.8*	1.1	2.3*	1.2	0.7*	0.7	0.5*	0.5	0.1*	0.1	-0.0*	0.0	-0.0*	0.0	-0.0*	0.0	-0.0*	0.0

-T INTERVAL: 0.50 + 0.62 (GEV/C)**2

0.73+14	-0.0*	0.0	0.0*	0.0	0.0*	0.0	0.0*	0.0	0.0*	0.0	0.0*	0.0	0.0*	0.0	0.0*	0.0	0.0*	0.0	-0.0*	0.0	-0.0*	0.0	-0.0*	0.0	-0.0*	0.0
.04+.26	-0.0*	0.0	0.0*	0.0	0.0*	0.0	1.4*	1.3	-0.0*	0.0	-0.0*	0.0	-0.0*	0.0	-0.0*	0.0	-0.0*	0.0	-0.0*	0.0	-0.0*	0.0	-0.0*	0.0	-0.0*	0.0
.26+.50	-0.0*	0.0	0.3*	0.3	0.0*	0.0	0.0*	0.0	0.0*	0.0	0.0*	0.0	0.0*	0.0	0.0*	0.0	0.0*	0.0	-0.0*	0.0	-0.0*	0.0	-0.0*	0.0	-0.0*	0.0
.74+.96	-0.0*	0.0	0.6*	0.4	0.0*	0.0	0.0*	0.0	0.0*	0.0	0.0*	0.0	0.0*	0.0	0.0*	0.0	0.0*	0.0	-0.0*	0.0	-0.0*	0.0	-0.0*	0.0	-0.0*	0.0

DIFFERENTIAL CROSS SECTION OF N+p->(P+PI-)+P REACTION FOR THE MOMENTUM RANGE 55 + 65 GEV/C,
 COS THETA* INTERVAL 0.1 + 0.50 (IN MICROBARN/(GEV**4/C**5*STERAD))

M* GEV: 1.09+1.12 1.12+1.18 1.18+1.24 1.24+1.30 1.30+1.36 1.36+1.42 1.42+1.48 1.48+1.54 1.54+1.62 1.62+1.70 1.70+1.78 1.78+1.86
 C**2

0*/3.14
 0.0+ 0.0 2.9+ 1.7 5.5+ 4.5 -0.0+ 0.0 -0.0+ 0.0 -0.0+ 0.0 -0.0+ 0.0 -0.0+ 0.0 -0.0+ 0.0 -0.0+ 0.0 -0.0+ 0.0
 2.5+ 1.5 4.8+ 1.7 14.0+ 5.1 8.9+ 2.9 4.0+ 3.0 -0.0+ 0.0 -0.0+ 0.0 -0.0+ 0.0 -0.0+ 0.0 -0.0+ 0.0 -0.0+ 0.0
 4.7+ 2.4 10.2+ 2.0 15.7+ 3.1 22.2+ 4.5 19.9+ 6.3 7.0+ 0.0 -0.0+ 0.0 -0.0+ 0.0 -0.0+ 0.0 -0.0+ 0.0 -0.0+ 0.0
 1.7+ 0.9 21.4+ 3.3 39.4+ 4.4 53.4+ 5.1 75.0+ 6.9 86.9+ 8.3 79.2+ 8.5 66.4+11.3 -0.0+ 0.0 -0.0+ 0.0 -0.0+ 0.0 -0.0+ 0.0

-T INTERVAL: 0.05 + 0.10 (GEV/C)**2
 0.04+0.26 2.6+ 3.2 9.3+ 0.3 9.9+ 0.9 0.0+ 0.0 -0.0+ 0.0 -0.0+ 0.0 -0.0+ 0.0 -0.0+ 0.0 -0.0+ 0.0 -0.0+ 0.0
 2.6+ 1.5 4.8+ 1.7 14.0+ 5.1 8.9+ 2.9 4.0+ 3.0 -0.0+ 0.0 -0.0+ 0.0 -0.0+ 0.0 -0.0+ 0.0 -0.0+ 0.0 -0.0+ 0.0
 4.7+ 2.4 10.2+ 2.0 15.7+ 3.1 22.2+ 4.5 19.9+ 6.3 7.0+ 0.0 -0.0+ 0.0 -0.0+ 0.0 -0.0+ 0.0 -0.0+ 0.0 -0.0+ 0.0
 1.7+ 0.9 21.4+ 3.3 39.4+ 4.4 53.4+ 5.1 75.0+ 6.9 86.9+ 8.3 79.2+ 8.5 66.4+11.3 -0.0+ 0.0 -0.0+ 0.0 -0.0+ 0.0

-T INTERVAL: 0.10 + 0.16 (GEV/C)**2
 0.04+0.26 2.6+ 3.2 9.3+ 0.3 9.9+ 0.9 0.0+ 0.0 -0.0+ 0.0 -0.0+ 0.0 -0.0+ 0.0 -0.0+ 0.0 -0.0+ 0.0 -0.0+ 0.0
 2.6+ 1.5 4.8+ 1.7 14.0+ 5.1 8.9+ 2.9 4.0+ 3.0 -0.0+ 0.0 -0.0+ 0.0 -0.0+ 0.0 -0.0+ 0.0 -0.0+ 0.0 -0.0+ 0.0
 4.7+ 2.4 10.2+ 2.0 15.7+ 3.1 22.2+ 4.5 19.9+ 6.3 7.0+ 0.0 -0.0+ 0.0 -0.0+ 0.0 -0.0+ 0.0 -0.0+ 0.0 -0.0+ 0.0
 1.7+ 0.9 21.4+ 3.3 39.4+ 4.4 53.4+ 5.1 75.0+ 6.9 86.9+ 8.3 79.2+ 8.5 66.4+11.3 -0.0+ 0.0 -0.0+ 0.0 -0.0+ 0.0

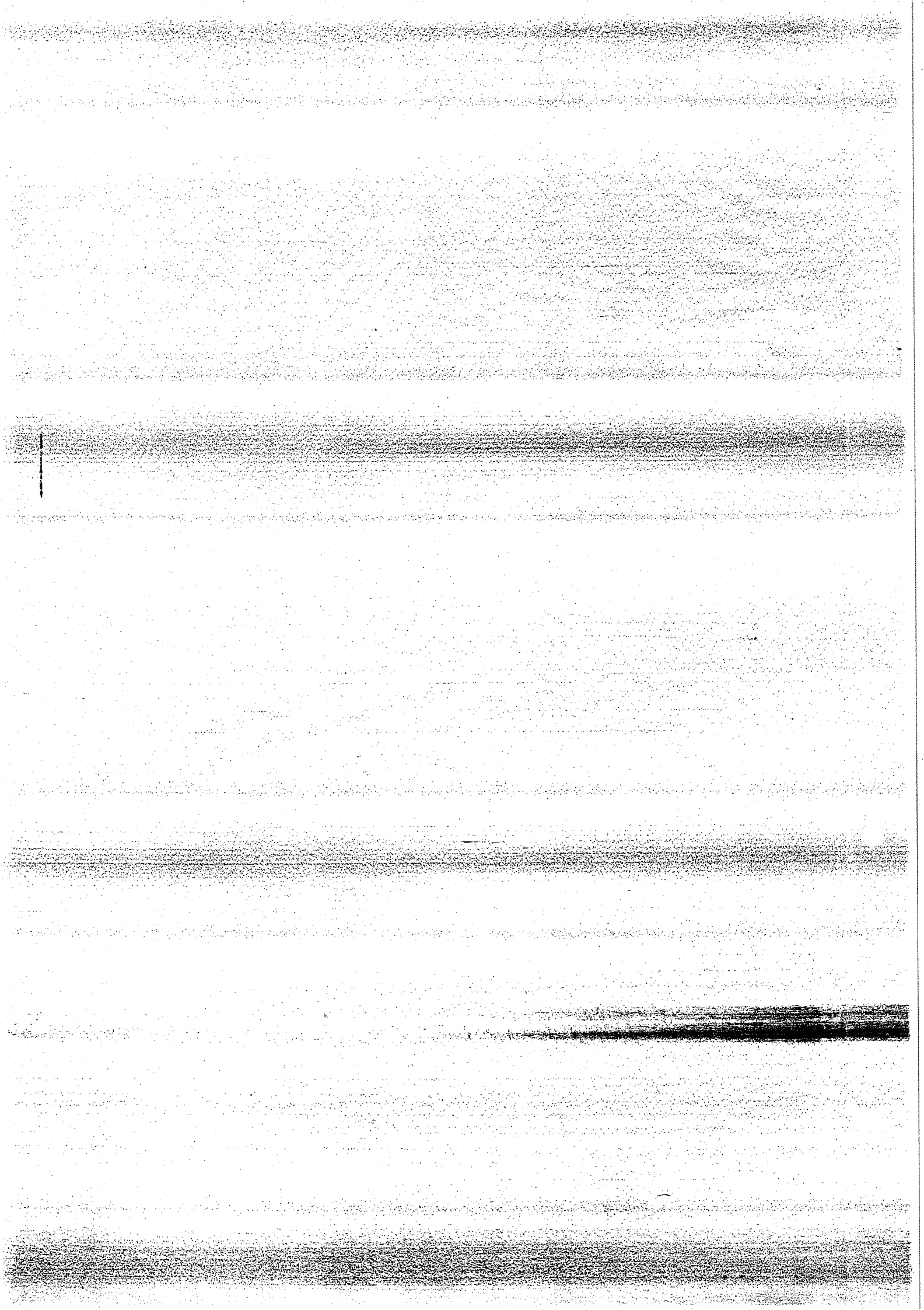
-T INTERVAL: 0.15 + 0.23 (GEV/C)**2
 0.04+0.26 2.6+ 3.2 9.3+ 0.3 9.9+ 0.9 0.0+ 0.0 -0.0+ 0.0 -0.0+ 0.0 -0.0+ 0.0 -0.0+ 0.0 -0.0+ 0.0 -0.0+ 0.0
 2.6+ 1.5 4.8+ 1.7 14.0+ 5.1 8.9+ 2.9 4.0+ 3.0 -0.0+ 0.0 -0.0+ 0.0 -0.0+ 0.0 -0.0+ 0.0 -0.0+ 0.0 -0.0+ 0.0
 4.7+ 2.4 10.2+ 2.0 15.7+ 3.1 22.2+ 4.5 19.9+ 6.3 7.0+ 0.0 -0.0+ 0.0 -0.0+ 0.0 -0.0+ 0.0 -0.0+ 0.0 -0.0+ 0.0
 1.7+ 0.9 21.4+ 3.3 39.4+ 4.4 53.4+ 5.1 75.0+ 6.9 86.9+ 8.3 79.2+ 8.5 66.4+11.3 -0.0+ 0.0 -0.0+ 0.0 -0.0+ 0.0

-T INTERVAL: 0.23 + 0.31 (GEV/C)**2
 0.04+0.26 2.6+ 3.2 9.3+ 0.3 9.9+ 0.9 0.0+ 0.0 -0.0+ 0.0 -0.0+ 0.0 -0.0+ 0.0 -0.0+ 0.0 -0.0+ 0.0 -0.0+ 0.0
 2.6+ 1.5 4.8+ 1.7 14.0+ 5.1 8.9+ 2.9 4.0+ 3.0 -0.0+ 0.0 -0.0+ 0.0 -0.0+ 0.0 -0.0+ 0.0 -0.0+ 0.0 -0.0+ 0.0
 4.7+ 2.4 10.2+ 2.0 15.7+ 3.1 22.2+ 4.5 19.9+ 6.3 7.0+ 0.0 -0.0+ 0.0 -0.0+ 0.0 -0.0+ 0.0 -0.0+ 0.0 -0.0+ 0.0
 1.7+ 0.9 21.4+ 3.3 39.4+ 4.4 53.4+ 5.1 75.0+ 6.9 86.9+ 8.3 79.2+ 8.5 66.4+11.3 -0.0+ 0.0 -0.0+ 0.0 -0.0+ 0.0

-T INTERVAL: 0.31 + 0.40 (GEV/C)**2
 0.04+0.26 2.6+ 3.2 9.3+ 0.3 9.9+ 0.9 0.0+ 0.0 -0.0+ 0.0 -0.0+ 0.0 -0.0+ 0.0 -0.0+ 0.0 -0.0+ 0.0 -0.0+ 0.0
 2.6+ 1.5 4.8+ 1.7 14.0+ 5.1 8.9+ 2.9 4.0+ 3.0 -0.0+ 0.0 -0.0+ 0.0 -0.0+ 0.0 -0.0+ 0.0 -0.0+ 0.0 -0.0+ 0.0
 4.7+ 2.4 10.2+ 2.0 15.7+ 3.1 22.2+ 4.5 19.9+ 6.3 7.0+ 0.0 -0.0+ 0.0 -0.0+ 0.0 -0.0+ 0.0 -0.0+ 0.0 -0.0+ 0.0
 1.7+ 0.9 21.4+ 3.3 39.4+ 4.4 53.4+ 5.1 75.0+ 6.9 86.9+ 8.3 79.2+ 8.5 66.4+11.3 -0.0+ 0.0 -0.0+ 0.0 -0.0+ 0.0

-T INTERVAL: 0.40 + 0.50 (GEV/C)**2
 0.04+0.26 2.6+ 3.2 9.3+ 0.3 9.9+ 0.9 0.0+ 0.0 -0.0+ 0.0 -0.0+ 0.0 -0.0+ 0.0 -0.0+ 0.0 -0.0+ 0.0 -0.0+ 0.0
 2.6+ 1.5 4.8+ 1.7 14.0+ 5.1 8.9+ 2.9 4.0+ 3.0 -0.0+ 0.0 -0.0+ 0.0 -0.0+ 0.0 -0.0+ 0.0 -0.0+ 0.0 -0.0+ 0.0
 4.7+ 2.4 10.2+ 2.0 15.7+ 3.1 22.2+ 4.5 19.9+ 6.3 7.0+ 0.0 -0.0+ 0.0 -0.0+ 0.0 -0.0+ 0.0 -0.0+ 0.0 -0.0+ 0.0
 1.7+ 0.9 21.4+ 3.3 39.4+ 4.4 53.4+ 5.1 75.0+ 6.9 86.9+ 8.3 79.2+ 8.5 66.4+11.3 -0.0+ 0.0 -0.0+ 0.0 -0.0+ 0.0

-T INTERVAL: 0.50 + 0.62 (GEV/C)**2
 0.04+0.26 2.6+ 3.2 9.3+ 0.3 9.9+ 0.9 0.0+ 0.0 -0.0+ 0.0 -0.0+ 0.0 -0.0+ 0.0 -0.0+ 0.0 -0.0+ 0.0 -0.0+ 0.0
 2.6+ 1.5 4.8+ 1.7 14.0+ 5.1 8.9+ 2.9 4.0+ 3.0 -0.0+ 0.0 -0.0+ 0.0 -0.0+ 0.0 -0.0+ 0.0 -0.0+ 0.0 -0.0+ 0.0
 4.7+ 2.4 10.2+ 2.0 15.7+ 3.1 22.2+ 4.5 19.9+ 6.3 7.0+ 0.0 -0.0+ 0.0 -0.0+ 0.0 -0.0+ 0.0 -0.0+ 0.0 -0.0+ 0.0
 1.7+ 0.9 21.4+ 3.3 39.4+ 4.4 53.4+ 5.1 75.0+ 6.9 86.9+ 8.3 79.2+ 8.5 66.4+11.3 -0.0+ 0.0 -0.0+ 0.0 -0.0+ 0.0



ADDENDUM II

to

DIFFRACTION DISSOCIATION OF NEUTRONS INTO ($p\pi^-$) ON PROTONS
IN THE MOMENTUM RANGE 35 TO 65 GeV/c

by

A. Babaev et al.,

ITEP, Moscow, IEKP, Karlsruhe and CERN, Geneva

Description of the pion and baryon exchange Deck-model.

Geneva - June 1976

The experimental data on $n + p \rightarrow (p + \pi^-) + p$ are described by the pion pole exchange graph (a) and the nucleon pole exchange graphs (b) and (c) in the region of low excited masses and low-momentum transfer.

Let Q_1 and Q_2 be the four-momenta of the initial nucleons, and q_1, q_2 and k be the momenta of the produced protons and pion.

The following invariants will be used

$$\begin{aligned} s &= (Q_1 + Q_2)^2, & s_1 &= (q_1 + k)^2 = M^2, & s_2 &= (q_2 + k)^2, & \tilde{s} &= (q_1 + q_2)^2 \\ t_1 &= (Q_1 - q_1)^2, & t &= (Q_2 - q_2)^2, & U &= (Q_1 - k)^2. \end{aligned} \quad (\text{II.1})$$

The off-mass shell corrections to the graph (a) are considered by Reggeizing the exchanged pion following the Reggeized one-pion-exchange (OPER) model^{a,b}. The main features of the reaction $p + p \rightarrow p + n + \pi^+$ have been successfully described by this model in the momentum range ($2 < P_{\text{lab}} < 28.5$ GeV/c).

The amplitude corresponding to the graph (a) reads in the OPER model as follows:

$$M_a = G \sqrt{2} \bar{u}(q_1) \gamma_5 u(Q_1) \frac{F_\pi(t_1, \dots)}{t_1 - \mu^2} T_{\pi^- p}(s_2, t, t_1) \quad (\text{II.2})$$

with the following notations:

- i) G is the $NN\pi$ coupling constant ($G^2/4\pi = 14.6$).
- ii) $T_{\pi^- p}(s_2, t, t_1) = \bar{u}(q_1) [A(s_2, t, t_1) + B(s_2, t, t_1) \hat{k}] u(Q_1)$ is the amplitude of the off-shell $\pi^- p$ scattering. It depends on the virtual pion mass only through the vacuum pole contribution. Let us write $T_{\pi p} = T_{\pi p}^R + T_{\pi p}^P$, where $T_{\pi p}^P$ corresponds to the pomeron contribution and $T_{\pi p}^R$ stands for contributions of resonances and P', ρ Regge poles. We then have the off-mass-shell amplitude

$$T_{\pi p}(s_2, t, t_1) = T_{\pi p}^R(s_2, t, \mu^2) + T_{\pi p}^P(s_2, t, \mu^2) \exp [R_p^2(t_1 - \mu^2)]. \quad (\text{II.3})$$

In Ref. b it was shown that in order to describe correctly the energy dependence of $p + p \rightarrow p + n + \pi^+$, it is necessary to have $R_p^2 \neq 0$. The Regge-pole parametrization for functions A and B was used according to Ref. b.

- iii) $F_\pi(t_1, \dots)$ is a form factor giving the off-mass shell dependence of the total amplitude. In the OPER model

$$F_\pi(t_1, \dots) = \exp \left[\left\{ R_1^2 + \alpha'_\pi \ln \left(\frac{s(k_T^2 + \mu^2)}{s_2 s_0} \right) \right\} (t_1 - \mu^2) \right], \quad (\text{II.4})$$

where k_T^2 is the square of the transverse momentum of the pion in the rest frame of the reaction; $s_0 = 1 \text{ GeV}^2$; α'_π is the pion trajectory slope ($\alpha'_\pi = 0.7 \text{ GeV}^{-2}$); and R_1^2 is a free parameter, characterizing the pion pole residue in graph (a).

The graphs (b) and (c) correspond to the soft pion bremsstrahlung. Their amplitudes depend on the off-mass shell NN-scattering amplitudes. For the on-shell scattering a single invariant amplitude, namely the vacuum pole non-spin flip amplitude

$$T_{NN}(s,t) = iA_0 e^{B(s)} t_{\bar{u}(P_2)} \frac{\hat{P}_4 + \hat{P}_3}{2\sqrt{s}} u(P_1) \bar{u}(P_4) \frac{\hat{P}_1 + \hat{P}_2}{2\sqrt{s}} u(P_3) \quad (\text{II.5})$$

dominates^{*}).

The value A_0 is connected to the total cross-section by the relation $A_0 = \sigma_t/0.39 \text{ (GeV}^{-2}\text{)}$ and $B(s)$ determines the dependence of the NN-scattering amplitude on the momentum transfer. A good approximation for $B(s)$ is

$$B(s) = (3.5 + 0.4 \ln s) \text{ GeV}^{-2} . \quad (\text{II.6})$$

By using Eq. (II.5) the amplitudes corresponding to the graphs (b) and (c) can be expressed in the following way:

$$M_b = iG\sqrt{2}A_0 e^{B(\tilde{s})} t_{\bar{u}(q_2)} \frac{\hat{Q}_1 + \hat{q}_1 - \hat{k}}{2\sqrt{s}} u(Q_2) \bar{u}(q_1) \frac{\hat{Q}_2 + \hat{q}_2}{2\sqrt{s}} \frac{\hat{Q}_1 - \hat{k} + m}{(Q_1 - k)^2 - m^2} \gamma_5 u(Q_1) F_u$$

$$M_c = iG\sqrt{2}A_0 e^{B(s)} t_{\bar{u}(q_2)} \frac{\hat{Q}_1 + \hat{q}_1 + \hat{k}}{2\sqrt{s}} u(Q_2) \bar{u}(q_1) \gamma_5 \frac{\hat{q}_1 + \hat{k} + m}{(q_1 + k)^2 - m^2} \frac{\hat{Q}_2 + \hat{q}_2}{2\sqrt{s}} u(Q_1) F_s , \quad (\text{II.7})$$

where $F_u(u)$ and $F_s(s_1)$ are functions describing the off-mass shell corrections which satisfy the conditions: $F_u(m^2) = F_s(m^2) = 1$.

Using an exponential parametrization for F_u and F_s one obtains a satisfactory description of the data with the following functions

$$F_u = \exp [a_u(u - m^2)] , \quad F_s = \exp [- \{a_s + b_s(s_1 - m^2)\}(s_1 - m^2)] \quad (\text{II.8})$$

^{*}) On mass shell equivalent representations for this amplitude become different in the off-mass shell region.

and with the following parameters

$$a_u = 2.9 \text{ GeV}^{-2}, \quad a_s = 0.7 \text{ GeV}^{-2}, \quad b_s = 2.7 \text{ GeV}^{-4}. \quad (\text{II.9})$$

The value of R_1^2 (II.4) was taken from Ref. b: $R_1^2 = 1.9 \text{ GeV}^{-2}$; and for R_p^2 (II.3) the value obtained was $R_p^2 = 2 \text{ GeV}^{-2}$.

To find the matrix element squared we use the following approximations in Eq. (II.7):

$$\bar{u}(q_2)(\hat{Q}_1 + \hat{q}_1 - \hat{k})u(Q_2) \approx 2\bar{u}(q_2)\hat{q}_1 u(Q_2), \quad \bar{u}(q_2)(\hat{Q}_1 + \hat{q}_1 + \hat{k})u(Q_2) \approx 2\bar{u}(q_2)\hat{Q}_1 u(\hat{Q}_2).$$

Then one gets for the square of the separate amplitudes (II.2), (II.7), and their interference terms after summation over the spins of the initial and final particles:

$$\begin{aligned} \overline{|M_a|^2} &= 2f_\pi^2 \{ |A|^2(Q_2 q_2 + m^2) + |B|^2[2(q_2 k)(Q_2 k) - \mu^2(Q_2 q_2) + \mu^2 m^2] + \\ &+ 2 \text{Re} (AB^*) (Q_2 + q_2, k)_m \} (-t_1) \end{aligned}$$

$$\begin{aligned} \overline{|M_b|^2} &= 4|f_b|^2 [2(q_2 q_1)(Q_2 q_1) - m^2(Q_2 q_2) + m^4] \{ 2(Q_1 k)[2(q_2 q_1)(q_2 k) - m^2(q_1 k)] - \\ &- \mu^2[2(q_2 q_1)(Q_1 q_2) - m^2(Q_1 q_1) + m^4] \} \end{aligned}$$

$$\begin{aligned} 2 \text{Re} (M_b M_a^*) &= 8 \text{Re} \{ f_b f_\pi^* [A^* m(q_1 q_2 + Q_2 q_1) + B^* ((q_2 q_1)(Q_2 k) + (q_2 k)(Q_2 q_1) + \\ &+ m^2(q_1 k) - (q_1 k)(Q_2 q_2))] [(q_1 q_2)(Q_1 k) + (Q_1 q_1)(q_2 k) - \\ &- (q_1 k)(Q_1 q_2) - m^2(q_2 k)] \} \end{aligned}$$

$$\begin{aligned} 2 \text{Re} (M_b M_c^*) &= 8 \text{Re} \{ f_b f_c^* [(q_1 q_2)(Q_1 Q_2) + (Q_1 q_2)(Q_2 q_1) - (Q_2 q_2)(Q_1 q_1) + m^2(Q_1 q_1)] \times \\ &\times [-2\mu^2(Q_1 q_2)(q_1 q_2) + 2(q_2 k)((q_1 q_2)(Q_1 k) + (q_1 k)(Q_1 q_2) - (Q_1 q_1)(q_2 k)) - \\ &- m^2(2(q_1 k)(Q_1 k) - \mu^2(Q_1 q_1) - 2(q_2 k)^2 + \mu^2 m^2)] \}. \end{aligned}$$

The expressions for $|M_c|^2$ and $2 \text{Re} (M_c M_a^*)$ can be obtained from $|M_b|^2$ and $2 \text{Re} (M_b M_a^*)$ by the substitutions: $Q_1 \rightleftharpoons q_1$ and $f_b \rightleftharpoons f_c$.

Here

$$f_\pi = G\sqrt{2} \frac{F_\pi}{t - \mu^2}, \quad f_b = \frac{iG\sqrt{2}}{\tilde{s}} A_0 \exp [B(\tilde{s})t] \frac{F_u}{(Q_1 - k)^2 - m^2}$$

$$f_c = \frac{iG\sqrt{2}}{s} A_0 \exp [B(s)t] \frac{F_s}{(q_1 + k)^2 - m^2}.$$

REFERENCES TO ADDENDA

- a) K.G. Borekov et al., Yadernaya Fiz. 15, 361 (1972) [English translation: Soviet J. Nuclear Phys. 15, 203 (1972)].
- b) L.A. Ponomarev, report ITEP-9 (1975) and Fiz. Elementarnykh Chastik i Atomnogo Yadra 7, 186 (1976), to be translated in Soviet J. Particles and Nuclei.

